Spring 5-16-2014

Detection and inhibition of influenza using synthetic sialosidesc

Yun He

DETECTION AND INHIBITION OF INFLUENZA VIRUSES USING SYNTHETIC SIALOSIDES

by

YUN HE

Under the Direction of Dr. Suri S. Iyer

ABSTRACT

Influenza infection remains constant threat to human health and results in huge financial loss every year. Rapid and accurate detection of influenza can help governments and health organizations monitor influenza activity and take measurements when necessary. In addition, influenza detection in a timingly manner can help doctors make diagnosis and provide effective treatment. On the other hand, novel inhibitors of influenza virus are in high demand because circulating strains have started to develop resistance to currently available anti-viral drugs.

Influenza virus has two surface glycoproteins: hemagglutinin (HA) and neuraminidase (NA), which play important roles in the influenza infection. The binding of HA to sialic acid-containing carbohydrates on cell surface initiates virus internalization, while cleavage of terminal sialic acid by NA facilitates viral particle release. In this dissertation, we focus on the development of glycan microarray that is comprised of a panel of NA resistant sialosides, and demonstrate the application of microarray to capture influenza virus at ambient temperature without the addition of NA inhibitors. We also describe a

novel electrochemical biosensor for the detection of influenza virus. In addition, we have developed a new class of bivalent NA inhibitors that show promising inhibitory activities against influenza viruses.

INDEX WORDS: Influenza, sialosides, microarray, NA inhibition

DETECTION AND INHIBITION OF INFLUENZA VIRUSES USING SYNTHETIC SIALOSIDES

by

YUN HE

A Dissertation Submitted in Partial Fulfillment of the Requirements for the Degree of

PhD

in the College of Arts and Sciences

Georgia State University

2014

DETECTION AND INHIBITION OF INFLUENZA VIRUSES USING SYNTHETIC SIALOSIDES

by

YUN HE

Committee Chair: Suri Iyer

Committee: Binghe Wang

Peng Wang

Gangli Wang

Electronic Version Approved:

Office of Graduate Studies

College of Arts and Sciences

Georgia State University

May 2014

DEDICATION

This dissertation is dedicated to my grandma Ruiqi Yu who wished to see her granddaughter graduate college and would be proud to see her one step further.

ACKNOWLEDGEMENTS

I would like to express my deepest appreciation to all those who have supported me in my long journey of pursuing my PhD degree and to complete this thesis. A special gratitude I give to my research advisor Dr. Suri S. Iyer, who introduced me into the excited research area and offered continuous encouragement, help and advices not only on research. I wouldn't have gone so far without your help. I would also like to thank my thesis committee members Dr. Alison Weiss, Dr. William Connick, Dr. Alan Pinhas (University of Cincinnati), Dr. Binghe Wang, Dr. Peng George Wang and Dr. Gangli Wang (Georgia State University) for guidance and feedbacks regarding my research. In addition, a thank you to my group members: Dr. Yang Yang, Dr. Abassahab, Ms. Joyce Sweeney, Mr. Hieu T. Dinh, Mr. Xiaohu Zhang. Our collaboration, both intelligently and experimentally, is a boost to my PhD research.

I'm grateful to my parents Weiwen He and Fengyan Zhu who raised me up and never stopped supporting me through my life. I would also like to express my gratitude to my parents-in-law, my other family members and friends who have always been there for me. Last but not the least, I want to thank my husband and soul mate, Xingzhe Li, who has been my role model since seven years ago. The journey of pursuing my PhD was rough but knowing I was not alone made it somewhat pleasant.

TABLE OF CONTENTS

LIST OF TABLES

LIST OF FIGURES

LIST OF SCHEMES

1 INFLUENZA: DIAGNOSIS AND THERAPY

ABSTRACT

Influenza infection remains constant threat to human health and results in huge financial loss every year. Rapid and accurate detection of influenza can help governments and health organizations monitor influenza activity and take measurements when necessary. In addition, influenza detection in a timingly manner can help doctors make diagnosis and provide effective treatment. On the aspect of clinical management of influenza, antiviral medications used along with vaccination. In this chapter, we present a thorough literature survey of salient features influenza virus, existing detection techniques and development of anti-influenza agents.

1.1 Introduction

Influenza virus is an acute respiratory pathogen that causes considerable harm to humans and livestock. According to CDC and WHO, annual seasonal outbreak of influenza infection accounts for approximately 36,000 deaths and 200,000 hospitalizations in the United States alone and 250,000 to 500,000 deaths worldwide. (*1, 2*) Pandemic outbreaks are more devastating. Each of the three documented influenza pandemic outbreaks (1918 Spanish H1N1, 1957 Asian H2N2, 1968 Hongkong H3N2) caused more than one million deaths worldwide. (*3*) Young, elderly and immune compromised populations are particularly vulnerable.(*4*) Early detection of influenza is essential to disease control due to the fast spreading nature of influenza infection.(*5*) It could also be useful in administration of antiviral drugs. The therapeutic window of antiviral drug oseltamivir is within 48 hours of the infection onset for immunocompromised people, beyond which the efficacy greatly decreases. (*6, 7*) Detection accuracy is also important due to the unspecific clinical symptoms of influenza infection, which may be confused with bacterial or other viral infection.(*8*) Addiitonally, new antiviral agents are in high demand due to the emergence of resistance to currently available anti-influenza drugs.(*9*) In this chapter, salient features influenza virus, existing detection techniques and anti-influenza agents will be discussed.

1.2 Influenza virus structure

Influenza virus is an enveloped single stranded RNA virus, belonging to orthomyxoviridae family. (*10*) There are three types of influenza: A, B and C, among which type A is commonly found in human and associated with annual influenza epidemics. (*11*) Influenza virion is roughly spherical with a diameter of approximately 100 nm. The envelope consists of a lipid membrane, an embedded protein M2 and two spiked and clustered glycoproteins, hemagglutinin (HA) and neuraminidase (NA). M2 protein is a small and hydrophobic protein, which functions as an ion channel. HA and NA are the major viral antigens and play important roles in influenza infection of host cells. Serological antibody cross-reactivity studies have identified 16 types of HA (H1-H16) and 9 types of NA (N1-N9) in avian population, while

only H1-H3 and N1-N2 are responsible for human influenza. Influenza A virus can be subtyped and expressed as a combination of HA and NA, e.g. H1N1, H3N2, etc. (*12-15*) Underneath the lipid membrane is the matrix protein M1, which surrounds the core of ribonucleoprotin complex (RNP) and helps retain the spherical structure. RNP is consists of a single strand RNA of 12,000 to 15,000 nucleotides, which is bound to a single polymerase protein, PB1, PB2 or PA and encapsulated with viral nucleoprotein (NP). RNP resembles a large loop and forms a helix structure. Influenza A and B each has eight segments of genome RNA while C has seven. The classification of influenza A, B and C is based on the antigenicity of abundant M1 and NP. An illustration of influenza virus structure is shown in figure 1.1.

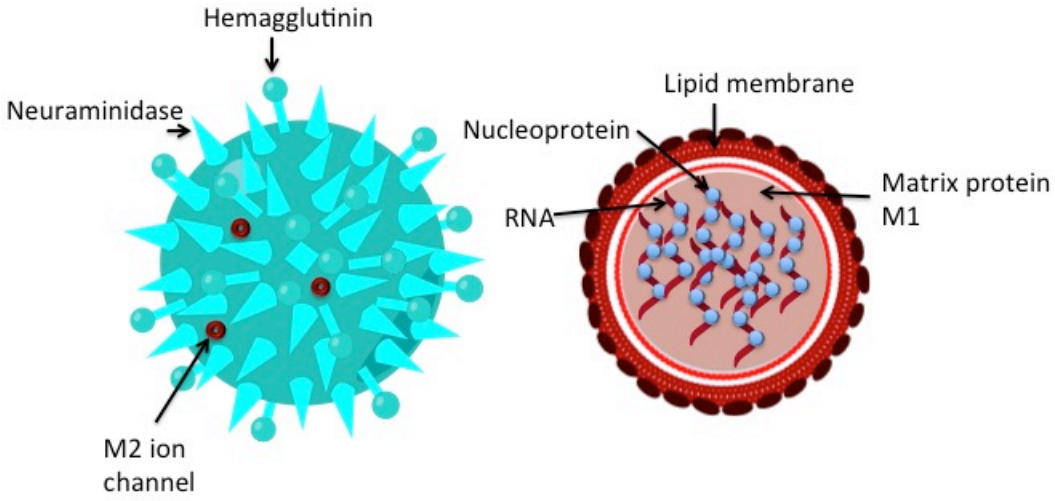

Figure 1.1 Structure of influenza virus

1.3 Antigenic shift and drift

One feature of influenza virus is the high mutation rate, (*16, 17*) which enables the mutant virus to escape immune surveillance and results in antigenic drift. For instance, as many as 35% of the substitutions have been reported to occur at only 18 of the 329 codons of the A (H3) virus. (*18*) The structural basis is that viral RNA polymerase prone to tolerate a high error rate. When the mutation occurs at the antigenic region of viral surface protein HA, NA or both, the antigenic drift arises. The process of anti-

genic drift is rather subtle, as point mutations occur potentially each time the virus replicates in a way that they do not change the conformation of the proteins. However, some mutations can significantly affect the conformation of the antigenicity site that results in loss of inhibition effect of antibodies raised to previously circulating strains. Antigenic drift is observed in all strains of influenza A and B with various patterns depending on the strain. Co-circulation of various drifted strains is observed in influenza B and A (H1), which allows re-emergence of old strains. While the influenza A (H3) strains are more prone to antigenic drift and complete replacement of old strains by new ones is more common.

Compared to the average 2 to 8 years occurrence rate of antigenic drift, antigenic shift is rather rare, estimated to happen three times every 100 years. However, once an antigenic shift occurs, it might result in pandemic or world wide epidemic outbreaks and lead to huge numbers of morbidity and mortality. The three major influenza pandemic outbreaks in 20^{th} century are believed to associate with antigenic shift. (*14, 19*)

Antigenic shift is referred to replacement of influenza A subtypes by novel ones.The cause is genetic reassortment, referring to the genetic material mixing between different viral subtypes that co-circulate. Genetic reassortment can also occur between co-infecting viral strains from different species, such as human and avian. As a result, virulent strain may be produced. Antigenicly drifted strains remain as susceptible to antigenic shift as any influenza virus. (*20*)

1.4 Influenza life cycle

Infection of influenza to host cell is initiated by the binding of HA to a cellular receptor: N-acetylneuraminic acid or sialic acid, a terminal residue on glycolipids or glycoproteins on the cell surface. The binding promotes the fusion of viral membrane to the host plasma membrane. The virion particle is incorporated into endosome via endocytosis. Inside the low pH environment of the endosome, proton influx is triggered and pumped into virion through M2 ion channel, resulting in conformational change of HA protein and fusion of the viral membrane and endosome membrane. The low pH also promotes dis-

association of viral RNP from matrix protein M1, which facilitate the RNP release through M2 ion channel into the cytoplasm. RNPs are transported into cell nucleus, where the viral RNAs are transcribed and replicated by trimeric viral RNA polymerase (PB1, PB2 and PA). Viral mRNAs are also synthesized utilizing host cell nucleus machinery. Viral proteins are translated in cytoplasm and assembled together with the newly synthesized RNPs to form virions at the apical surface of the cell membrane. NA of the progeny virus cleaves off the glycosidic bond between terminal sialic acid and galactose to facilitate budding virion escape from cell membrane and seek for new hosts. Influenza life cycle is briefly illustrated in figure 1.2.

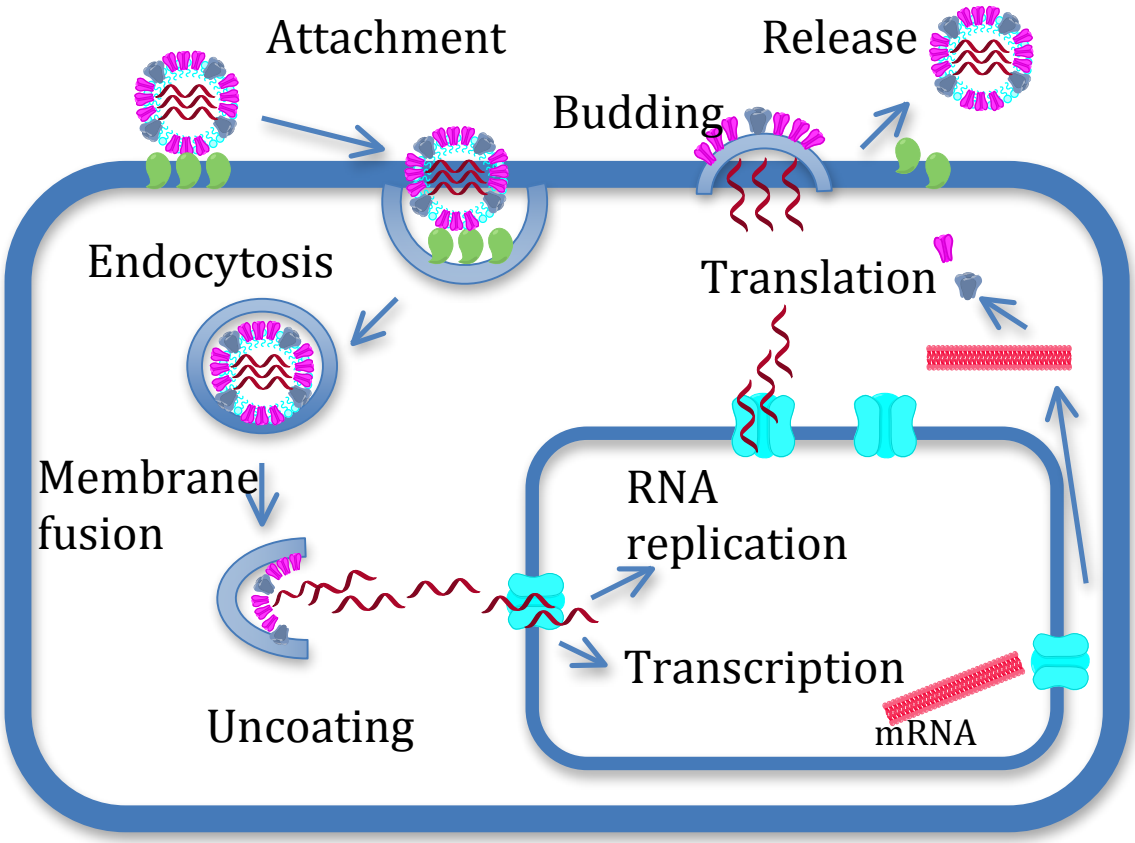

Figure 1.2 Illustration of influenza virus life cycle

1.5 Detection of influenza: Current methods

1.5.1 Viral culture

Viral culture is called "gold standard" for virus detection and a well established technique. Pri-

mary clinical specimens may have low virus titers and therefore, amplification is required for accurate detection. Cell lines such as primary epithelial cells of human adenoid, Vero cells, MRC-5, primary monkey kidney cells and Madin–Darby canine kidney (MDCK) cells have been used for isolation and propagation of influenza virus. (*21*)MDCK cells are the most commonly used cell line because it supports the growth of both influenza A and B. The traditional way of reading the result is observing cytopathic effect (CPE). Since the concentration of virus is unknown, multiple passages might be required before CPE can be observed. A minimum of two passages is required before considering a sample negative, which increases the processing time, varying from 4 to 10 days. (*22*) Using MDCK shell vials (a commercial cell culture kit with enhanced centrifugation feature) can significantly shorten the processing time to 48 to 72h. (*23*) This technique allows cell monolayers to grow on coverslips contained in flat-bottomed shell vials. After centrifugation of the cultures after inoculation, enhanced viral infection of the cells, and increased sensitivity to virus isolation is obtained. Prior to the development of CPE, the viral antigens could be identified. However, a negative result does not rule out the viral etiology. Beside cell lines, embryonated chicken eggs can also be used. Following the viral culture, rapid immunoassays such as immunofluorescent assay or membrane enzyme-linked immunosorbent assay(ELISA) are used to characterize the virus. (*22*)

1.5.2 Polymerase Chain Reaction (PCR)

In recent years, PCR has been accepted widely as new “gold standard” for influenza virus detection as PCR detects viruses and provides type and subtype information. (*24*) Briefly, viral nucleic acids extracted from clinical specimens are used as a template for cDNA synthesis by in vitro reverse transcription. The RNA primers are either specific synthetic oligonucleotides that match known nucleotide sequences on the viral genes or random hexamers. The cDNA then is amplified with specific primers and DNA polymerase and monitored on real time by fluorescence and luminescence. The processing time is much shorter compared to viral culture and sensitivity is very high, usually 5-100 TCID50 (tissue culture

infection dose at 50% end point) is sufficient. While viral culture requires 10^4 TCID50 and ELISA requires a minimum of 10^5 TCID50. (*25*) While highly precise, PCR generally is not preferred in point of care diagnosis because of it's high cost, lack of primers for emerging strains and it requires specialized training and equipment. (*26, 27*)

1.5.3 Immuno-based rapid influenza diagnostic test (RIDT)

In low resource settings, and/or during an influenza season, hospitals usually lack the facility to run standard flu test on hundreds or thousands of patient samples. Under such circumstances, rapid influenza diagnostic tests (RIDTs) may be used to guide diagnosis and treatment decisions. Currently, there are several FDA approved RIDTs in the marketplace, which are immuno-based assays targeting at influenza A and B nucleoprotein from respiratory specimens, with various readout methods such as fluorescent, direct color, etc. These RIDTs can yield results within a short time frame, usually 10 to 15 minutes, with relatively simple instructions. Some of the RIDTs are approved for office/bedside use. The 3M™ Rapid Detection Flu A+B test as an example, it is a new immunochromatography (IC) assay that is designed to detect and differentiate between influenza A and B nucleoprotein in nasal swab, aspirates, and nasopharyngeal swab specimens. The format of this assay is a self-contained cartridge and only single specimens are required without the need of test batching. The assay can be completed in 15 min and a reader detects the fluorescent signal. (*28*)However, interpreting the RIDT test result is not always straightforward. Several factors including clinical symptoms, types and collecting time of specimens, disease prevalence must also be considered. (*29*)This is due to possible false negative results caused by the relatively lower sensitivity of RIDTs compared to the "golden standard" viral culture or RT-PCR. A systematic study analyzing most commercial available RIDTs shows that the sensitivity to detect different strains of influenza viruses varies among RIDTs, which complicates the result interpretation. (Table 1.1)

RIDT Names	Influenza virus types	Specimens	Ability to distinguish A and B
3M™ Rapid Detection Flu A+B Test	A and B	NP swab/aspirate, Nasal wash/aspirate	Yes
Alere Influenza A & B	A and B	Nasal swab	Yes
BD Veritor System for Rapid Detection of Flu A+B	A and B	NP swab/nasal swab	Yes
BinaxNOW® Influenza A&B	A and B	NP swab,Nasal wash/aspirate/swab	Yes
BioSign® Flu A+B	A and B	NP swab/aspirate/wash, nasal swab	Yes
Directigen™ EZ Flu A+B	A and B	NP wash/aspirate/swab, Throat swab	Yes
OSOM® Influenza A&B	A and B	Nasal swab	Yes
QuickVue® Influenza Test	A or B	Nasal wash/aspirate/swab	Yes
QuickVue® Influenza A+B Test	A and B	NP swab, Nasal wash/aspirate/swab	No
SAS™ FluAlert A&B	A and B	Nasal wash/aspirate	Yes
SAS™ FluAlert A	A only	Nasal wash/aspirate	N/A
SAS™ FluAlert B	B only	Nasal wash/aspirate	N/A
Sofia Influenza A+B	A and B	NP aspirate/swab/wash, Nasal wash	Yes
TRU FLU®	A and B	NP aspirate/swab,Nasal wash	Yes
XPECT™ Flu A&B	A and B	Nasal wash/swab, Throat swab	Yes

Table 1.1 Commercial influenza RIDTs and characteristics

1.5.4 Glycan-based detection method for influenza virus

Another method of detection of influenza is the use of small molecules. Since sialylated glycoconjugates have been found to be essential in cell entry of influenza viruses, sialosidescan be used as probes for the detection of influenza viruses. In general, oligosaccharides/glycoconjugates represent the most abundant class of organic molecules with the capacity of structural diversity far exceed proteins and nucleic acids. The structural diversity enables them to play a variety of roles in cell biological processes such as cellular communication, cell signaling, differentiation, etc. 95% of the mammalian cell surface is covered with glycans in the form of glycoproteins or glycolipids, which are in the front line for pathogen recognition.(*31*) Therefore, using glycans as probes for the detection of pathogens have at-

tracted much attention. Since glycans typically bind through a multivalent effect, we discuss multivalency below.

1.5.4.1 Multivalency effect

Multivalency effect is observed widely in receptor-ligand binding process in the form of higher apparent affinity of multivalent ligand to receptor compared to monovalent ligand. The receptor-ligand binding process can be summarized into four categories and the proposed mechanisms are shown in Figure 1.2. The first widely observed type of interaction is the binding of multivalent ligand to oligomeric receptors. In this case, the translational entropy is paid only for the initial contact of receptor and multivalent ligand but not the subsequent binding interactions, thus the total entropy cost is much lower. The second type is the binding of multivalent ligand to multiple monomeric receptors. Binding of the ligand to the first receptor "recruit" other receptors in the fluid bilayer by the two-dimensional diffusion. The third type is the binding of one multivalent ligand to one monomeric receptor, which possesses binding subsites in addition to the primary binding site. In the case of binding to monomeric receptor without diffusion, multivalent ligands still possesses higher functional affinities due to higher local concentration of binding element. (*32*)

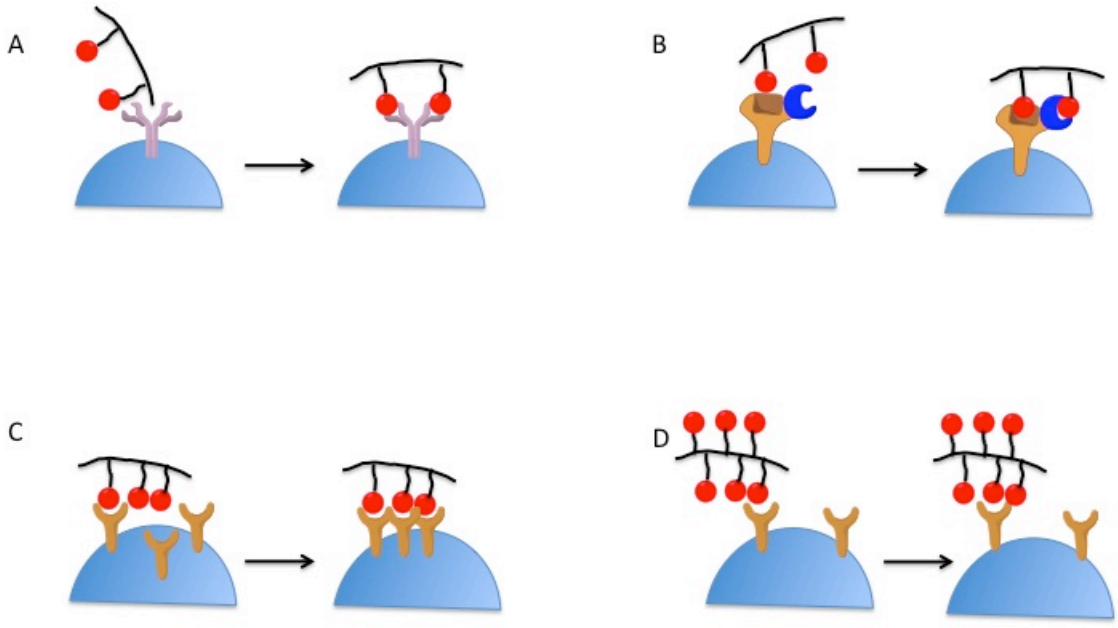

Figure 1.3 Mechanism of multivalent ligand interaction with cellular receptors: (A) Multivalent ligands bind to receptors with multiple binding sites. (B) Multivalent ligands occupy both primary and secondary binding sites of receptors. (C) Multivalent ligands binding cause receptors to cluster. (D) Multivalent ligands display high local concentration and result in high apparent binding affinity.

1.5.4.2 Glycan microarray

Since multivalency is a requirement for glycan based diagnosis of influenza, clustering of glycans can be achieved by attaching the same glycan to a surface. When multiple glycans are printed at different regions of a glass slide, it gives rise to a glycan microarray, which can be used to detect influenza virus.

Binding affinity of a single carbohydrate molecule to proteins are usually weaker (dissociation constant K_D: 10^{-3} to 10^{-6}M) compared to antigen-antibody interactions (10^{-8} to 10^{-12} M).(*33*)Due to the structural complexity of carbohydrates and difficulties in synthesis, obtaining structure-defined oligo- or polysaccharides in large quantties is very challenging. A method that can analyze carbohydrate-protein interactions with high sensitivity is in high demand. Taking the multivalent effect into account and inspired by the success of high-throughput DNA and protein microarray technique, glycan microarray was

first introduced in 2002 by several independent groups.(*34-36*)Glycan microarrays are composed of various oligo- or polysaccharides, which are immobilized on a chip-like surface in a spatially defined arrangement. Before the introduction of microarray, glycan arrays on different surfaces, such as silica plates, beads or ELISA wells have been around for many years.(*37-39*)Only after the invention of robotic arraying and high-resolution scanning technique, a miniature form of glycan array on a standard size microscope slide was realized. Hundreds of glycans can be spotted on a single microscope slide and screened with various target proteins.(*40*) In the past decade, progress in development of immobilization chemistry of carbohydrate has been made and the application of glycan microarray has been expanded, which will be discussed in the following paragraphs.

The first generation of glycan microarray was fabricated using non-covalent method to immobilize polysaccharides, proteoglycans and neoglycoproteins on nitrocellulose(*41*) or oxidized polystyrene surface(*42*) through adsorption or electrostatic interactions. This method does not require any modification of carbohydrates, however, the application scope was limited to carbohydrates with large molecular weight.

For the immobilization of low molecular weight oligosaccharides, structural modification is required. Generally, linkers with various properties or different functional groups are chemically attached to oligosaccharides. For instance, oligosaccharides with long alkyl linker can be arrayed on polystyrene surface by hydrophobic adsorption(*43, 44*). Similarly, oligosaccharides with fluorous tag (C_8F_{17}) showed high affinity to a surface coated with the same chains (C_8F_{17}). (*45*)Other tightly binding pairs such as biotinylated glycan-streptavidin coated slide,(*46, 47*) or oligosaccharides with complementary DNA sequence have also been applied. (*48*)

The strategy of attaching linkers with certain functional group into glycans is also well developed. Thiol and primary amine are two widely used functional groups that serve the purpose of covalently immobilizing glycans onto solid surface. Thiol group is reactive to maleimide (*49*)while primary

amine can be coupled with cyanuric chloride, (*50*)NHS ester(*51, 52*) or epoxide.(*53*) “Click” reaction is also used in the fabrication of glycan microarray. Generally, glycans are functionalized with azide and reacted with alkyne functionalized surface with Copper(I) as catalyst, resulting in the formation of triazole ring. (*54*)The reactions are shown in figure 1.4.

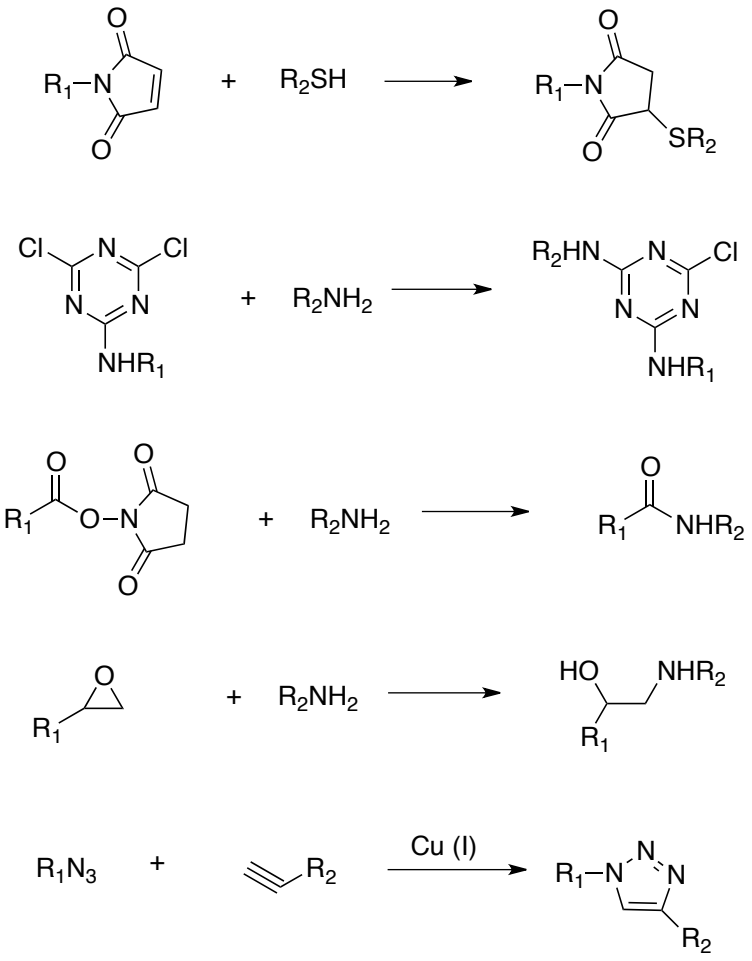

Figure 1.4 Typical coupling reactions of thiol, primary amine and "click" chemistry

Direct immobilization or modification of free reducing glycans through reductive amination(*55, 56*), glycosylamine formation and trapping(*53*), hydrazine chemistry(*57*), condensation of oxyamines(*58*)/N-alkyl oxyamines(*59*) with aldehydes have also been reported. This strategy shows its merit in modifying naturally derived glycans since complex protection/deprotection synthetic strategy is not required. Different direct conjugation reactions are shown in figure 1.5.

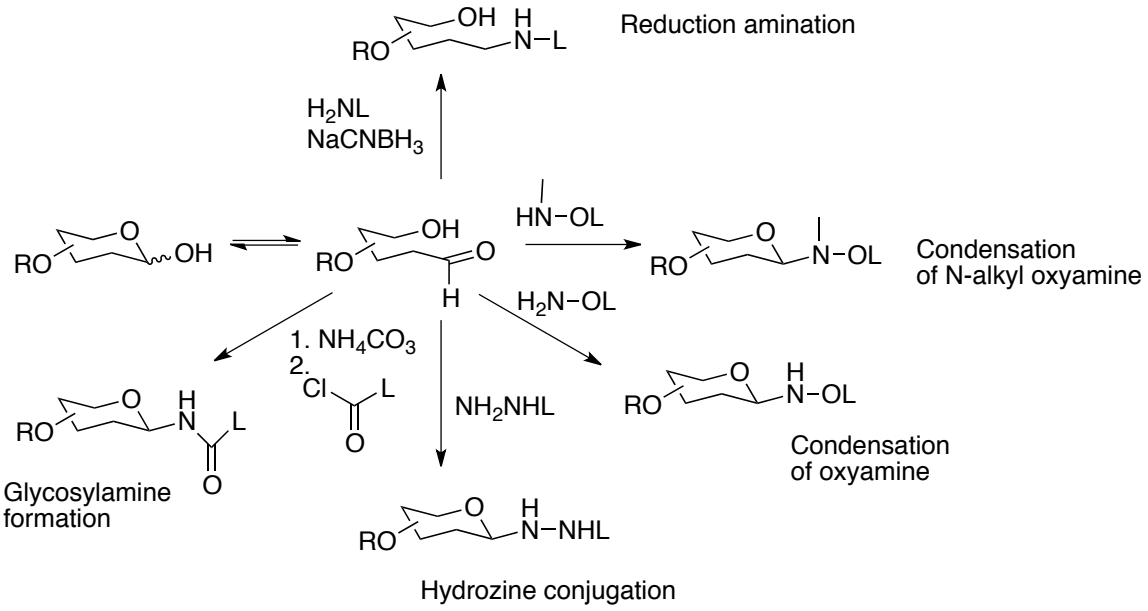

Figure 1.5 Direct conjugation of reducing glycans

To summarize, three major types of conjugation can be used to immobilize glycans, including non-covalent, covalent and direct conjugation at the reducing end. The progress in the development of the immobilization methodology has greatly advanced the glycan microarray technique. Different types of glycan conjugation are summarized in table 1.2.

Type of conjugation	Type of immobilization interaction or chemistry	Application
Noncovalent	Mix of hydrophilic and hydrophobic	Polysaccharides, proteoglycan, Neoglycoprotein on nitrocellulose or oxidazed polystyrene surface
	Hydrophobic	Neoglycolipid on nitrocellulose surface
	Fluorophilic	Glycans with fluorous linker on fluorous surface
	Electrostatic	Sulfated GAG on poly-lysine surface
	Small molecule/protein interaction	Biotinylated glycan on streptavidin coated surface
	Complimentary hybridization	Single-stranded DNA conjugated glycan on surface with complimentary DNA se-

		quence
Functionalized glycans (Covalent)	Amine chemistry	Primary amine with NHS ester slide
		Primary amine with epoxide slide
		Primary amine with cyanuric chloride coated surface
	Thiol chemistry	Thiolated glycans with maleimide surface or vice versa
	"Click" chemistry	Azide functionalized glycans with alkyne functionalized surface
Reduced end modification or conjugation	Reductive amination	Conjugate glycans with linkers (with reducing end monosaccharides in ring-open form)
	Glycosamine formation and trapping	First react with acid chloride then with linker (with reducing end monosaccharides in ring-closed form)
	Hydrazine chemistry	Directly immobilize glycan on hydrozine modified surface (with reducing end monosaccharides predominantly in ring-closed form)
	Oxyamine condensation	Generate neoglycolipid for noncovalent immobilization (with reducing end monosaccharides partially in ring-closed form)
	N-alkyl oxyamine condensation	Incorporate bifunctional linker for glycan immobilization (with reducing end monosaccharides in ring-closed form)

Table 1.2 Summary of different types of glycan conjugation

Progress made in chemical, enzymatic, chemoenzymatic synthesis of glycans has enormously enlarged the library of structure-defined carbohydrates. Combining with various immobilization techniques, glycan microarrays with different composition have been applied broadly to analyze the binding

properties of several classes of proteins such as lectins from plants, animals, virus and bacteria, antibodies, cytokines and growth factors, etc. In addition, studies that determine the binding profiles of larger and more complex targets such as cells and pathogens including bacteria on glycan microarray platforms have also been reported.

Glycan microarrays have revealed a lot of biological secrets. A comprehensive dataset of hundreds of examples of the application of glycan microarrays can be found at the Consortium for Functional Glycomics website: http://www.functionalglycomics.org/.We describe briefly, a few examples that demonstrate the power of glycan microarrays.

1.5.4.3 Glycan-protein interactions using glycan microarrays

Lectins are proteins that bind to carbohydrate with high specificities, which are commonly used to probe glycans and characterize glycan microarrays. A comprehensive understanding of the binding profile of lectins to carbohydrate can expand their applications. For instance, a screening of plant lectins ConA Concanavalin A (ConA) and Erythrina cristagalli lectin ECA binding profile by Consortium for Functional Glycomics (CFG) confirmed that ConA specifically bound to glycans with at least one a-D-mannose residue; while ECA bound exclusively to various terminal N-acetyllactose amine structure. (*52*)Another example was demonstrated by Feizi laboratory. A membrane-anchored ER protein malectin that is highly conservative in animals was found to recognize glucose oligomers by NMR studies, however, the exact structure of ligand was not clear. (*60*)The profiling study on glycan microarrays revealed that malectin selectively bound to diglucosylated high mannose-N-glycan structure. The binding profiles of some novel lectins such as galectin 8, human ficolin and *Candida glabrata* have also been determined using glycan microarrays by different groups. (*61-63*)

Array of synthetic glycan fragments of large natural polysaccharides such as glycosamineglycans can be used to elucidate the structure-binding correlation of such macromolecules to their receptors. Seeberger group has constructed glycan microarrays using synthetic heparin oligosaccharides and eval-

uated the heparin-like glycosaminoglycan (GAG)-fibroblast growth factors (FGF-1 and FGF-2) interation. They found that FGF-2 bound best to the hexamer and tetramer of heparin oligosaccharides but not with the unusual 2,4-O-sulfated monomer. In the contrary, FGF-1 showed comparable binding to all of the monomer, tetramer and hexamer. This finding may facilitate the inhibitor design of FGF.(*64*)Hsieh-Wilson group reported the first example of using chondroitin sulfate microarray with distinct sulfation sequence to probe GAG-cytokine interactions. They studied both TNF-α as well as midkine-derived and brain-derived neurotrophic factor. They observed selective binding of these growth factors to CS-E but not CS-A or CS-C tetrasaccharide. (*65*)Followed-up experiments have proven the merit of the binding studies. A brain neuron growth experiment confirmed that the CS-E motif stimulated neurite outgrowth by about 50%.(*66*)

Quantitative study of carbohydrate-mediated cell adhesion to glycan array was reported by Nimrichter *et al.* They used a microarray comprised of 45 glycans to screen the binding profile of fluorescent-labeled primary chicken hepatocytes and $CD4^+$ human T-cells and found that chicken hepatocytes bound to nonreducing terminal GlcNAc residues in different linkages and orientations but not to galactose or N-acetylgalactosamine residues, while $CD4^+$ human T-cells specifically adhered to the sialyl Lewis x structure.(*67*)Seeberger *et al.* used a microarray containing five monosaccharides: mannose, glucose, N-acetyl glucose, galactose and fucose to determine the binding specificity of *E. coli*. They demonstrated that *E. coli* strain of ORN178 cells specifically bound to mannose but no the rest of monosaccharides. In comparison, a mutant strain ORN209 showed much lower binding to mannose. (*68*) In addition, the binding properties of *Helicobacter pylori* has been determined by Walz *et al.* They found that the binding profile of different *H. pylori* strains was highly dependent on the expression level of two adhesins: SabA (sialic acid binding adhesin) and BabA (Le^b-binding adhesin).(*69*)

Pathogens usually possess unique polysaccharides on the surface, which play important roles in interaction with host cells and can trigger immune response in infected human bodies. Microarrays that

are comprised of these pathogenic polysaccharides or their fragments are valuable tools in analyzing patient serum samples and evaluating the reactivity of antibodies, which can shed light to the production of vaccines. (*70*)A study aimed at the development of HIV vaccine incorporated the utilization of glycan microarray. Human antibody 2G12, which shows broad neutralization range to HIV-1 isolates, recognizes a highly conservative oligomannose cluster on HIV-1 envelope glycoprotein gp120. Based on this finding, oligomannose derivatives can be potentially used as HIV vaccines. However, the key structure was not clear. A serial of oligomannose derivatives with different length and branching patterns (Man_4 to Man_8) were synthesized and arrayed by Chi-Huey Wong and Ian A. Wilson groups. They found that a minimum element of Man_4 was required in binding, and Man_4 bound as effective to 2G12 as the Man9GlcNAc2-high mannose core.(*71*) The inhibition study using these oligomannose was also in agreement with the binding study. (*72*)These results have great impact in guiding the design of immunogens to elicit 2G12-like neutralizing antibodies as a component of an HIV vaccine. Seeberger group demonstrated another example that targeted at malaria parasites. They arrayed analogues of malaria parasite glycosylphosphatidylinositol (GPI) toxin with different mannoside units and analyzed serum samples from African donors living in a malaria endemic area and European donors. They were able to show correlation of anti-GPI antibody levels and protection from severe malaria using the synthetic GPI glycan array. (*73*)

Glycan microarrays have also been applied in cancer-induced antibody recognition, since cancer cells usually possess aberrant glycosylation pattern. Globo H hexasaccharide, a cancer marker epitope that is found on the surface of breast, prostate and ovarian cancer cells, and its truncated sequences were arrayed to analyze two monoclonal antibodies (MBr1 and VK-9) and serum samples from breast cancer patients. The terminal tetrasacchride with fucose residue was identified as the key element for effective binding to monoclonal antibodies. This study opened a door of using glycan microarray to monitor immune response to carbohydrate epitopes at different stages during differentiation, metastasis, or

treatment.(*74*) Another study used an array containing 37 carbohydrates to compare the serum antibody (IgG and IgM) levels of classical Hodgkin's lymphoma (cHL) patients and age/sex-matched healthy controls. The two groups of samples showed remarkable deviation in glycan-binding specificity. (*75*) All of these examples demonstrate the importance of glycan microarrays to further our knowledge on the fundamental understanding of protein-glycan interactions.

Another important application of glycan microarray, which is highly relevant to our research focus, is analyzing the binding properties of viral proteins and intact viruses. The carbohydrate binding profiling of influenza viruses and envelope glycoprotein HAs has attracted much research interest, mostly due to the well recognized binding specificity of HAs to sialosides. In addition, mutations of HAs occur frequently which have impact on the binding profiling. Sialoside microarray can also be used to gain better understanding of the species barrier of influenza virus transmission (avian vs human). This point is described in detail below.

1.5.4.4 Elucidating HA-glycan interactions using focused sialoside microarrays

HA is a trimeric glycoprotein with each monomer comprised of two disulfide-linked subunits HA1 and HA2. The tip of the HA spike is formed from globular regions of HA1, and the transmembrane stem region is formed from portions of both HA1 and HA2. The receptor binding domain, vestigial esterase domain and most of the epitopes for antibody recognition locate at the HA1 globular cap. The transmembrane region located close to the C terminus of HA2 anchors HA in the viral membrane. The region near the N terminus of HA2 contains the fusion peptide sequence, which undergoes conformational change at lower pH and induces membrane fusion of virus and host cell. The structure of the trimeric HA is shown in figure 1.5. Superimposition of Viet04 HA monomer with another H5 HA and 1918 pandemic virus HA reveals more similarity of this avian HA to human H1 HA than a more sequence-related H5 HA.

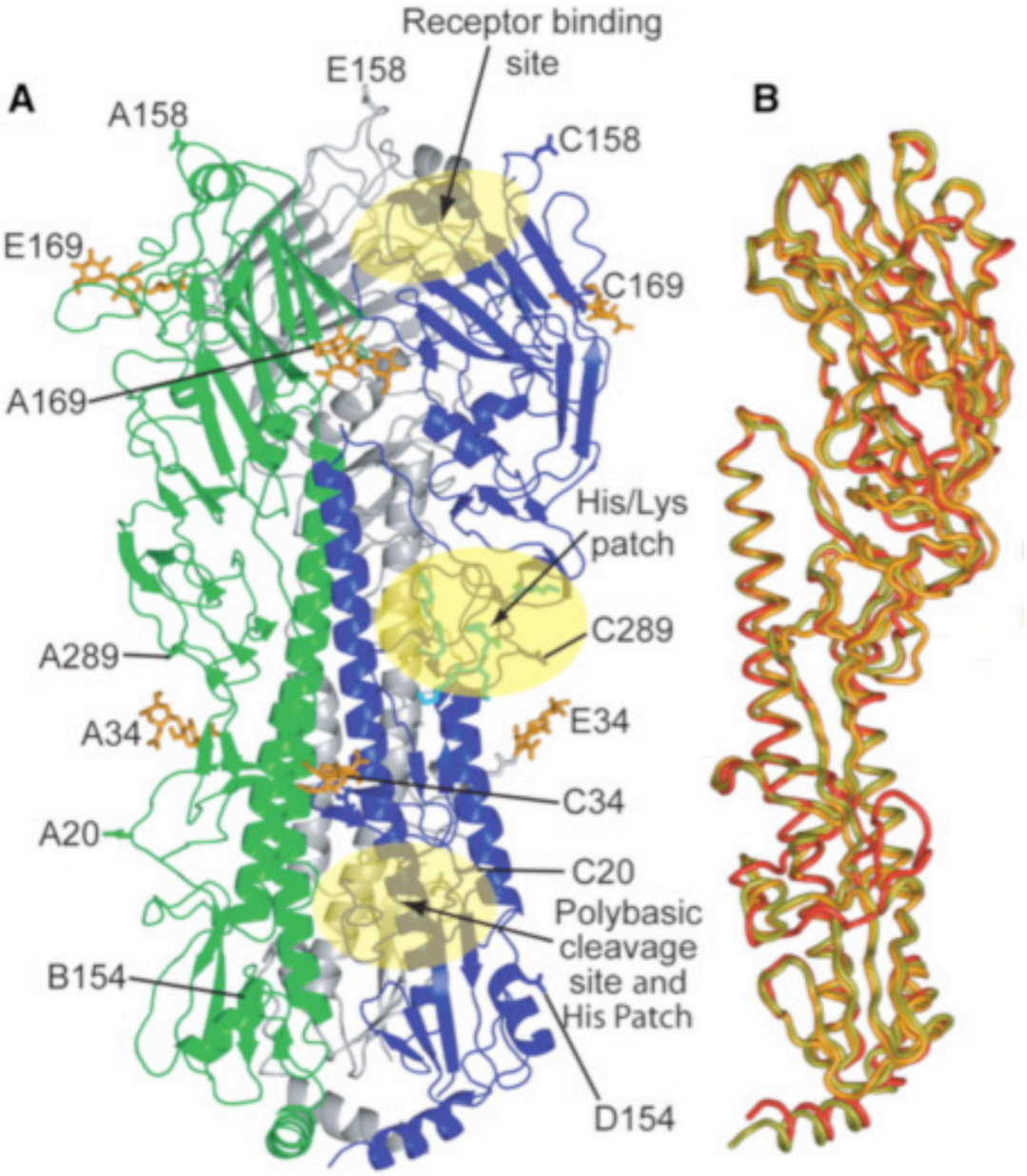

Figure 1.6 Structure of HA: (A) Overview structure of of the H5N1 Viet04 trimer. Each monomer has been colored differently. Carbohydrates observed in the electron-density maps are colored orange. (B) Structural comparison of the Viet04 monomer (olive) with duck H5 (orange) and 1918 H1 (red) HAs. (Figure 1.6 is adapted from (76)with permission)

Influenza A virus specificity for the host is mediated by HA. HA binds to receptors containing glycans with terminal sialic acids, where their precise linkage determines species preference. Avian viral HA preferentially binds to sialic acids connected to galactose in α-2,3-linkages, which are commonly found on receptors of avian intestinal epithelial cells, whereas human viral HA prefers the α-2, 6 linkage, the

dominant form on epithelial cells of the lungs and upper respiratory tract. A switch in receptor specificity is a major obstacle for influenza A viruses to cross the species barrier and to adapt to a new host. The structures of sialosides with different connections to galactose and their configurations adopted in the HA binding site with electron density maps are shown in figure 1.7. The α-2, 6-linked human receptor analog 6'-SLN adopt a compact, folded configuration in the receptor-binding site of HA (Figure 1.7C); while α-2, 3-linked avian receptor analog 3'-SLN is linear (Figure 1.7D).

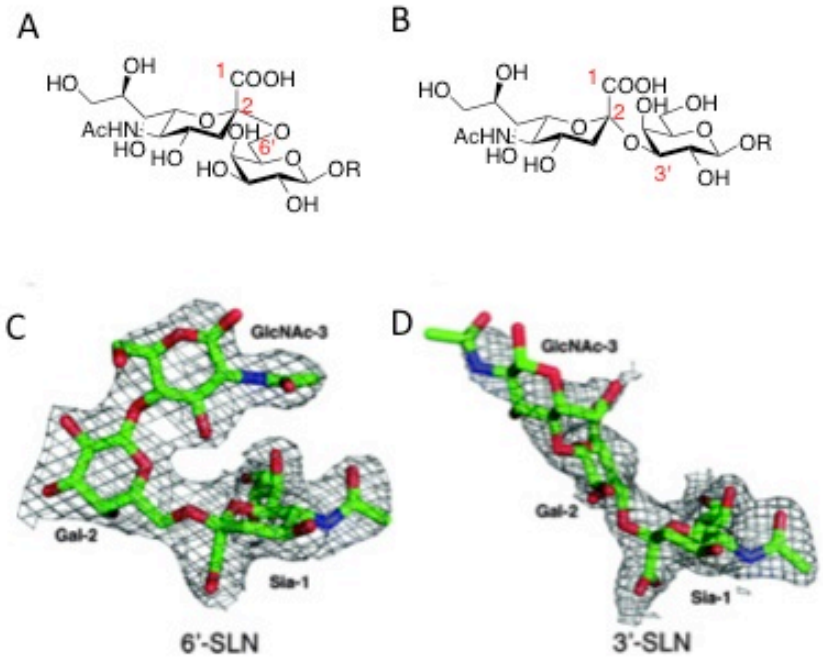

Figure 1.7 Structures and configuration of human and avian receptor analogues: (A) Structure of α-2, 6-sialosides. (B) Structure of α-2, 3-sialosides. (C) Electron density map of 6'-SLN. (D) Electron density map of 3'-SLN. (C and D are adapted from (77) with permission)

A study of the crystal structures of HA from the 2009 H1N1 pandemic viruses bound to sialodes(*77*) with different length and linkages demonstrates s that the H1 HA preferentially recognizes α-2, 6-sialylated receptors, which is achieved by hydrogen bonds between the glycan and HA mediated mainly by Asp190 and Asp225. Asp190 interacts with GlcNAc-3 while Asp225 contacts Gal-2 of α-2, 6-

sialylated receptors (human like). However, no significant interaction is observed with α-2, 3-sialylated receptors (Avian like) due to differences in the overall configurations of α–2, 6- versus α–2-3-linked sialylated glycans, which explains the considerably weaker HA avidity to avian-like receptor analogs. Another observation is that the trisaccharide and pentasaccharide adopt similar configuration at the binding site and only the three terminal glycans interact with the binding pocket. (Figure 1.7) Although differences in individual HA/glycan affinity are small, when amplified by multivalent binding, the property becomes distinguishable(*78, 79*). The microarray binding study also shows the binding preferences of 2009 H1 HA to α-2, 6-sialylated receptors. These corresponding results demonstrate that sialoside microarray is a powerful tool in studying influenza binding profile.

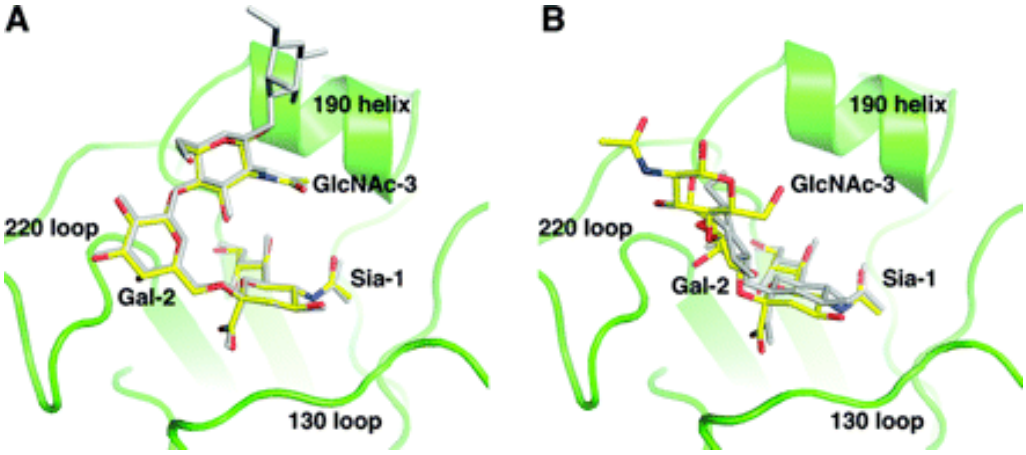

Figure 1.8 Receptor-binding specificity of CA04 HA to pentasaccharide or trisaccharide receptor analogs in the CA04 receptor binding site (green). The trisaccharide receptor analogs are shown in yellow the pentasaccharide analogs in gray. (A) α-2, 6-linked glycans; (B) α-2, 3-linked glycans. (Figure 1.7 is adapted from (77) with permission)

The diversity of sialoside microarray has been greatly increased resulted from the development of synthetic methodologies and increase interest of using microarray technique to profile the binding properties of newly emerged influenza or to differentiate different strains of viruses. Chi-Huey Wong group reported the preparation of a microarray composed of 30 synthetic sialosides of different length, branching sulfation pattern with either 2,3- or 2,6-linkage.(*80*) They used the sialoside microarray to

screen binding profiles of HAs as well as intact viruses. They observed that human influenza HA had higher binding to longer sialoside(a linear heptasaccharide shows maximum binding to almost all human HAs that were tested).

1.6 Inhibitors of influenza virus

Two major tools of combating influenza are vaccine and anti-influenza drugs. Vaccination is the prevention and control strategy, which has been proven to provide adults (aged 18-65 years) moderate protection against virologically confirmed influenza. However, vaccine efficacy varies for seasonal flu, even absent in some seasons. As mentioned before, influenza vaccines are usually produced several months in advance base on the prediction of circulating strains of the upcoming season and in case of pandemic outbreaks, production of effective vaccines might lag behind virus rapid spread. Finally, if is virtually impossible to vaccinate everybody against influenza virus every single year. Taken together , relying solely on vaccination is not a realistic strategy for fighting against influenza infection.

Antiviral medications provide alternative options to treat and control influenza infection. When administrated within the therapeutic window, antiviral drugs can significantly shorten illness onset and prevent serious flu complications such as pneumonia. (*81*) FDA has approved four antiviral drugs in treating influenza infection, including two NA inhibitors, oseltamivir (Tamiflu®) and zanamivir (Relenza®), two M2 channel blockers, amantadine (Symmetrel®) and rimantadine (Flumadine®). As circulating strains of influenza viruses have started to develop resistance to these drugs, new drug candidates are in high demand (*82*).

The clear illustration of influenza life cycle provides a number of targets for antiviral drug design. In fact, almost all viral proteins are becoming potential therapeutic targets. These target proteins, inhibitors and inhibition mechanisms are summarized in Table 1.3. Inhibitors targeting different sites are discussed in detail in the following section.

Viral proteins	Inhibitors	Inhibition mechanisms
M2	Amantadine; Rimitadine	Inhibit endosomal acidification and uncoating of endosome-entrapped virus; disable the dissociation of RNPs from M1 matrix
HA	Neu5Ac; TBHQ	Inhibit HA binding to sialic acid on cell surface and virus entry
NA	Oseltamivir; zanamivir; peramivir; laninamivir	Inhibit virus release
Polymerase	marchantin E; Ribavirin; viramidine; favipiravir	Inhibit viral replication
NP	Nucleozin	Inhibit RNP formation

Table 1.3 Inhibitors and inhibition mechanisms of influenza proteins (Table 1.3 is adapted from (83)

1.6.1 Small molecules target at HA

HA binds to sialylated glycoproteins or glycolipids on cell surface and initiates virus entry. Also, HA undergoes conformational change inside endosome at low pH and promotes RNP release. Designing inhibitors that block the binding function of HA have proven to be challenging because of the shallow binding pocket of HA. The structure of HA inhibitors are shown in figure 1.9. Most drug designs use Neu5Ac as template but the binding affinity of the Neu5Ac derivatives to HA is not very high. For instance, the dissociation constant K_D of Neu5Ac2Me (Compound 1) is in the milimolar range. (*78*)Introducing hydrophobic substituents at the anomeric carbon of Neu5Ac increases binding affinity to a certain extend. E.g. Ki of compound 2 to is 40 uM against influenza virus X-31. (*84*) Another strategy of increasing the binding affinity of Neu5Ac derivatives to HA is increasing valency. Compound 3 has been reported to inhibit hemagglutination with an IC_{50} of 3 uM against a recombinant influenza virus X-31 (Kilbourne, 1969). (*85*)

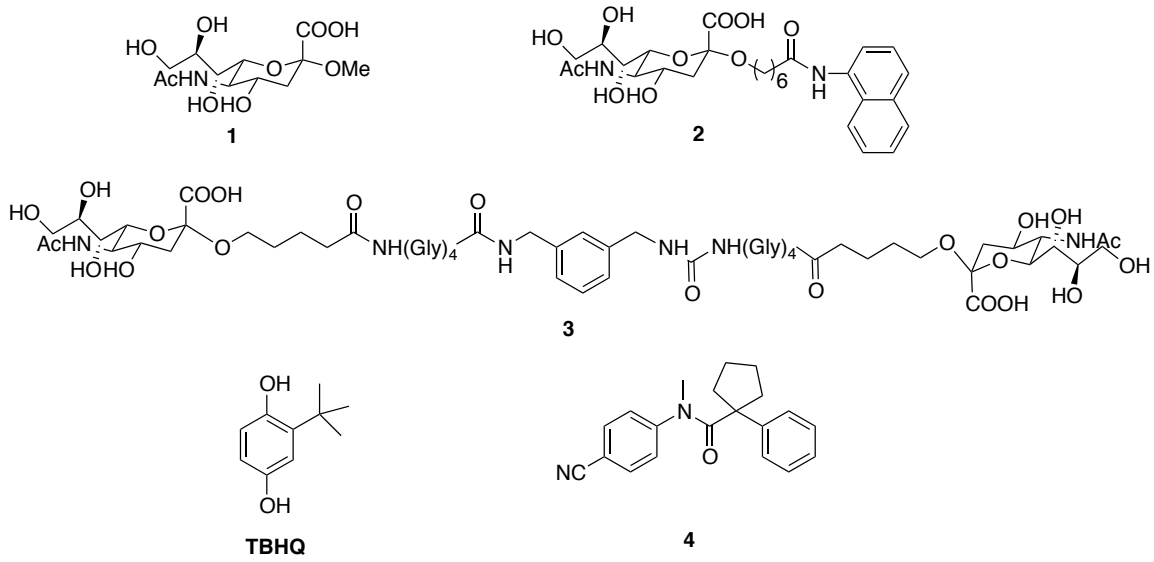

Figure 1.9 Influenza HA inhibitors targeting at sialic acid binding site (1-3) or inhibit membrane fusion (TBHQ and 4)

Progress has been reported in the discovery of HA inhibitors that interfere with membrane fusion. One lead compound is tert-butylhydroquinone (TBHQ). The binding site has been identified in two group-2 HAs (H14 and H3) at the prefusion trimeric interface of the stem region. The TBHQ binding stabilizes the prefusion trimer conformation and prevent HA1 undergo conformational change at low pH, which is essential for membrane fusion. (*86*) However, the inhibition is not observed with group-1 HAs because the binding site is blocked. Fusion inhibitors designed for group-1 HAs bind to a neighboring site. Compound 4 was found to be potent in inhibiting group-1 HAs. The crystal structure of H14 HA bound to TBHQ is shown in figure 1.10.

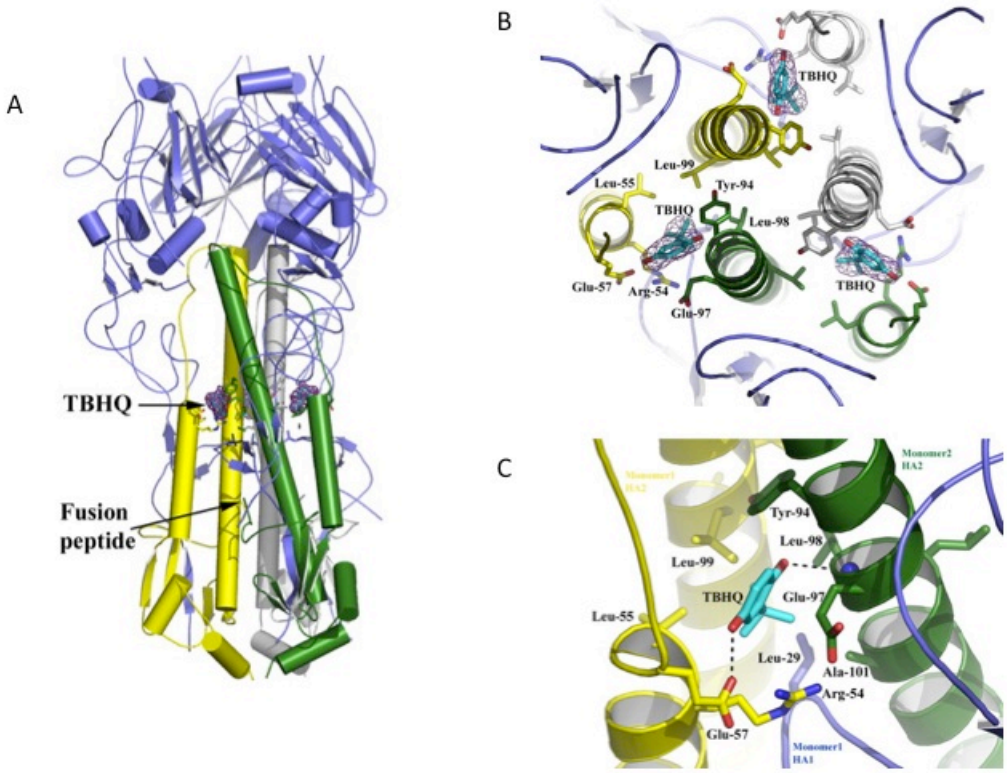

Figure 1.10 TBHQ binding to fusion peptide on H2 subunit of a group-2 HA (H14). (A) H14 HA trimer: 3 H1 subunits are colored in blue and 3 H2 subunits are colored in yellow, green or grey. The locations of TBHQ and fusion peptide are highlighted. (B) View down the 3-fold axis of H14 HA to show the 3 TBHQ binding sites. (C) Close-up view of a single TBHQ binding site. Selected residues are shown as sticks, and potential hydrogen bonds are shown as dotted lines. (Figure 1.10 is adapted from (86))

The strategy of inhibiting membrane fusion has been adopted to guide vaccine production. Seasonal flu vaccines are neutralizing antibodies that recognize epitopes on the surface of HA head region, which is highly variable. For this reason, the vaccines have to be changed every year based on prediction of circulating strains. Innovate antibodies that target at the highly conservative stem region instead of the globular cap have been discovered. (*12, 87, 88*)This type of antibodies can provide broad neutralization to different strains of influenza viruses and have higher tolerance to virus mutation because the change at the distal globular head has minimal impact on the stem region. The same concept was also used in designing proteins that bind to the stem region of HAs and inhibit conformational change. (*89*)

1.6.2 Ion channel M2 blocker

The M2 protein is a small integral membrane protein of 97 amino acid residues. The intracellular cytoplasmic domain has 54 residues at the C-terminal; 24 residues at the N-terminal comprise the extracellular domain and the rest of 19 residues are the transmembrane domain. (*90*) M2 proteins exist in the form of oligomers, minimally a tetramer. Disulfide bonds between subunits help retain the oligomer structure. (*91*) Although M2 protein is present in low abundance in the viral membrane, it plays important roles in influenza virus life cycle since low pH environment is essential for the conformational change of HA, which leads to viral-endosomal membrane fusion. On the other hand, the RNPs can only dissociate with matrix protein M1 at low pH and being released into the cytoplasm. Blockade of M2 ion channel results in accumulation of M1-associated RNPs in cytoplasm, which are unable to penetrate the nucleus. (*92, 93*)

M2 ion channel inhibitor amantadine and rimitadine are the first two FDA approved antiviral drugs for influenza infection and have demonstrated efficacy in clinical settings. Amantadine is believed to bind to the channel pore near Ser31 of the M2 protein, at which site mutations occur and results in resistance.(*94, 95*) Rimitadine is a derivative of amantadine and shows efficacy against some amantadine resistant strains, however, resistance to rimitadine has occurred in high incidence in recent years. Amantadine and rimitadine also show side effect on central nervous system, thus are not used wildly.

The most common mutation of amantadine binding site of M2 protein is S31N while V27A and L26F have also been observed. New drug designs based on amantadine structure target at these mutants. Structures of these compounds are shown below. Compound 5 shows inhibition to V27A and L26F mutants but not S31N mutant. (*96-99*) Actually, no effective inhibitor against the most common S31N mutant of M2 protein has been reported.

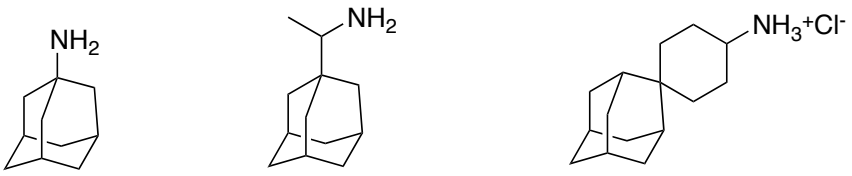

Amantadine **Rimantadine** **5**

Figure 1.11 Structures of M2 ion channel blockers

1.6.3 NA inhibitor

NA inhibitors represent the most successful effort of structure-based anti-influenza drug discovery. The inhibition mechanism is that the inhibitors block the active site of NA, thereby NA is unable to cleave off sialic acid from cell membrane glycoproteins and hinders progeny virions release. The two most commonly used antiviral drugs oseltamivir and zanamivir NA inhibitors. Other NA inhibitors are also being developed such as peramivir and laninamivir. The reason for success is that the deep binding pocket of NA is highly conservative and well defined. (Figure 1.6) In the active site of NA, substrate α-N-acetylneuraminic acid adopts a boat like conformation and in direct contact with eight highly conservative amino acid residues, forming hydrogen bond with these charged residues. (*100*)

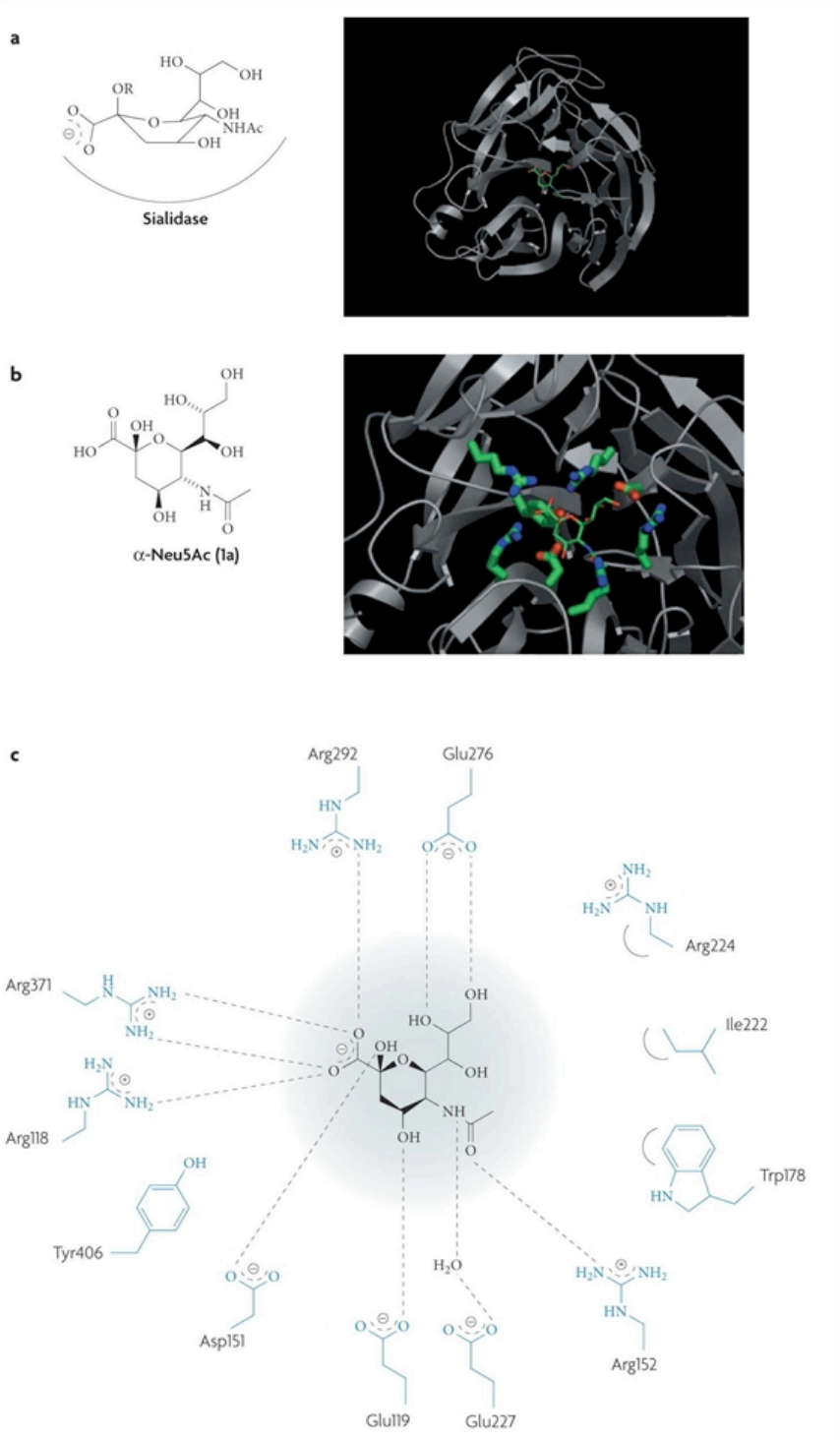

Figure 1.12 Interaction of a-N-acetylneuraminic acid(a-Neu5Ac) inside NA active site. (a) a-Neu5Ac bound in a boat-like conformation. (b) Zoom view of the NA active site.with a-Neu5Ac. (c) Eight invariant amino-acid residues make direct contact with a-Neu5Ac. (Figure 1.12 is adapted from Ref.(100))

The nine NA subtypes are phylogenetically divided into to groups: N1, N4, N5 and N8 belong to group 1; N2, N3, N6, N7 and N9 compose group 2. The grouping is highly relevant to the active site structure. Superposition of group-1 NAs N1, N4 and N8 reveals identical active site, however, a large cavity adjacent to the active site in group-1 NAs is absent in group-2 NAs (Figure 1.13) (*101*)

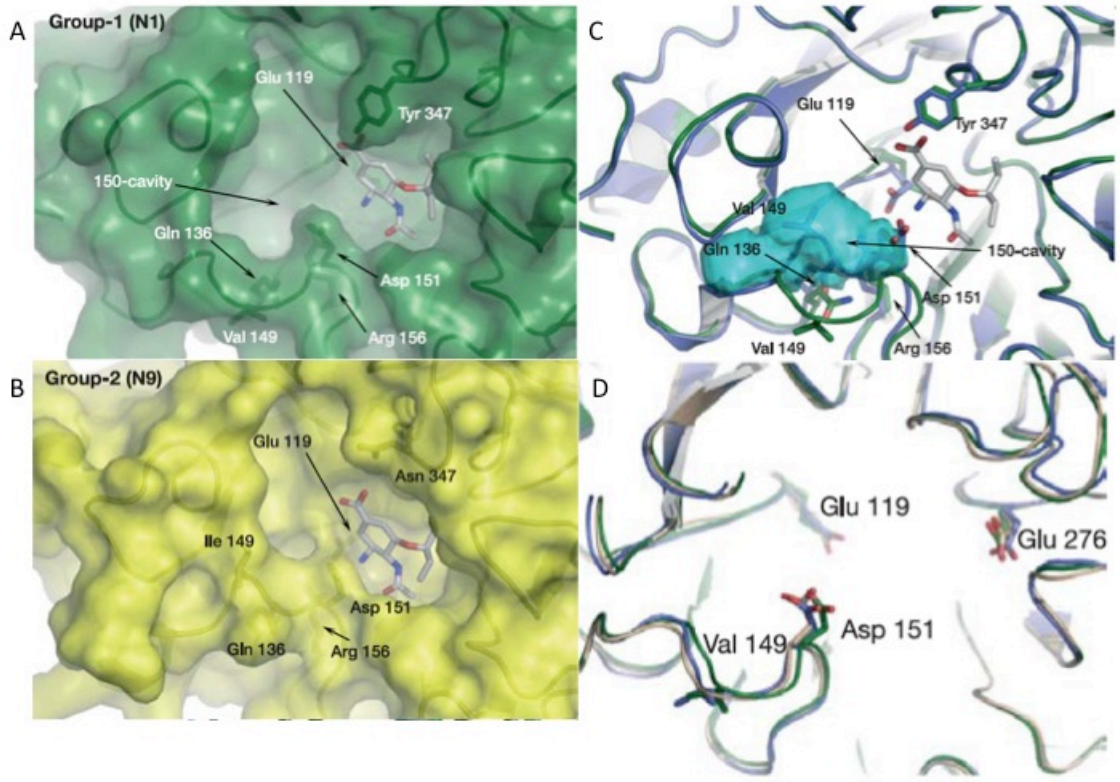

Figure 1.13 Active site structure comparisons of group-1 and group-2 NAs. (A) N1 active site with oseltamivir. (B) N9 active site with oseltamivir. (C) Superposition of the active sites of apo-N1 (green) and N1 complexed with oseltamivir (blue). (D) Superposition of the active site of N1 (green) and N9 (yellow). (Figure 1.13 is adapted from (101) with permission)

2-Deoxy-2,3 -didehydro-N-acetylneuraminic acid (DANA) was developed by Meidle *et al.* in 1974 as NA inhibitor. The double bond structure mimics the transition state of the sialosyl cation. Replacement of C4 hydroxyl group with positively charged amino group increases the inhibitory effect by 100 fold. The reason is that a negatively charged amino acid residue Glu119 at the binding pocket is aligned with the C4 position, and the amino group can form a salt bridge with Glu119 to further stabilize the

interaction with the active site. Following this lead, introduction of a highly positively charged guanidinyl group at the C4 position brings the inhibition IC_{50} to nanomolar range. The guanidinyl group of zanamivir shows interaction with both Glu227 and Glu119 of the NA active site. (*100, 102, 103*)Due to the high positive charge nature of zanamivir, oral administration is not suitable. Instead, it is administered as an inhaler. This is also the major drawback of zanamivir because inhalation may increase the risk of bronchospasms in patients with respiratory diseases. (*104*)Laninamivir is a pro-drug of zanamivir. With a methyl ether group, a prolonged duration of antiviral activity in animal models was observed as well as a prolonged presence in human. Laninamivir is also administrated through inhalation and shows similar antiviral spectrum as zanamivir.

Oseltamivir is a pro-drug with an ethyl ester group, which can be cleaved off in liver after ingestion by human carboxylesterase 1 and form the active compound oseltamivir carboxylate. Compare to DANA and its derivatives, oseltamivir is derived from non-carbohydrate template shikimic acid with a lipophilic pentane 3-oyl group instead of the glycerol group with C8 and C9 hydroxyl groups, which inside the NA catalytic site can induce a conformational change in Glu276 to interact with Arg244 through charge-charge interaction. The induced fit of oseltamivir carboxylate into active site is essential for the achievement of potent antiviral activity. A neighboring amino acid residue His274 helps in the conformational change. The induced fit model explains the drug resistance against oseltamivir when point mutation H274Y occurs.(*105-108*) (Figure 1.14) Different from zanamivir, oseltamivir is usually administrated orally thus used more commonly.

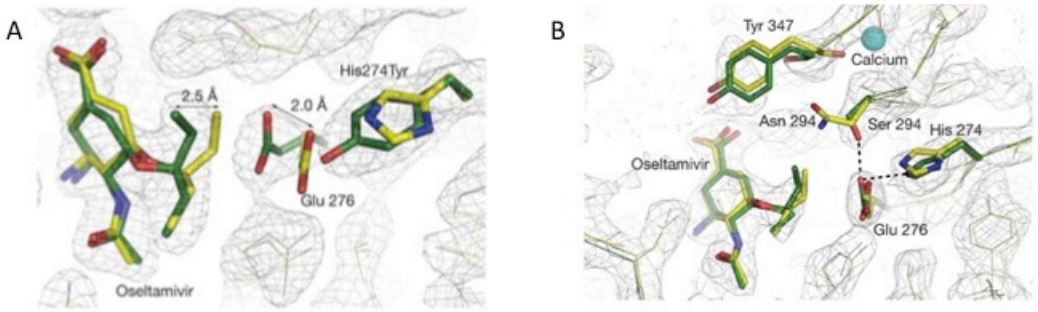

Figure 1.14 Structure of oseltamivir N1 neuraminidase complexes (A) His274Tyr in complex with oseltamivir. (B) Asn294Ser in complex with oseltamivir. (Figure 1.8 is adapted from (108)with permission).

As more and more resistance to oseltamivir has been reported, new NA inhibitors are in great need. Peramivir and its analogue A315675 retain inhibition activity against oseltamivir and zanamivir resistant strains of influenza A and B viruses. A prolonged half-life of peramivir from N9 was also observed (1 day vs 1.25 h of oseltamivir and zanamivir). (*109*)The design of peramivir follows similar concept as oseltamivir, which is replacing the carbohydrate core structure with quinic acid. At the same time, a lipophilic 3-pentyl side chain is also introduced. One feature of peramivir is that it's injectable, which might be beneficial for patients who cannot take drug orally or through inhalation.

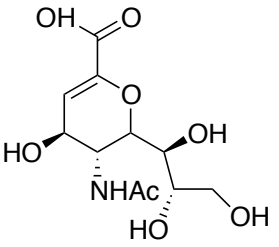

DANA

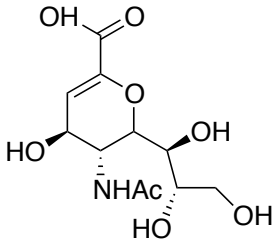

4-amino DANA

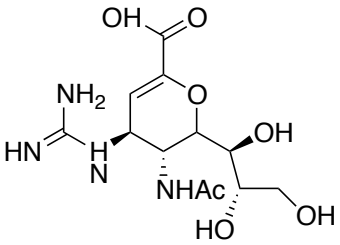

Zanamivir

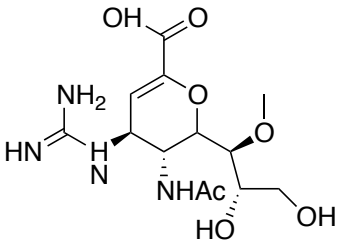

Laninamivir

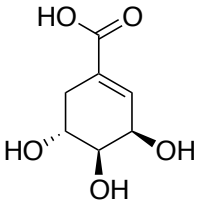

Shikimic acid

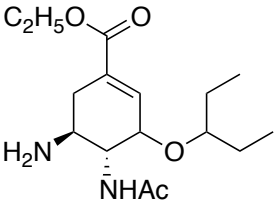

Oseltamivir

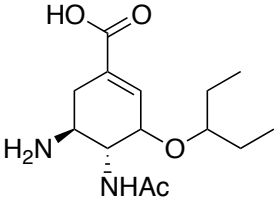

Oseltamivir carboxylate

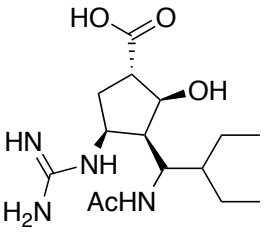

Peramivir

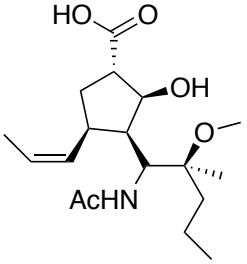

A315675

Figure 1.15 Influenza NA inhibitors

1.6.4 Viral polymerase inhibitor

Influenza RNA polymerase complex is a heterotrimer of PB1, PB2 and PA. Studies show that PB2 binds to host cell mRNA at the 5' end and PA functions as an endonuclease to cleave off 9-15 nucleotides down-stream to generate a primer for viral mRNA synthesis. (*110, 111*)Through docking models, Iwai et al identified a 33 macrocyclic bisbibenzyl compound marchantin E as an inhibitor of PA endonuclease activity and showed inhibition of influenza A virus growth. (*112*)

Several small molecules have been identified with anti endonuclease activity as well. Compound 6 is a lead compound identified by SAR study and its isomer compound 7 shows submilimolar IC_{50}. Another class of viral polymerase inhibitors is simple phosphate derivatives (compound 8-11). The proposed inhibition mechanism is that these compounds coordinate to zinc ion at the active site of the polymerase and sterically interfere with nucleotide phosphate binding or prevent the pyrophosphate release after chain extension. However, this class of compounds has no selectivity between viral DNA and RNA polymerase. (*113, 114*)

Guanosine analogues ribavirin and viramidine can inhibite inosine 5'-monophosphate dehydrogenase (IMPDH), which functions in the de novo synthesis of guanine nucleotides thus lower intracellular GTP. They also inhibit transcription and elongation by interfering with RNA dependent RNA polymerase. Inhibition of ribavirin to seasonal isolates of H1N1 and H3N2 viruses, influenza B viruses and pandemic H1N1 influenza A viruses has been shown in mouse model with early administration after infection. Viramidine is less potent, but better tolerated. Ribavirin also shows efficacy in preventing mortality in mice infected with lethal H5N1 virus. (*115*)

T-705, also called favipiravir, shows broad spectrum in inhibition of RNA viruses, including influenza A, B and C. T-705 is first converted to monophosphate T705RMP by phosphoribosyl transferase and subsequently to triphosphate T-705RTP by

nucleotide kinase in host cell. T-705RTP is the active form of inhibition, which can compete with GTP in RNA synthesis. Compare to ribavirin, T-705 has much lower inhibitory effect on cellular DNA and RNA synthesis as well as the IMPDH. It also shows merit in treating oseltamivir resistant H5N1 strains in mouse models.(*116*)

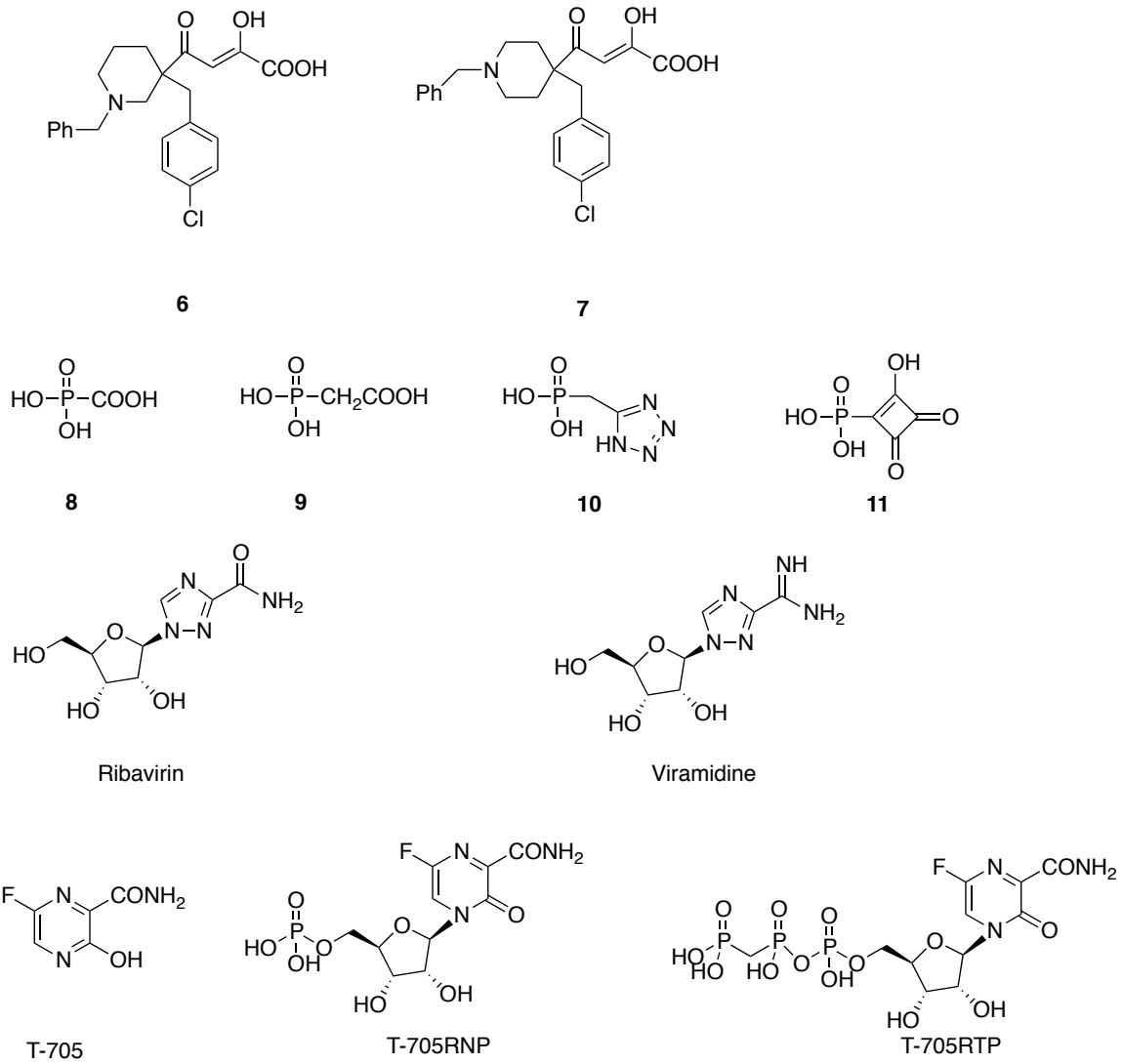

Figure 1.16 Viral polymerase inhibitors

1.6.5 Nucleoprotein (NP) inhibitor

NP is a key component of RNP, which encapsidates viral RNA segment and bind with polymerase heterotrimer. (*117*)Kao *et al*. discovered a compound nucleozin, which can induce NP aggregation and inhibit NP accumulation in nucleus, thereby inhibit RNP formation and viral replication. The NP tail-loop

binding pocket and RNA binding groove are potential drug targets.(*118*) Shen *et al*. identified compound as potent inhibitor of NP oligomerization and replication of influenza virus by binding to tail-loop of NP. Fedichev et al. identified compound M as a potential NP binder by docking model of this compound and RNA binding groove. (*119*)

1.6.6 Summary

To summarize, all these proteins are viable targets that could be exploited to inhibit the spread of the virus. Since the virus mutates by two mechanisms, it is very important that we pursue two methods of fighting the virus. Early detection and development of small molecules asdrug candidates. In this thesis, we have developed novel methods of capturing the virus and developed first generation potential drug candidates against the virus.

REFERENCE

1. World Health Organization. Influenza (seasonal) Fact Sheet, (Accessed Janurary 2, 2014, at http://www.who.int/mediacentre/factsheets/fs211/en/index.html)
2. Centers for Disease Control and Prevention. Seasonal Influenza (Flu), (Accessed Janurary 2, 2014, at http://www.who.int/mediacentre/factsheets/fs211/en/index.html)
3. World Health Organization. Influenza Fact Sheet, (Accessed Janurary 2, 2014, at http://www.who.int/mediacentre/factsheets/2003/fs211/en/)
4. N. M. Smith *et al.*, Prevention and Control of Influenza: recommendations of the Advisory Committee on Immunization Practices (ACIP). *MMWR Recomm Rep* **55**, 1 (2006).
5. K. Mitamura *et al.*, Clinical evaluation of highly sensitive silver amplification immunochromatography systems for rapid diagnosis of influenza. *J. Virol. Methods* **194**, 123 (2013).

6. Y. Amano, Q. Cheng, Detection of influenza virus: traditional approaches and development of biosensors. *Anal. Bioanal. Chem.* **381**, 156 (2005).

7. A. Linde, The importance of specific virus diagnosis and monitoring for antiviral treatment. *Antiviral Res.* **51**, 81 (2001).

8. A. S. Monto, S. Gravenstein, M. Elliott, M. Colopy, J. Schweinle, Clinical signs and symptoms predicting influenza infection. *Arch Intern Med* **160**, 3243 (2000).

9. A. J. Hay, F. G. Hayden, Oseltamivir resistance during treatment of H7N9 infection. *Lancet* **381**, 2230 (2013).

10. A. Moeller, R. N. Kirchdoerfer, C. S. Potter, B. Carragher, I. A. Wilson, Organization of the Influenza Virus Replication Machinery. *Science (Washington, DC, U. S.)* **338**, 1631 (2012).

11. T. Horimoto, Y. Kawaoka, Pandemic threat posed by avian influenza A viruses. *Clin. Microbiol. Rev.* **14**, 129 (2001).

12. D. C. Ekiert *et al.*, Antibody Recognition of a Highly Conserved Influenza Virus Epitope. *Science (Washington, DC, U. S.)* **324**, 246 (2009).

13. R. A. M. Fouchier *et al.*, Characterization of a novel influenza A virus hemagglutinin subtype (H16) obtained from black-headed gulls. *J. Virol.* **79**, 2814 (2005).

14. J. Treanor, Influenza vaccine--outmaneuvering antigenic shift and drift. *N Engl J Med* **350**, 218 (2004).

15. P. Palese, J. F. Young, Variation of influenza A, B, and C viruses. *Science (Washington, D. C., 1883-)* **215**, 1468 (1982).

16. D. A. Steinhauer, J. J. Holland, Rapid evolution of RNA viruses. *Annu. Rev. Microbiol.* **41**, 409 (1987).

17. J. D. Parvin, A. Moscona, W. T. Pan, J. M. Leider, P. Palese, Measurement of the mutation rates of animal viruses: influenza A virus and poliovirus type 1. *J. Virol.* **59**, 377 (1986).

18. N. M. Ferguson, A. P. Galvani, R. M. Bush, Ecological and immunological determinants of influenza evolution. *Nature (London, U. K.)* **422**, 428 (2003).

19. C. W. Potter, A history of influenza. *J Appl Microbiol* **91**, 572 (2001).

20. N. J. Cox, K. Subbarao, Global epidemiology of influenza: past and present. *Annu. Rev. Med.* **51**, 407 (2000).

21. R. Youil *et al.*, Comparative study of influenza virus replication in Vero and MDCK cell lines. *J. Virol. Methods* **120**, 23 (2004).

22. Wiley, *Influenza viruses disease modeling and laboratory methods*. (Wiley-Blackwell, Chichester, 2013).

23. M. Peiris, W. C. Yam, K. H. Chan, P. Ghose, K. F. Shortridge, Influenza A H9N2: aspects of laboratory diagnosis. *J Clin Microbiol* **37**, 3426 (1999).

24. W. D. Zhang, D. H. Evans, Detection and identification of human influenza viruses by the polymerase chain reaction. *J Virol Methods* **33**, 165 (1991).

25. P. R. Murray, *Manual of clinical microbiology*. (ASM Press, Washington, D.C., 1999).

26. R. L. Atmar, B. D. Baxter, E. A. Dominguez, L. H. Taber, Comparison of reverse transcription-PCR with tissue culture and other rapid diagnostic assays for detection of type A influenza virus. *J. Clin. Microbiol.* **34**, 2604 (1996).

27. J. S. Ellis, M. C. Zambon, Molecular diagnosis of influenza. *Rev. Med. Virol.* **12**, 375 (2002).

28. S. E. Dale, C. Mayer, M. C. Mayer, M. A. Menegus, Analytical and clinical sensitivity of the 3M rapid detection influenza A+B assay. *J Clin Microbiol* **46**, 3804 (2008).

29. A. Balish, R. Garten, A. Klimov, J. Villanueva, Analytical detection of influenza A(H3N2)v and other A variant viruses from the USA by rapid influenza diagnostic tests. *Influenza Other Respir. Viruses* **7**, 491 (2013).

30. Centers for Disease Control and Prevention. Rapid Diagnostic Testing for Influenza: Information for Clinical Laboratory Directors, (Accessed Janurary 2, 2014, at http://www.cdc.gov/flu/professionals/diagnosis/rapidlab.htm - table2)

31. C. R. Bertozzi, L. L. Kiessling, Chemical glycobiology. *Science (Washington, DC, U. S.)* **291**, 2357 (2001).

32. L. L. Kiessling, J. E. Gestwicki, L. E. Strong, Synthetic multivalent ligands in the exploration of cell-surface interactions. *Curr. Opin. Chem. Biol.* **4**, 696 (2000).

33. P.-H. Liang, S.-K. Wang, C.-H. Wong. (American Chemical Society, 2007), pp. GEN-149.

34. M. Schena, D. Shalon, R. W. Davis, P. O. Brown, Quantitative monitoring of gene expression patterns with a complementary DNA microarray. *Science (Washington, D. C.)* **270**, 467 (1995).

35. A. Lueking *et al.*, Protein Microarrays for Gene Expression and Antibody Screening. *Anal. Biochem.* **270**, 103 (1999).

36. D. J. Rogers, S. E. Randolph, The global spread of malaria in a future, warmer world. *Science (Washington, D. C.)* **289**, 1760 (2000).

37. P. W. Tang, H. C. Gooi, M. Hardy, Y. C. Lee, T. Feizi, Novel approach to the study of the antigenicities and receptor functions of carbohydrate chains of glycoproteins. *Biochem. Biophys. Res. Commun.* **132**, 474 (1985).

38. R. Liang *et al.*, Parallel synthesis and screening of a solid phase carbohydrate library. *Science (Washington, D. C.)* **274**, 1520 (1996).

39. R. Roy, Syntheses and some applications of chemically defined multivalent glycoconjugates. *Curr. Opin. Struct. Biol.* **6**, 692 (1996).

40. S. Park, M.-R. Lee, I. Shin, Carbohydrate microarrays as powerful tools in studies of carbohydrate-mediated biological processes. *Chem. Commun. (Cambridge, U. K.)*, 4389 (2008).

41. D. Wang, S. Liu, B. J. Trummer, C. Deng, A. Wang, Carbohydrate microarrays for the recognition of cross-reactive molecular markers of microbes and host cells. *Nat. Biotechnol.* **20**, 275 (2002).

42. W. G. T. Willats, S. E. Rasmussen, T. Kristensen, J. D. Mikkelsen, J. P. Knox, Sugar-coated microarrays: A novel slide surface for the high-throughput analysis of glycans. *Proteomics* **2**, 1666 (2002).

43. S. Fukui, T. Feizi, C. Galustian, A. M. Lawson, W. Chai, Oligosaccharide microarrays for high-throughput detection and specificity assignments of carbohydrate-protein interactions. *Nat. Biotechnol.* **20**, 1011 (2002).

44. M. C. Bryan *et al.*, Saccharide Display on Microtiter Plates. *Chem. Biol.* **9**, 713 (2002).

45. K.-S. Ko, F. A. Jaipuri, N. L. Pohl, Fluorous-Based Carbohydrate Microarrays. *J. Am. Chem. Soc.* **127**, 13162 (2005).

46. Y. Guo *et al.*, Structural basis for distinct ligand-binding and targeting properties of the receptors DC-SIGN and DC-SIGNR. *Nat. Struct. Mol. Biol.* **11**, 591 (2004).

47. B. S. Bochner *et al.*, Glycan array screening reveals a candidate ligand for Siglec-8. *J. Biol. Chem.* **280**, 4307 (2005).

48. J. Zhang *et al.*, Specific recognition of lectins by oligonucleotide glycoconjugates and sorting on a DNA microarray. *Chem. Commun. (Cambridge, U. K.)*, 6795 (2009).

49. B. T. Houseman, E. S. Gawalt, M. Mrksich, Maleimide-functionalized self-assembled monolayers for the preparation of peptide and carbohydrate biochips. *Langmuir* **19**, 1522 (2003).

50. M. Schwarz *et al.*, A new kind of carbohydrate array, its use for profiling antiglycan antibodies, and the discovery of a novel human cellulose-binding antibody. *Glycobiology* **13**, 749 (2003).

51. C.-C. Wang *et al.*, Glycans on influenza hemagglutinin affect receptor binding and immune response. *Proc. Natl. Acad. Sci. U. S. A.* **106**, 18137 (2009).

52. O. Blixt *et al.*, Printed covalent glycan array for ligand profiling of diverse glycan binding proteins. *Proc. Natl. Acad. Sci. U. S. A.* **101**, 17033 (2004).

53. X. Song, Y. Lasanajak, B. Xia, D. F. Smith, R. D. Cummings, Fluorescent Glycosylamides Produced by Microscale Derivatization of Free Glycans for Natural Glycan Microarrays. *ACS Chem. Biol.* **4**, 741 (2009).

54. F. Fazio, M. C. Bryan, O. Blixt, J. C. Paulson, C.-H. Wong, Synthesis of Sugar Arrays in Microtiter Plate. *J. Am. Chem. Soc.* **124**, 14397 (2002).

55. X. Song *et al.*, Novel Fluorescent Glycan Microarray Strategy Reveals Ligands for Galectins. *Chem. Biol. (Cambridge, MA, U. S.)* **16**, 36 (2009).

56. B. Xia *et al.*, Versatile fluorescent derivatization of glycans for glycomic analysis. *Nat. Methods* **2**, 845 (2005).

57. M.-r. Lee, I. Shin, Facile Preparation of Carbohydrate Microarrays by Site-Specific, Covalent Immobilization of Unmodified Carbohydrates on Hydrazide-Coated Glass Slides. *Org. Lett.* **7**, 4269 (2005).

58. Y. Liu *et al.*, Neoglycolipid Probes Prepared via Oxime Ligation for Micro-array Analysis of Oligosaccharide-Protein Interactions. *Chem. Biol. (Cambridge, MA, U. S.)* **14**, 847 (2007).

59. O. Bohorov, H. Andersson-Sand, J. Hoffmann, O. Blixt, Arraying glycomics: a novel bi-functional spacer for one-step microscale derivatization of free reducing glycans. *Glycobiology* **16**, 21C (2006).

60. T. Schallus *et al.*, Malectin: a novel carbohydrate-binding protein of the endoplasmic reticulum and a candidate player in the early steps of protein N-glycosylation. *Mol. Biol. Cell* **19**, 3404 (2008).

61. S. Diskin, Z. Cao, H. Leffler, N. Panjwani, The role of integrin glycosylation in galectin-8-mediated trabecular meshwork cell adhesion and spreading. *Glycobiology* **19**, 29 (2009).

62. A. Krarup, D. A. Mitchell, R. B. Sim, Recognition of acetylated oligosaccharides by human L-ficolin. *Immunol. Lett.* **118**, 152 (2008).

63. M. L. Zupancic *et al.*, Glycan microarray analysis of Candida glabrata adhesin ligand specificity. *Mol. Microbiol.* **68**, 547 (2008).

64. P. J. L. de, C. Noti, P. H. Seeberger, Microarrays of Synthetic Heparin Oligosaccharides. *J. Am. Chem. Soc.* **128**, 2766 (2006).

65. S. E. Tully, M. Rawat, L. C. Hsieh-Wilson, Discovery of a TNF-α Antagonist Using Chondroitin Sulfate Microarrays. *J. Am. Chem. Soc.* **128**, 7740 (2006).

66. C. I. Gama *et al.*, Sulfation patterns of glycosaminoglycans encode molecular recognition and activity. *Nat. Chem. Biol.* **2**, 467 (2006).

67. L. Nimrichter *et al.*, Intact cell adhesion to glycan microarrays. *Glycobiology* **14**, 197 (2004).

68. M. D. Disney, P. H. Seeberger, The Use of Carbohydrate Microarrays to Study Carbohydrate-Cell Interactions and to Detect Pathogens. *Chem. Biol.* **11**, 1701 (2004).

69. A. Walz, S. Odenbreit, J. Mahdavi, T. Boren, S. Ruhl, Identification and characterization of binding properties of Helicobacter pylori by glycoconjugate arrays. *Glycobiology* **15**, 700 (2005).

70. P.-H. Liang, C.-Y. Wu, W. A. Greenberg, C.-H. Wong, Glycan arrays: biological and medical applications. *Curr. Opin. Chem. Biol.* **12**, 86 (2008).

71. D. A. Calarese *et al.*, Dissection of the carbohydrate specificity of the broadly neutralizing anti-HIV-1 antibody 2G12. *Proc. Natl. Acad. Sci. U. S. A.* **102**, 13372 (2005).

72. D. M. Ratner, P. H. Seeberger, Carbohydrate microarrays as tools in HIV glycobiology. *Curr. Pharm. Des.* **13**, 173 (2007).

73. F. Kamena *et al.*, Synthetic GPI array to study antitoxic malaria response. *Nat. Chem. Biol.* **4**, 238 (2008).

74. C.-Y. Huang *et al.*, Carbohydrate microarray for profiling the antibodies interacting with Globo H tumor antigen. *Proc. Natl. Acad. Sci. U. S. A.* **103**, 15 (2006).

75. C. H. Lawrie *et al.*, Cancer-associated carbohydrate identification in Hodgkin's lymphoma by carbohydrate array profiling. *Int. J. Cancer* **118**, 3161 (2006).

76. J. Stevens *et al.*, Structure and receptor specificity of the hemagglutinin from an H5N1 influenza virus. *Science (Washington, DC, U. S.)* **312**, 404 (2006).

77. R. Xu, R. McBride, C. M. Nycholat, J. C. Paulson, I. A. Wilson, Structural characterization of the hemagglutinin receptor specificity from the 2009 H1N1 influenza pandemic. *J. Virol.* **86**, 982 (2012).

78. N. K. Sauter *et al.*, Hemagglutinins from two influenza virus variants bind to sialic acid derivatives with millimolar dissociation constants: a 500-MHz proton nuclear magnetic resonance study. *Biochemistry* **28**, 8388 (1989).

79. J. Stevens *et al.*, Glycan Microarray Analysis of the Hemagglutinins from Modern and Pandemic Influenza Viruses Reveals Different Receptor Specificities. *J. Mol. Biol.* **355**, 1143 (2006).

80. H.-Y. Liao *et al.*, Differential Receptor Binding Affinities of Influenza Hemagglutinins on Glycan Arrays. *J. Am. Chem. Soc.* **132**, 14849 (2010).

81. Centers for Disease Control and Prevention. Recommendations of the Advisory Committee on Immunization Practices (ACIP): Information for Health Care Professionals, (Accessed Janurary 2, 2014, at http://www.cdc.gov/flu/professionals/antivirals/index.htm)

82. Q.-S. Du, H. Wei, R.-B. Huang, K.-C. Chou, Progress in structure-based drug design against influenza A virus. *Expert Opin. Drug Discovery* **6**, 619 (2011).

83. J. Du, T. A. Cross, H.-X. Zhou, Recent progress in structure-based anti-influenza drug design. *Drug Discovery Today* **17**, 1111 (2012).

84. P. L. Toogood, P. K. Galliker, G. D. Glick, J. R. Knowles, Monovalent sialosides that bind tightly to influenza A virus. *J. Med. Chem.* **34**, 3138 (1991).

85. G. D. Glick, P. L. Toogood, D. C. Wiley, J. J. Skehel, J. R. Knowles, Ligand recognition by influenza virus. The binding of bivalent sialosides. *J. Biol. Chem.* **266**, 23660 (1991).

86. R. J. Russell *et al.*, Structure of influenza hemagglutinin in complex with an inhibitor of membrane fusion. *Proc. Natl. Acad. Sci. U. S. A.* **105**, 17736 (2008).

87. J. Sui *et al.*, Structural and functional bases for broad-spectrum neutralization of avian and human influenza A viruses. *Nat. Struct. Mol. Biol.* **16**, 265 (2009).

88. D. Corti *et al.*, A Neutralizing Antibody Selected from Plasma Cells That Binds to Group 1 and Group 2 Influenza A Hemagglutinins. *Science (Washington, DC, U. S.)* **333**, 850 (2011).

89. S. J. Fleishman *et al.*, Computational Design of Proteins Targeting the Conserved Stem Region of Influenza Hemagglutinin. *Science (Washington, DC, U. S.)* **332**, 816 (2011).

90. L. H. Pinto, L. J. Holsinger, R. A. Lamb, Influenza virus M2 protein has ion channel activity. *Cell (Cambridge, Mass.)* **69**, 517 (1992).

91. M. Sharma *et al.*, Insight into the Mechanism of the Influenza A Proton Channel from a Structure in a Lipid Bilayer. *Science (Washington, DC, U. S.)* **330**, 509 (2010).

92. A. L. Stouffer *et al.*, Structural basis for the function and inhibition of an influenza virus proton channel. *Nature (London, U. K.)* **451**, 596 (2008).

93. T. A. Cross, H. Dong, M. Sharma, D. D. Busath, H.-X. Zhou, M2 protein from Influenza A: from multiple structures to biophysical and functional insights. *Curr. Opin. Virol.* **2**, 128 (2012).

94. J. Hu *et al.*, Backbone structure of the amantadine-blocked trans-membrane domain M2 proton channel from influenza A virus. *Biophys. J.* **92**, 4335 (2007).

95. M. Yi, T. A. Cross, H.-X. Zhou, A Secondary Gate As a Mechanism for Inhibition of the M2 Proton Channel by Amantadine. *J. Phys. Chem. B* **112**, 7977 (2008).

96. W. Hu *et al.*, Identification of Hits as Matrix-2 Protein Inhibitors through the Focused Screening of a Small Primary Amine Library. *J. Med. Chem.* **53**, 3831 (2010).

97. X. Zhao, C. Li, S. Zeng, W. Hu, Discovery of highly potent agents against influenza A virus. *Eur. J. Med. Chem.* **46**, 52 (2010).

98. J. Wang *et al.*, Exploring the Requirements for the Hydrophobic Scaffold and Polar Amine in Inhibitors of M2 from Influenza A Virus. *ACS Med. Chem. Lett.* **2**, 307 (2011).

99. M. D. Duque *et al.*, Exploring the Size Limit of Templates for Inhibitors of the M2 Ion Channel of Influenza A Virus. *J. Med. Chem.* **54**, 2646 (2011).

100. M. von Itzstein, The war against influenza: discovery and development of sialidase inhibitors. *Nat Rev Drug Discov* **6**, 967 (2007).

101. R. J. Russell *et al.*, The structure of H5N1 avian influenza neuraminidase suggests new opportunities for drug design. *Nature (London, U. K.)* **443**, 45 (2006).

102. N. R. Taylor, I. M. von, Molecular Modeling Studies on Ligand Binding to Sialidase from Influenza Virus and the Mechanism of Catalysis. *J. Med. Chem.* **37**, 616 (1994).

103. I. M. von *et al.*, A Study of the Active Site of Influenza Virus Sialidase: An Approach to the Rational Design of Novel Anti-influenza Drugs. *J. Med. Chem.* **39**, 388 (1996).

104. F. G. Hayden, Perspectives on antiviral use during pandemic influenza. *Philos Trans R Soc Lond B Biol Sci* **356**, 1877 (2001).

105. V. P. Mishin, F. G. Hayden, L. V. Gubareva, Susceptibilities of antiviral-resistant influenza viruses to novel neuraminidase inhibitors. *Antimicrob. Agents Chemother.* **49**, 4515 (2005).

106. J. W. Park, W. H. Jo, Infiltration of Water Molecules into the Oseltamivir-Binding Site of H274Y Neuraminidase Mutant Causes Resistance to Oseltamivir. *J. Chem. Inf. Model.* **49**, 2735 (2009).

107. Q. Li *et al.*, Functional and structural analysis of influenza virus neuraminidase N3 offers further insight into the mechanisms of oseltamivir resistance. *J Virol* **87**, 10016 (2013).

108. P. J. Collins *et al.*, Crystal structures of oseltamivir-resistant influenza virus neuraminidase mutants. *Nature (London, U. K.)* **453**, 1258 (2008).

109. W. M. Kati *et al.*, In vitro characterization of A-315675, a highly potent inhibitor of A and B strain influenza virus neuraminidases and influenza virus replication. *Antimicrob. Agents Chemother.* **46**, 1014 (2002).

110. R. M. Krug, B. A. Broni, M. Bouloy, Are the 5' ends of influenza viral mRNAs synthesized in vivo donated by host mRNAs? *Cell (Cambridge, Mass.)* **18**, 329 (1979).

111. C. Zhao *et al.*, Nucleoside monophosphate complex structures of the endonuclease domain from the influenza virus polymerase PA subunit reveal the substrate binding site inside the catalytic center. *J. Virol.* **83**, 9024 (2009).

112. Y. Iwai *et al.*, Anti-influenza activity of marchantins, macrocyclic bisbibenzyls contained in liverworts. *PLoS One* **6**, e19825 (2011).

113. P. A. Cload, D. W. Hutchinson, The inhibition of the RNA polymerase activity of influenza virus A by pyrophosphate analogs. *Nucleic Acids Res.* **11**, 5621 (1983).

114. D. W. Hutchinson, M. Naylor, P. M. Cullis, Thio-analog of inorganic pyrophosphate inhibit the replication of influenza virus A in vitro. *Antiviral Res.* **5**, 67 (1985).

115. B. B. Goswami, E. Borek, O. K. Sharma, J. Fujitaki, R. A. Smith, The broad spectrum antiviral agent ribavirin inhibits capping of mRNA. *Biochem. Biophys. Res. Commun.* **89**, 830 (1979).

116. M. Kiso *et al.*, T-705 (favipiravir) activity against lethal H5N1 influenza A viruses. *Proc. Natl. Acad. Sci. U. S. A.* **107**, 882 (2010).

117. A. Portela, P. Digard, The influenza virus nucleoprotein: a multifunctional RNA-binding protein pivotal to virus replication. *J. Gen. Virol.* **83**, 723 (2002).

118. R. Y. Kao *et al.*, Identification of influenza A nucleoprotein as an antiviral target. *Nat. Biotechnol.* **28**, 600 (2010).

119. Y.-F. Shen *et al.*, E339...R416 salt bridge of nucleoprotein as a feasible target for influenza virus inhibitors. *Proc. Natl. Acad. Sci. U. S. A.* **108**, 16515 (2011).

2 NEURAMINIDASE RESISTANT SIALOSIDE MICROARRAY FOR THE DETECTION OF INFLUENZA VIRUSES

ABSTRACT

Glycan microarrays comprise of O-linked sialosides have become important tools for studying influenza virus binding profile. However, NA inhibitors or low temperature is required in performing the binding assays since the viral NA can hydrolyze O-linked terminal sialic acid. In this chapter, we describe the synthesis of NA resistant sialosides that include different glycosidic linkages (C-, S- and N-). We compare the stability of these sialosides with O-linked sialosides and demonstrate the ability of these molecules to capture influenza virus at ambient temperature without the addition of NA inhibitors. Every strain of influenza virus shows unique binding pattern on the microarray.

ABBREVIATION

Acetate, Ac; Acetic anhydride, Ac_2O; Acetonitrile, CH_3CN; Benzaldehyde dimethyl acetal, BDA or $PhCH(OMe)_2$; Benzyl bromide, BnBr; Camphorsulfonic acid, CSA; Carbon-13 nuclear magnetic resonance, 13C-NMR; Copper (I) Iodine, CuI; Deuterated chloroform, $CDCl_3$; Deuterated water, D_2O; Dichloromethane, DCM or CH_2Cl_2; Diethyl ether, Et_2O; N,N-dimethyl formamide, DMF; Ethanol, EtOH; Ethyl acetate, EtOAc; High resolution mass spectroscopy, HRMS; Hydrogen gas, H_2; Hydrazine acetate, NH_2NH_2.HOAc; Hydrochloric acid, HCl; Sodium sulfate, Na_2SO_4; Methanol, MeOH or CH_3OH; Palladium hydroxide on carbon, $Pd(OH)_2/C$; Proton nuclear magnetic resonance, 1H-NMR; Pyridine, py; Room temperature, RT; Sodium azide, NaN_3; Sodium bicarbonate, $NaHCO_3$; Sodium hydride, NaH; Sodium methox-

ide, NaOMe; Tetrahydrofuran, THF; Thin layer chromatography, TLC; Trifluoromethanesulfonic anhydride, Tf_2O; Trimethylsilyl p-Toluenesulfonic acid, p-TSA; Water, H_2O.

2.1 Introduction

Influenza virus is an acute respiratory pathogen that causes considerable harm to humans and livestock.(*1*) In addition to seasonal influenza that accounts for approximately 200,000 hospitalizations and 36,000 deaths per year in the United States alone, catastrophic pandemics such as the 1918 Spanish flu (H1N1) can be devastating.(*2*) Early detection is critical in our fight against this deadly virus because most antivirals lose their efficacy if it is not administered within 24-48 hours after onset of infection(*2*) and because influenza spreads very rapidly. For example, the 2009 H1N1 influenza virus spread rapidly across the globe within ten days, resulting in extraordinary measures(*3, 4*) and overwhelming public health care facilities.(*5*) Most public hospitals requested sick patients to stop coming to the emergency room during that time. PCR based technologies, although highly accurate and definitive, are cost prohibitive for use in a primary care setting. Antibody based tests are point-of-care with a test to result time of less than 30 minutes, but are generally used for surveillance because they suffer from a variety of issues that include sensitivity, antibody degradation at ambient temperature and cross reactivity.(*6, 7*) Procurement of antibodies for emerging strains is also a problem during an emergency. Finally, while antibody tests are less expensive than PCR, they are expensive (~ 50$) and prohibitive for use in a resource poor setting and are generally only used for surveillance purposes.

Since the virus binds to the terminal residues of N-acetyl neuraminic acid (or sialic acid) of glycoproteins and glycolipids to gain entry into the cell, an alternate receptor based approach based on synthetic glycans could potentially be used to identify and type the virus.(*1, 8, 9*) From a diagnostic perspective, synthetic small molecule analogs based on receptors (in this case, glycans) present a novel, but largely unexplored, opportunity as recognition molecules. Glycans can be synthesized in appreciable

yields economically, are highly robust under a variety of conditions and do not require refrigeration.(*10-12*) An added advantage is that glycans are small molecules and this provides them with an unique advantage over larger recognition elements such as antibodies or aptamers. Glycans could find use in for potential applications in nanobiosensors, where nanoparticle-glycan conjugates do not perturb the overall size of the nanoparticle.(*13*) Lastly, since a plethora of glycans can be synthesized with new advances in synthetic methodologies, a 'fingerprint' pattern of recognition can be obtained for every virus type that binds to a glycan microarray.(*14-16*) Indeed, multiple groups have used this approach to capture hemagluttinin, a surface glycoprotein, and the virus using microarrays of *O*-sialosides, synthesized from enzymatic and synthetic methods.(*17, 18*)

This approach has advanced our understanding of some of the fundamental aspects of virus-receptor interactions; glycan microarrays constructed using *O*-sialosides have been used (in conjunction with other methods) to explain why certain virus types prefer 2,3 linkages, in contrast to other viruses which seem to prefer 2,6 linkages.(*17-20*)However, this approach is limited in scope for point of care influenza diagnostics, because neuraminidase (NA) an influenza surface glycoprotein, cleaves *O*-glycoside linkages rapidly.(*21*) Indeed, most publications report performing the assays with influenza viruses at low temperatures (4 ^{0}C) and/or use NA inhibitors to avoid issues with NA cleaving the natural *O*-sialosides.(*22-24*) To overcome these issues towards our ultimate goal of using glycans as a practical approach to capture influenza viruses, we synthesized NA insensitive glycans with S-, N- or C-link, (Figure 2.1) which can be used to capture viral particles at ambient temperature and without NA inhibitors.

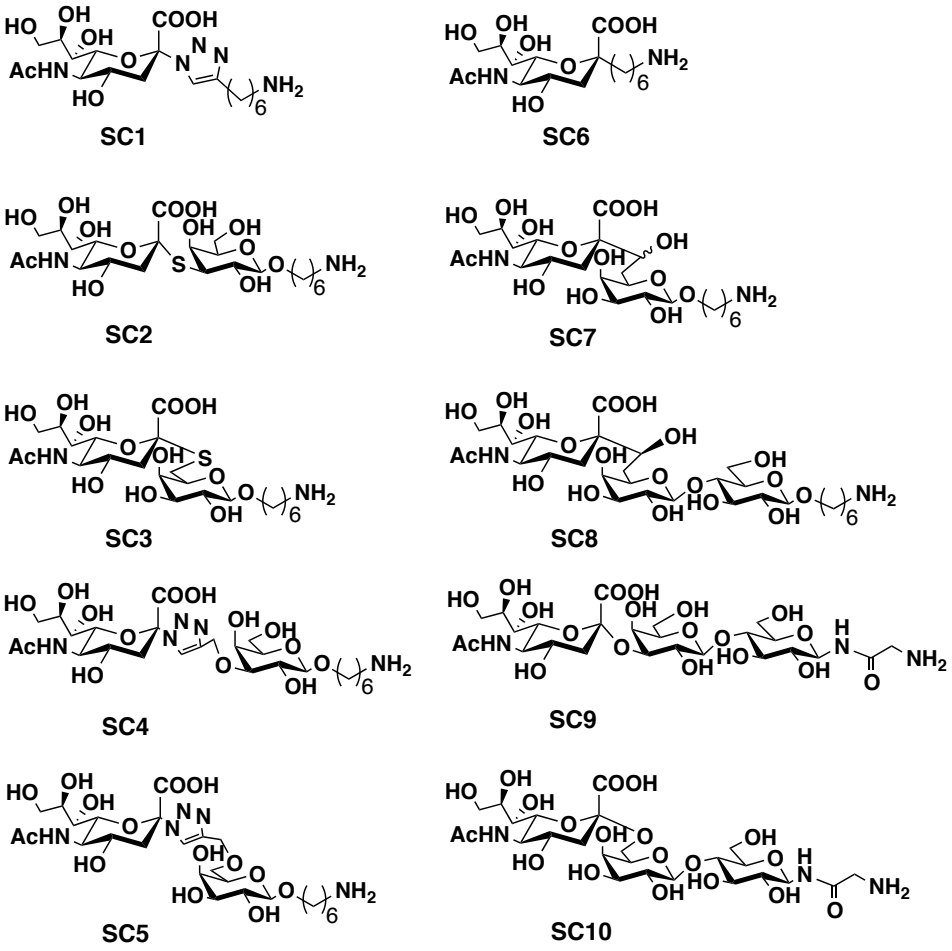

Figure 2.1 Structures of ten sialosides used to construct glycan microarray

2.1.1 Stability of thiosialoside

Thioglycosides generally exhibit enhanced stability toward enzyme-mediated hydrolysis compared to their oxygen-based counterparts. Meanwhile, they maintain the biochemical activities of the parent oligosaccharides. (*25, 26*)For instance, Suzuki et al. has shown that thioglycosidic analogues of gangliosides are not hydrolyzed by influenza NA.(*27*) Von Itzstein group reported a detailed study investigating the stability of thiosialosides towards sialidase hydrolysis by NMR spectroscopy. In this study, they compared the stability of O- and S-sialosides with α-2, 3 or α-2, 6 linkage to galactoside toward *Vibrio cholerae* sialidase. They found that O-sialosides were mostly hydrolyzed in 2h while S-sialosides

were still intact after 14 days. (*28*) Possible explanation for the stability of S-sialosides toward sialidase is that the slightly longer C-S bond causes minor alteration of glycoside conformation, making the structure less suitable for sialidase recognition. The reduced Lewis basicity of sulfur might also contribute to the stability of S-sialosides.(*29, 30*)

2.1.2 Synthesis of thiosialoside

The formation of S-glycosidic bond is usually through nucleophilic substitution reaction. Two general approaches can be adopted for the synthesis of thiosialosides, which are (a) installation of thioacetyl group at the anomeric carbon of sialic acid followed by selective deacetylation of the anomeric thioacetate and subsequent reaction with sialosyl acceptor bearing a good leaving group and (b) incorporation of the sulfur into the sialosyl acceptor and then coupling with the 2-chloro Neu5Ac derivative. (Scheme 1) The first approach has been widely used in the synthesis of α-S-2, 6-sialosides while both of the two approaches have been reported for the synthesis of α-S-2, 3-sialosides. In comparison, the reported overall yield in synthesizing the α-S-2, 3-sialosides following the second approach is higher. Therefore, we chose this method to synthesize our target molecule **SC2**.

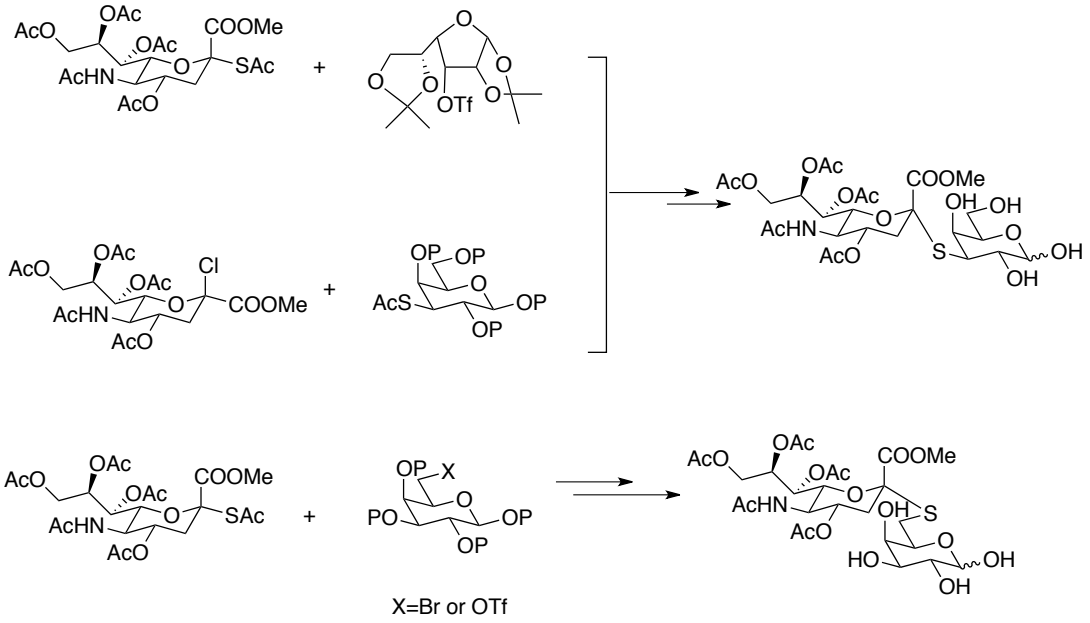

Scheme 2.1 Two approaches toward the synthesis of thiosialosides

2.2 Results and discussion

2.2.1 Synthesis of S- and N-linked sialosides

To probe and differentiate different strains of influenza viruses, I have synthesized S- and N-linked sialosides(**SC1-5**). The synthesis of **SC1** is shown in scheme 2. The β-2-Chloro-N-acetylneuraminic acid 2 was synthesized from an α, β mixture 1 by bubbling hydrochloric acid gas through. Formation of α-2-chloro-N-acetylneuraminic acid was not observed. 2 was not stable at room temperature therefore was used within a shore time frame to synthesize 3 or 4, which possesses thioacetyl or azido group respectively at the anomeric position. The glycosylation reaction was catalyzed by a phase transfer catalyst tetrabutylammonium hydrogen sulfate (TBAHS) under mild basic condition. TBAHS was chosen over other halide phase transfer catalyst such as tetrabutylammonium bromide to avoid the possibility of double halide displacement. In addition, in the presence of chloride, bromide, or iodide anions, scrambling of anomeric configuration could be observed. (*31*) As expected, compound 3 and 4 were obtained in pure α configuration through complete anomeric conversion of 2, which indicated SN2 mechanism. Another aspect that worth mentioning in this reaction is the choice of solvent. Ethyl acetate is a better solvant than dichloromethane, which has been broadly used in phase transfer catalyzed reactions, because a large proportions of the thiols reacted with dichloromethane to give products such as bis (4-nitrophenylthio)methane and lower the yield. (*32*) The 2-azido compound 4 was coupled with 8-chloro-1-octyne through Cu(I) catalyzed “Click” reaction to form N-linked compound 5 with almost quantitative yield. CuI was slightly soluble in acetonitrile and could be easily removed through filtration after the reaction was complete. The chloride on the 6-carbon linker was converted to azide (compound 6) then amine through palladium(II) catalyzed hydrogenation reaction.

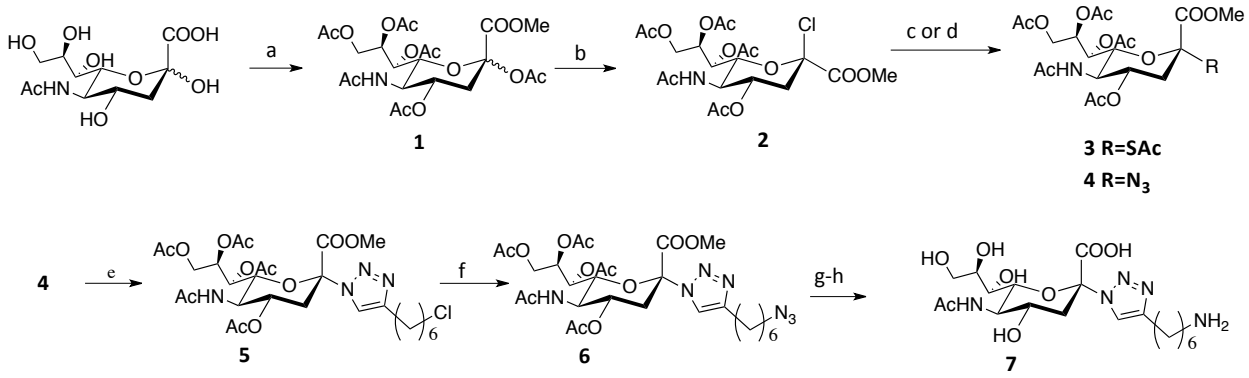

Scheme 2.2 Synthesis of **SC1** (**7**) (a) (i) H+ resin, MeOH, rt, 48h, (ii) Ac2O, DMAP, pyridine, rt, overnight, 82%; (b) HCl(g), DCM, rt, 8h, 100%; (c) KSAc, TBAHS, NaHCO3/EtOAc(1:1), rt, 10h, 75%; (d) NaN_3, TBAHS, $NaHCO_3$/EtOAc(1:1), rt, 10h, 83%; (e) 8-chloro-1-octyne, CuI, diisopropylethylamine, 50oC, MeCN, 6h, 98%; (f) NaN3, DMF, 60^{o}C, overnight, 82%; (g)(i) 0.5M NaOMe, MeOH, rt, 7h, (ii) 0.25M NaOH(aq), 8h; (h) H2, palladium hydroxide on carbon, EtOH, 24h, 52%.

The synthesis of **SC2** was shown in scheme 2.3. Our approach was to install the thiol group at the 3 position on the galactose acceptor and react it with β-chloro-N-acetylneuraminic acid **2** via a SN2 type reaction to obtain the desired disaccharide as the alternate strategy of introducing the thiol group on the N-acetylneuraminic acid and displacing a good leaving group on the galactoside acceptor leads to side reactions, especially if the leaving group is on a secondary carbon.(*33, 34*) The galactoside acceptor **14** was converted from guloside **13,** which was synthesized from the known β-galatoside derivative **8** (*35*) through a number of protection/deprotection steps. **8** was selectively protected with 4-methylbenzyl (PMB) through a two step reaction. The cis 3- and 4-OH were first temporarily protected with dibutyltin oxide. The formation of the Sn-O bonds enhanced the nucleophilicity of the oxygen atom. The oxygen atom at the equatorial position was more nucleophilic and exclusively reacted with 4-methylbenzylchloride, which was added stoichiometrically (1.2 eq). Next, the 4,6 and the 2 hydroxyl groups were protected in a one pot reaction using benzaldehyde dimethyl acetal and benzoyl chloride respectively to yield **10** in appreciable yield. Conversion of the chloride to the azide was achieved using sodium azide in a near quantitative yield. Selective removal of the PMB group through oxidative cleavage by ceric ammonium nitrate (CAN) was followed by inversion of the 3 hydroxyl group from the equa-

torial to the axial position. Treating compound **12** first with triflic anhydride to active the hydroxyl group and then inverting it using tetrabutyl ammonium nitrite at a slightly elevated temperature yielded guloside derivative **13**. We found that this reaction is not straightforward, specifically, the tetrabutylammonium nitrate has to be completely oxygen and moisture free, else the compound reverts to the galactoside derivative **12**. Activation of the axial hydroxyl using triflic anhydride, followed by SN2 type substitution by potassium thioacetate resulted in the desired installation of the thiol group on the 3 position of the galactoside derivative **14**. Selective removal of the acetate in **14** using hydrazinium acetate was followed by reaction with the N-acetylneuraminic acid chloride derivative **2** in the presence of a commercial cryptand to yield the 2,3 S-linked derivative **15**, in reasonable yield. The product was confirmed by NMR and mass spectroscopic analysis; the hydrogen and the carbon at the 3 position of galactose resonated at 4.60 and 101.0 ppm, respectively, and the anomeric carbon of sialic acid resonated at 96.6 ppm. After removal of the benzylidene group, deprotection of the acetate, benzoyl and ester functional groups in **15** under basic conditions, followed by hydrogenation of the azide yielded the desired 2,3 *S*-sialoside glycoconjugate **SC2** with a pendant amine for conjugation to activated carboxyl acid surfaces. The rest of the glycoconjugates were synthesized in a similar manner.

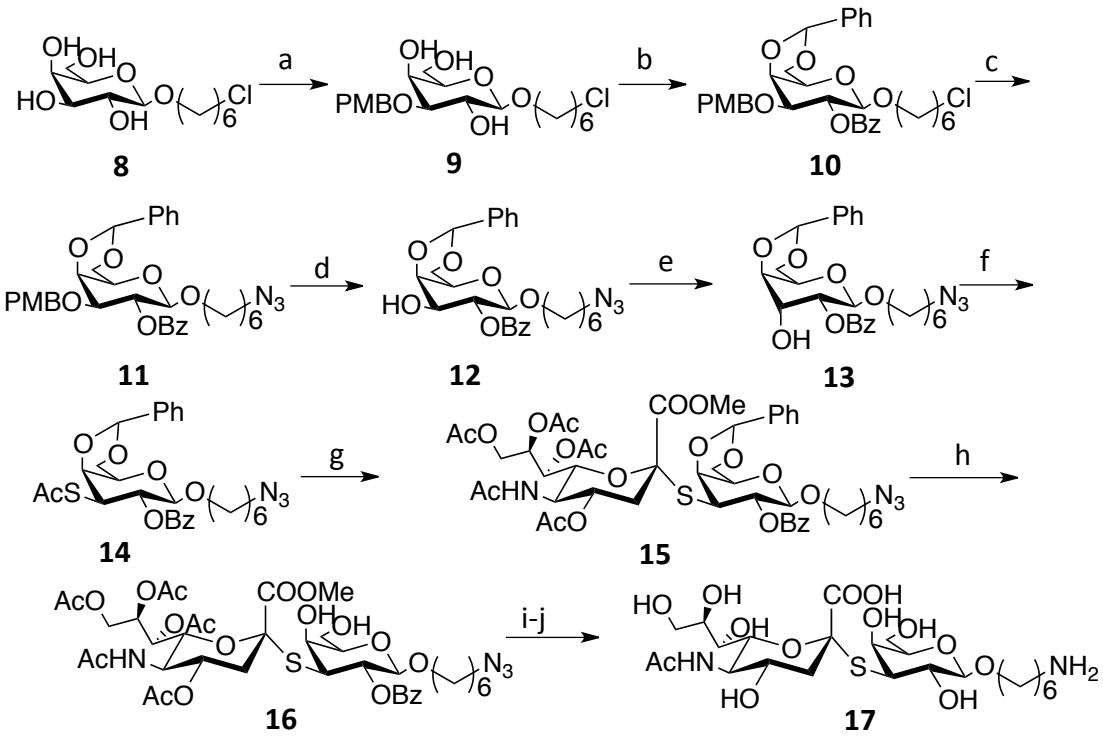

Scheme 2.3 Synthesis of **Sc2** (**17**) (a) (i) Bu_2SnO, MeOH, reflux, 8h, (ii) PMBCl, Bu_4NBr, toluene, 70°C, 8h, 80%; (b) (i)benzaldehyde dimethyl acetal, p-TSA, MeCN, rt, 5min, (ii) BzCl, pyridine, rt, 8h, 70%; (c) NaN_3, DMF, 60°C, 100%; (d) CAN, MeCN/H_2O(16:1), rt, 30min, 68%; (e) (i) Tf_2O, pyridine, DCM, -25°C, 25min, (ii) Bu_4NNO_2, MeCN, 50°C, overnight, 70%; (f) (i) Tf_2O, pyridine, DCM, -25°C to rt, 90min, (ii) KSAc, DMF, 60°C , overnight, 84%; (g) (i) hydrazinium acetate, DMF, rt, 2h, (ii) NaH, DMF, then **2**, Kryptofix 21, rt; (h) 80% AcOH(aq), 45°C, overnight, 32% over 3 steps; (i) (i) 0.5M NaOMe, MeOH, rt, overnight, (ii) 0.25M NaOH(aq), 8h; (j) H_2, palladium hydroxide on carbon, EtOH, 48h, 70%.

The synthesis of **SC3** has been previously reported. (*36*)The synthesis of **SC4** (**23**) and **SC5** were shown in scheme 4 and 5, respectively. Through proper protection/deprotection strategy, the free hydroxyl group at 3 or 6 position was reacted with propargyl chlororide and yielded propargylated compounds **20** and **27** respectively. The “click” reactions resulted in the formation of the triazole linkage were done under the same condition as the synthesis of SC1. Deprotection and convertion of azide to amine was the same as described in the synthesis of **SC2**.

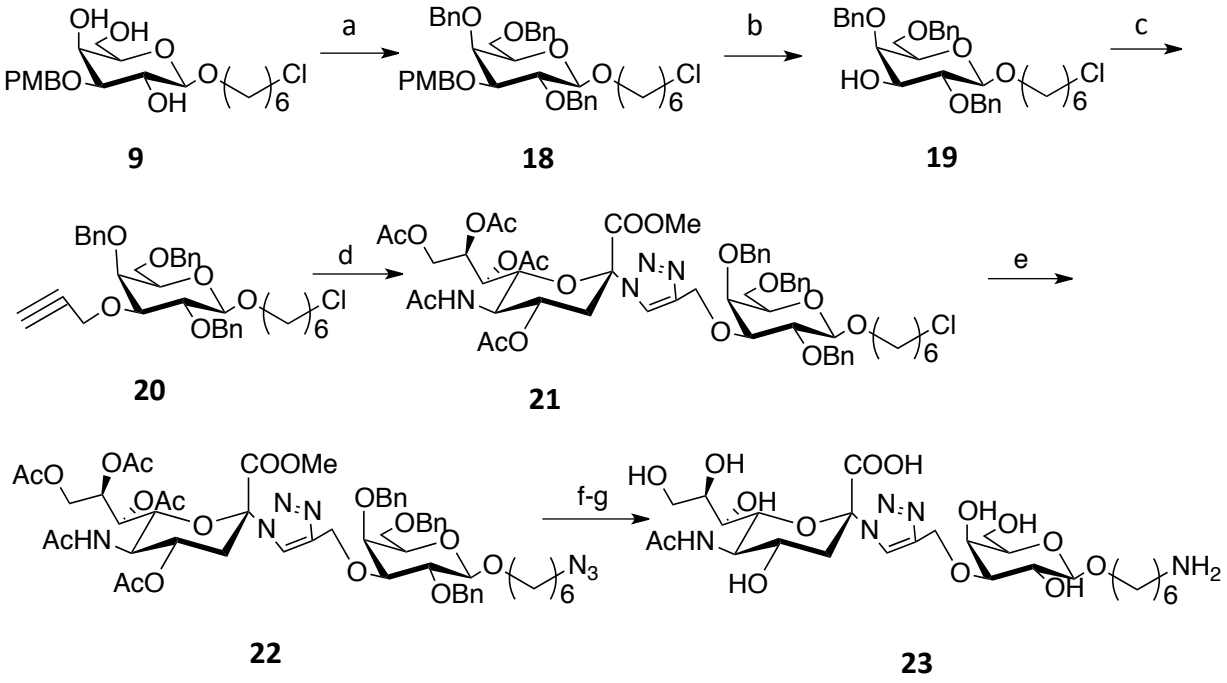

Scheme 2.4 Synthesis of **SC4** (**23**) (a) BnBr, NaH, THF, reflux, 6h, 83%; (b) CAN, MeCN/H_2O(16:1), rt, 2h, 55%; (c) propargyl bromide, NaH, THF, 60^oC, 3h, 75%; (d) 4, CuI, diisopropylethylamine, MeCN, rt, 91%; (e) NaN_3, DMF, 60^oC, overnight, 58%; (f) (i) 0.5M NaOMe, MeOH, rt, overnight, (ii) 0.25M NaOH(aq), 8h; (g) H_2, palladium hydroxide on carbon, EtOAc/EtOH(1:1), 48h, 56%.

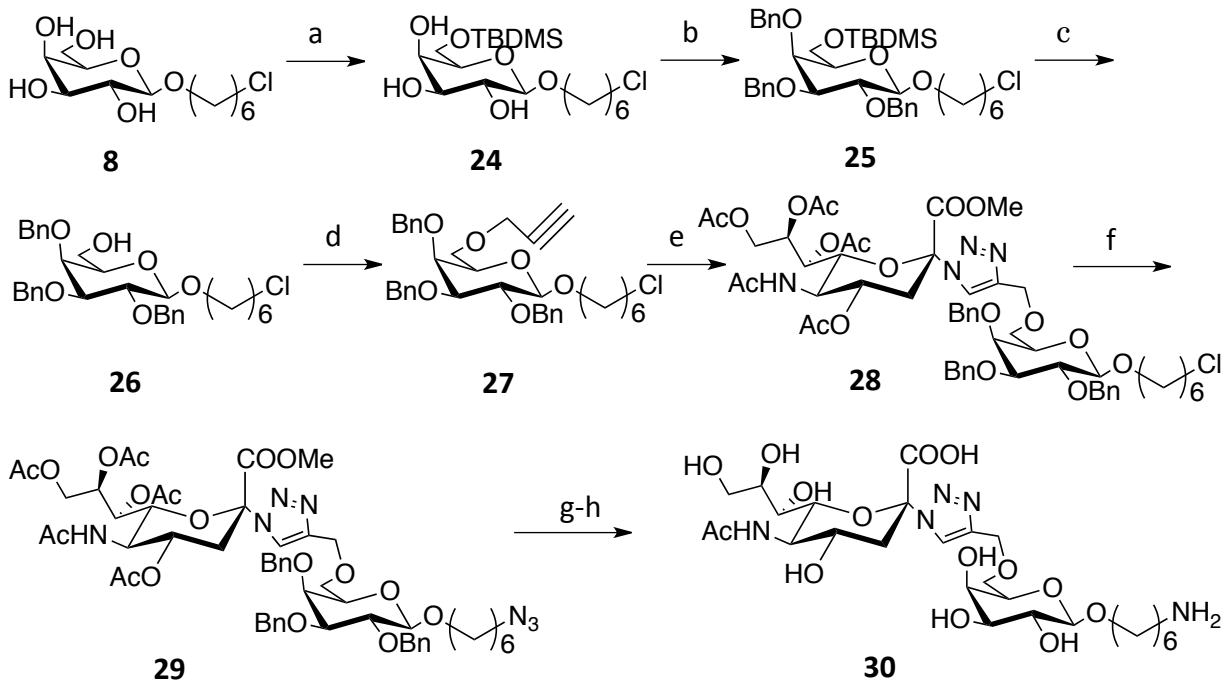

Scheme 2.5 Synthesis of **SC5** (**30**) (a) (i) Bu_2SnO, MeOH, reflux, 8h, (ii) TBDMSCl, toluene, 100°C, 6h, 63%; (b) BnBr, NaH, THF, reflux, 6h, 73%; (c) I_2, MeOH, reflux, 3h, 72%; (d) propargyl bromide, NaH, THF, 60°C, 17h, 83%; (e) **4**, CuI, diisopropylethylamine, MeCN, rt, 91%; (f) NaN_3, DMF, 60°C, overnight, 50%; (g) (i) 0.5M NaOMe, MeOH, rt, overnight, (ii) 0.25M NaOH(aq), 8h; (h) H_2, palladium hydroxide on carbon, EtOAc/EtOH(1:1), 48h, 60%.

The synthesis of C-linked sialosides (**SC6-8**) was performed by Dr. Yang Yang, a postdoctoral fellow in our laboratories. The detailed procedure is not discussed in the dissertation.

2.2.2 Glycan microarray fabrication

With the sialosides in hand, we first immobilized them on standard ELISA plate with maleimide coated wells and tested the binding ability toward recombinant HA proteins, as described by our group previously.(*35*) Unfortunately, despite several efforts that included a variety of blocking methods and using ELISA plates from different manufacturers, we found that the non-specific binding were substantial, therefore most of the binding signals were buried in the noise. Also, we were consuming significant amount of material for a single assay. For instance, a minimum of 30 μg of compounds were required in a single well (based on the minimum coating concentration of 750 μM volume of 100 μl) and 90 μg for

one target protein (triplicate is the minimum requirement for ELISA assay). To overcome this problem, we switched to microarray technology, which utilizes a miniature version of ELISA plate: microscope glass slide. The robotic printing technique is automatic, and most important, highly economic considering the consumption of precious glycans. The pin of the robotic microarray printer withdraws only ~0.6 µl of glycan solution and prints up to 8 replicate spots. (according to microarray printer manual)

Since our compounds all possess primary amine on the terminal of the linker, we chose slides that were prefabricated with PEG and N-hydroxysuccinimide (NHS) activated carboxyl groups. The hydrophilic long chain of PEG can significanlly decrease non-specific binding and the activated ester is ready to react with amine to form amide bond under neutral or mild basic conditions. In printing condition optimization study (data not shown), we printed amine-functionalized mannoside at different concentrations under different pHs (5.5, 7.4 and 8.4) and incubated with Alexa Fluor@633 labeled lectin Concanavalin A (ConA) to find out the optimal printing condition. We found that when the printing was done under pH 8.4, the binding of mannoside to ConA was significant even at a printing concentration of 6.25 µM. At pH 7.4, a minimum of 12.5 µM mannoside solution was required for printing. While at pH 5.5, the printing was much less efficient. We found that a glycan concentration of 200 µM provides an excellent signal to noise ratio and we used that concentration for all our studies. A systematic study that correlated the printing concentration and surface saturation also supported our findings. Liang *et al.*(*37*) used fluorescein isothiocyanate (FITC) cadaverine, a fluorescent dye as model molecule and printed it in concentrations ranging from 100 mM to 1 fM on the same commercial available NHS-ester slide that we used. They scanned the slide before and after washing and measured the surface coverage of FITC. They found that at concentrations below 100 µM, the fraction of surface coverage increased as the concentration increased, whereas the surface saturated over 500 µM. The density of maximum loading was found to be 10^{14} molecules/cm^2, which was similar to most peptides or sugars attached to an SPR biosensor surface. (*38, 39*)

2.2.3 Lectin and HA binding study

After the printing was complete, we tested the binding of sialosides with lectins that are known to bind to terminal sialic acid. The first lectin we tested was Wheat germ agglutinin (WGA), which showed binding to N-acetylglucosamine and N-acetylneuraminic acid (sialic acid) in previous studies. (*40, 41*) An NMR binding study showed that WGA preferred the α-2, 3 over α-2, 6-linkage when bound to sialic acid (K_D = 0.73mM with α-2, 3-sialyllactose; K_D = 5.3mM with α-2, 6-sialyllactose). (*40*) The binding profile of WGA on our sialoside microarray is shown in figure 2.3A. In accordance with the NMR binding study, WGA showed moderate binding to **SC9** (α-O-2, 3-sialyllactoside) while very weak binding to **SC10** (α-O-2, 6-sialyllactoside). A similar binding preference was also seen with the thiosialoside pair: WGA showed highest binding to **SC2** (α-S-2, 3-sialylgalactoside) among all ten sialosides, whereas only moderate binding to **SC3** (α-S-2, 6-sialylgalactoside). This results indicated that the replacement of O- with S- did not change the conformation of glycans to the extend that could alter the WGA binding specificity. On the contrary, this binding preference of WGA was not observed when bound to N-linked sialosides. In fact, both **SC4** and **SC5** showed only weak to moderate binding to WGA, which might be resulted from the conformational change induced by the insertion of a rigid ring to replace glycosidic bond. Moderate to strong binding were observed with the two N- and C-linked monosaccharides **SC1** and **SC6** and C-linked trisaccharide **SC8**, while binding to C-linked disaccharide **SC7** was hardly seen.

We also obtained the binding profile of three other lectins that have been reported to bound to sialic acid, including *Sambucus nigra* agglutinin (SNA) (Figure 2.3B), *Maackia amurensis* leukoagglutinin (MAL-I) and *M. amurensis* hemagglutinin (MAL-II) **(**Figure 2.3D**)**. SNA was first reported to bind to D-galactose and N-acetylgalatosamine, and then was found to be capable of recognizing terminal sialic acid, preferably with α-2, 6-linkage.(*42*) We observed the highest binding was with **SC10** (α-O-2, 6-sialyllactoside) while significant binding to **SC9** (α-O-2, 3-sialyllactoside) was also seen. The binding of **SC3** (α-S-2, 6-sialylgalactoside) was also strong, compared to its α-S-2, 3-linked analogue **SC2**. Similar to

WGA, SNA also showed moderate binding to the N-linked monosaccharides **SC1**, but did not bind well with N-linked disaccharides and all three C-linked sialosides. MAL-I and MAL-II showed very weak binding to S- and N-linked sialosides while weak to moderate binding to O- and C-linked sialosides depending on the structures.

Next we incubated the microarray slide with influenza hemagluttinin (HA) H1N1 A/Brisbane/59/2007, which was premixed with primary and secondary antibodies in the ratio of 4:2:1. We observed binding signals from **SC7**, **SC9** and **SC10**, but not the rest of the sialosides **(**Figure 2.3C**).** Combining the results from WGA (WGA bound to all sialosides except **SC7** and **SC10** in moderate to high level) and HA binding studies, we concluded that all ten sialosides were immobilized on the slide.

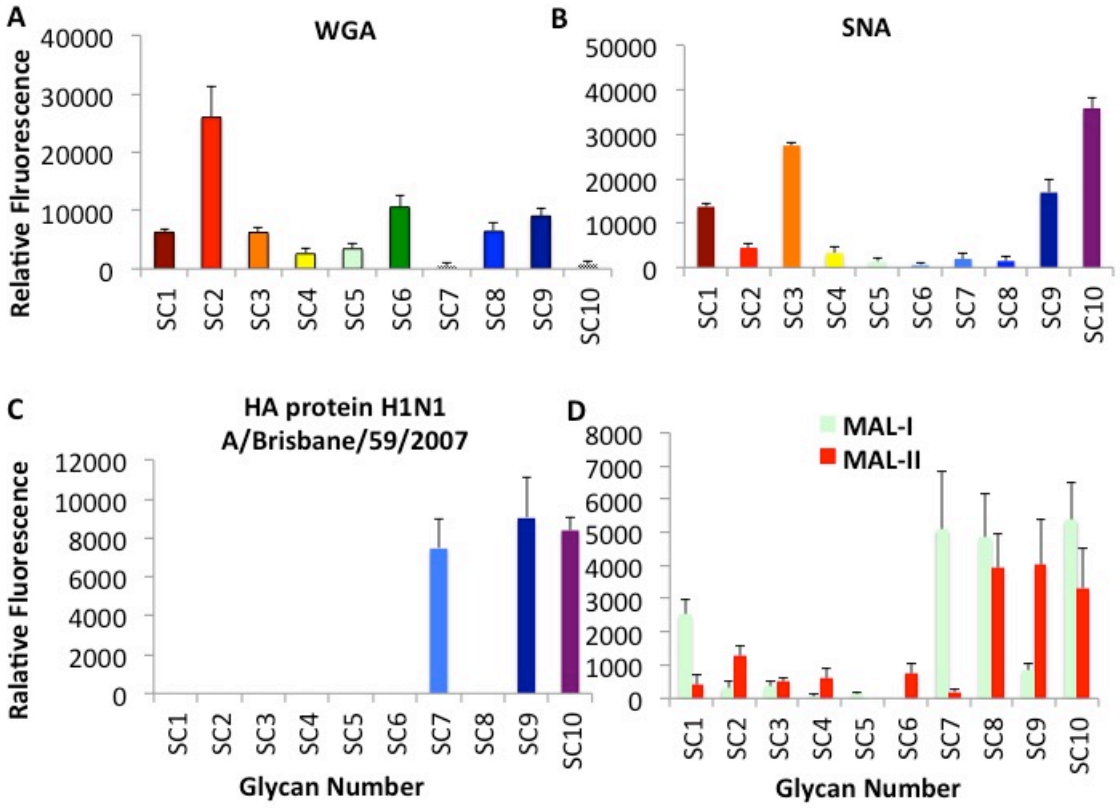

Figure 2.2 Lectin and HA protein binding profile on sialoside microarray. Microarray was incubated with (A) Rhodamine labeled WAG (100µg/ml). (B) Biotinylated SNA (100µg/ml) then rhodamine labeled streptavidin (C) Recombinant HA protein of H1N1 A/Brisbane/59/2007 (100µg/ml) premixed with anti-H1 rabbit polyclonal antibody and Alexa Fluor®633 labeled goat anti rabbit secondary antibody (4:2:1). (D) Biotinylated MAL-I and MAL-II (100µg/ml) then rhodamine labeled streptavidin.

2.2.4 NA resistance assay

Next, we compared the stability of sialosides with different linkages towards NA to evaluate the feasibility of using the microarray to detect virus at ambient temperature without adding NA inhibitors. We first treated the slide with H1N1 NA at rt for 2h and then incubated it with either fluorescent labeled WGA or HA (A/Brisbane/59/2007), which were premixed with primary and labeled secondary antibodies. The WGA binding profile before and after NA treatment of the printed slide is shown in **Figure 2.4A**. Through the side-to-side comparison, we can clearly see that the binding of WGA to S-, and N-linked sialosides (**SC1**-**SC5**) is almost unchanged, indicating NA did not hydrolyze these sialosides. We also still see the binding signal for **SC9** after NA treatment, which was expected to be hydrolyzed by NA. One possible reason is that the WGA can bind to the residual lactoside on the microarray after the NA cleaves the terminal O-linked sialic acid. However, when HA (A/Brisbane/59/2007) is used (**Figure 2.4B**), we see that the signal of **SC9**, the α-2, 3-*O*-linked sialoside, is completely lost, which is a clear indication that the viral NA cleaves α-2, 3-O-linkages very efficiently even when present on a solid surface. In contrast, the signal of the C-sialoside **SC7** binding remained unchanged. The signal intensity of the α-2, 6-*O*-linked sialoside, **SC10** decreases slightly, but is not completely lost as seen with α-2, 3-*O*-linked sialoside **SC9**. Increasing the NA incubation time doesn't produce a different result, we observed similar fluorescent readings (data not shown), indicating that the α-2, 3-*O*-linked sialoside is cleaved more rapidly than α-2, 6-*O*-linked sialoside. A NA substrate specificity study also shows similar result. (*43*) Li *et al.* screened the substrate specificity of 27 NAs (N1-N9), including both human and avian viral NA using a colorimetric assay with 1h duration of hydrolysis. They found that α-2, 3-linked sialosides were hydrolyzed more efficient than α-2, 6-linked sialosides in solution toward all NAs. When assuming the standard compound Siaα2 − 3GalβpNP(NP: para-nitrophenol) was completely hydrolyzed during the assay, only 40% or less of Siaα2 − 6GalβpNP was cleaved off by most NAs.

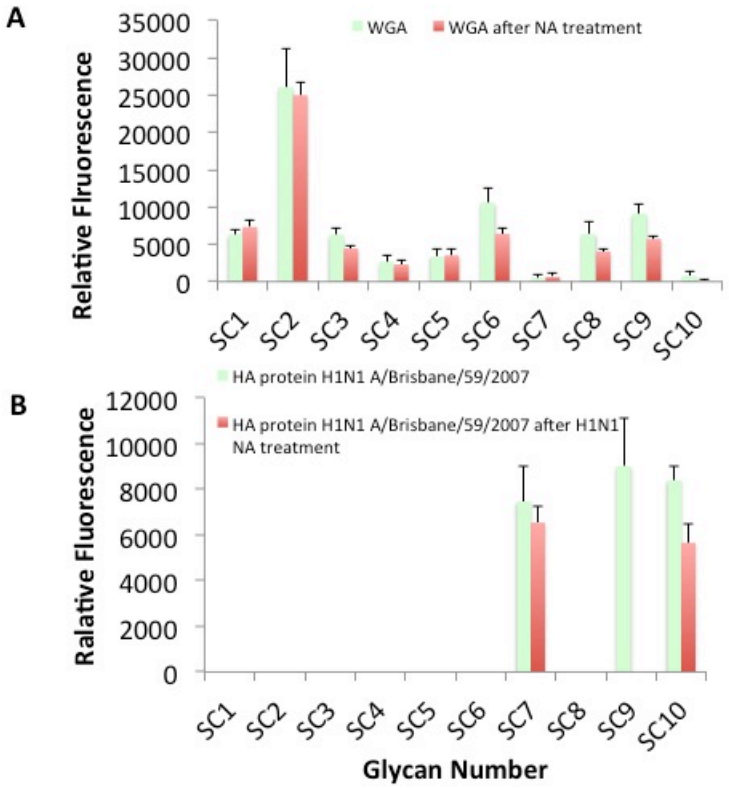

Figure 2.3 *Stability comparison of sialosides with S-, N-, C- and O-linkages towards NA.* (A) Rhodamine labeled WAG (100µg/ml) (Green); First NA (N1, 3.3 U, 1U=1,000 pmol/min), then rhodamine labeled WAG (100µg/ml) (Red). (B) H1 (100µg/ml) premixed with anti-H1 rabbit polyclonal antibody and Alexa Fluor®633 labeled goat anti rabbit secondary antibody (4:2:1)(Green); First NA (N1, 3.3 U, 1U=1,000 pmol/min), then H1-antibody complex (Red). All experiments were performed in triplicate on three different days. Error bars represent mean ± SEM of three independent experiments.

To understand this behavior, we performed molecular modeling studies. The crystal structures of 1, 3-sialyllactose and 6-siallylactose were downloaded from PDB and Sybyl-X® was used for docking studies. 3-sialyllactose and 6-sialyllactose was fitted into the known sialic acid binding pocket of N1. (**Figure 2.5**) Eight amino acids of NA have direct interactions with sialic acid in the binding pocket and two of them Asp151 and Tyr406 function as the acid and base in the catalytic process. As can be seen in the two structures, the distance between the glycosidic oxygen of 3-sialyllactose with the key amino acid, Asp151 (3.741 A) is smaller than that with 6-sialyllactose (4.042 A); meanwhile, the distance between the anomeric carbon of 3-sialyllactose with Tyr406 (3.778 A) is also smaller than that with 6-sialyllactose

(5.007 A), suggesting that the 2,3 *O*-sialosides provides a better fit for the hydrolysis as opposed to the 2,6 O-linkages. The longer hydrolysis time of 2,6 *O*-linked sialosides could potentially be exploited in the development of multivalent inhibitors of certain influenza types, which prefer 2,6 *O*-linkages.

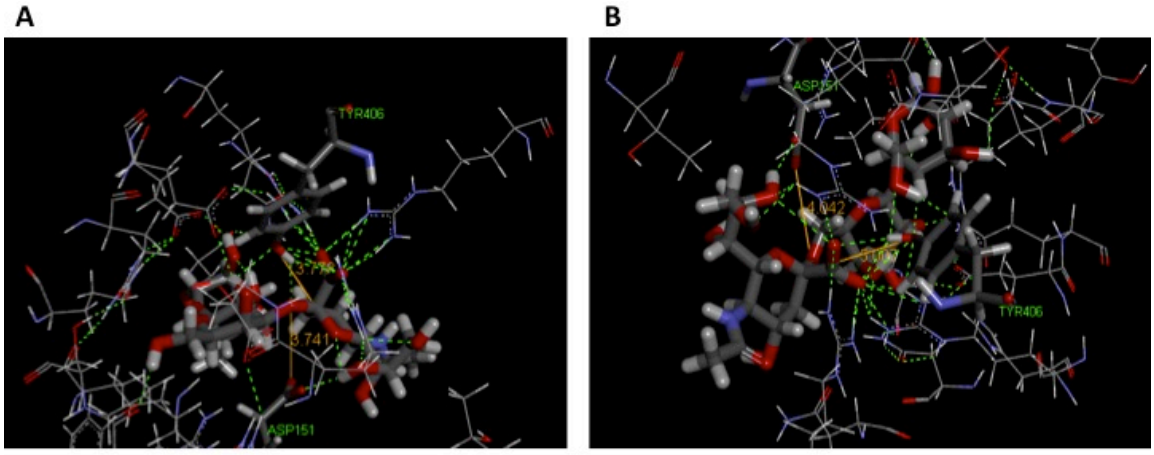

Figure 2.4 Molecular modeling of influenza N1 bound to (A) 2,3-sialyllactose and (B) 2,6-sialyllactose using SYBYL-X®. The 2,3 linkage is a better fit than the 2,6 linkage.

Acknowledging that S-, N- and C-linked sialosides are resistant to NA hydrolysis, we also want to demonstrate the stability of these sialosides toward intact influenza viruses in comparison to O-linked sialosides. The approach we adopted was different then the NA hydrolysis study because intact virus has more complex structure (HA and NA present at the same time) and binding behavior compared to re-combinant enzyme NA. Instead of detecting the binding signal of influenza virus, we designed an exper-iment that detects the residue after hydrolysis. Take SC9 for instance, if the terminal sialic acid is cleaved off, the remaining residue would be lactoside, which can be detected by lectin Ricinus Communis Agglu-tinin-120 (*RCA-120*). We included amine functionalized N-acetylgalactoside as a positive control on the printed slide as well as SC8 (C-linkage) and SC9 (O-linkage) for direct comparison. First we incubated the printed slide with two strains of influenza viruses (H1N1: A/Solomon Island/3/06; H3N2 A/Hongkong/8/68) at pH 5.5, 37^{o}C for 4h to ensure a complete cleavage. Then we incubated the virus-treated slide with biotinylated RCA120 followed by rhodamine labeled streptavidin. The binding result is shown in Figure 2.6. Neither SC8 or SC9 shows binding to RCA120 before treated with intact influenza

viruses. However, SC9 shows significant binding signal after incubated with H1N1 virus, whereas SC8 still don't show binding. This results indicate that the O-linked SC9 was hydrolyzed by virus while SC8 remained intact. The binding signal of SC9 to RCA120 after treated with H3N2 virus is lower, indicating that the hydrolysis is not complete.

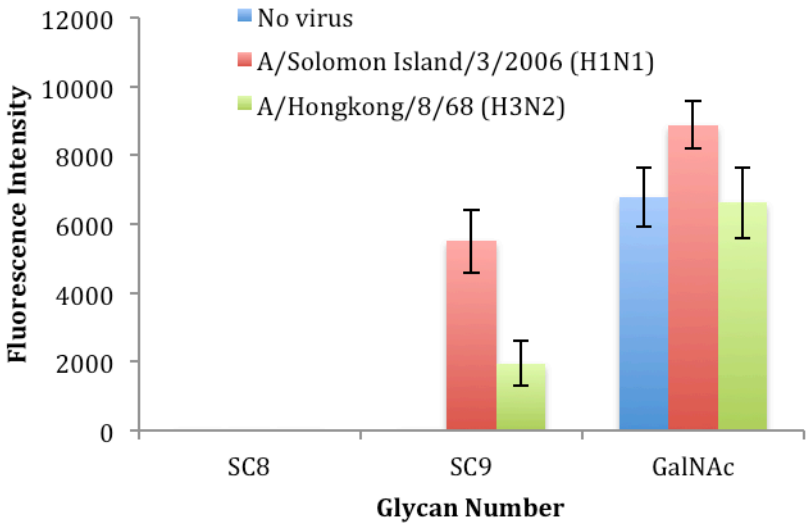

Figure 2.5 Stability comparison of sialosides with C- and O-linkages towards intact influenza viruses. Printed slide was first incubated with influenza virus (A/Solomon Island/3/2006 $2X10^3$ PFU or A/Hongkong/8/68 $8X10^2$ PFU) at 37°C, pH 5.5 for 4h, then biotinylated RCA120 and finally rhodamine labeled streptavidin.

2.2.5 Virus binding and detection sensitivity assay

Having demonstrated the stability of S-, N- and C-linked sialosides toward viral NA and intact influenza viruses, we wanted to test their capturing ability of influenza viruses. Without premixing with NA inhibitors, we introduced BLP (betapropiolactone) inactivated influenza virus A/Puerto Rico/8/34 (BEI resources) at different concentrations to the printed slides, incubated at rt for 1 h, followed by incubation of primary and fluorescently labeled rhodamine secondary antibody. This was followed by scanning the slides using a Genepix scanner at 635 nm. The fluorescence image shows that all eight sialosides captured the virus. (**Figure 2.7A**) We found non-specific binding is negligent to the control PEG ligand. We observe differential binding to the different glycans, the *N*-linked sialosides seems to bind with a

higher affinity than the *C*- or *S*- linked sialosides. (**Figure 2.7B**). Next, we determined the binding pattern of a different influenza strain A/Brisbane/59/2007 (BEI resources). As seen in **Figure 2.7D**, the binding pattern is markedly different for this strain. Finally, we wanted to find the limit of detection by using different concentrations of the virus. We choose **SC5** and we were excited to observe that we can detect the virus at a concentration as low as 35 CEID50 (Chicken Embryo Infectious Dose).

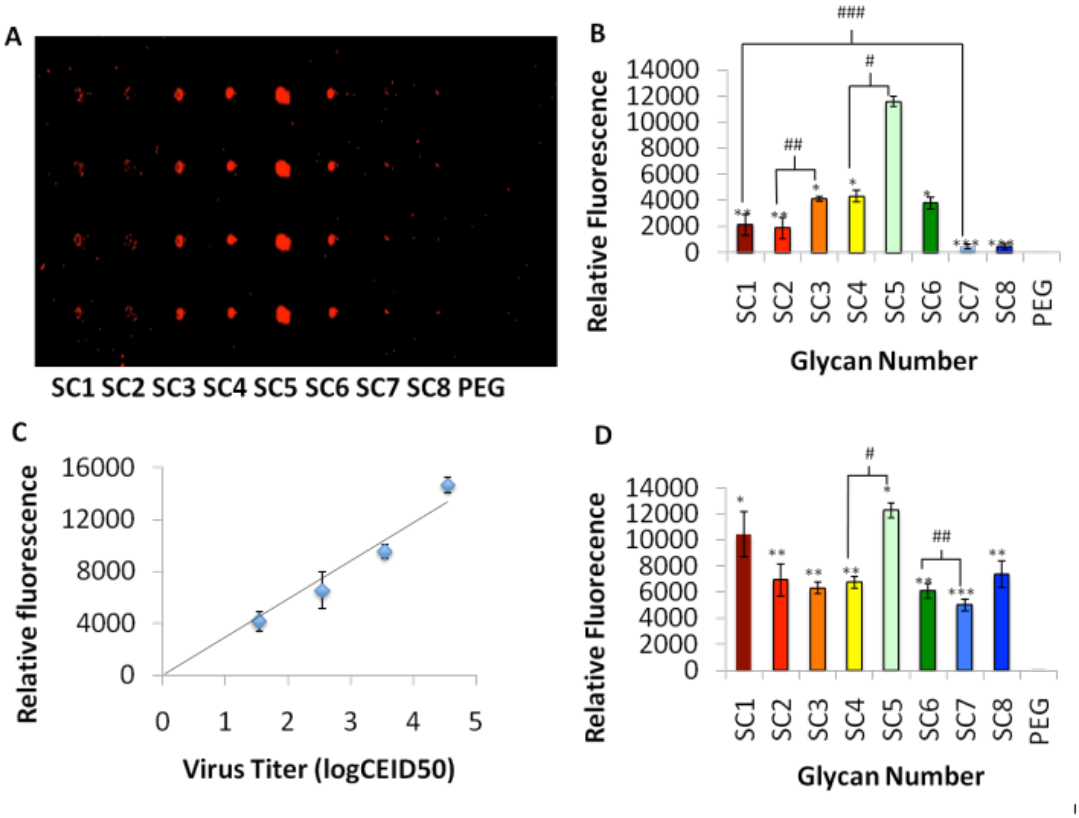

Figure 2.6 Influenza virus binding studies. (A) Fluorescence image of microarray containing 8 sialosides (SC1-SC8), which was incubated with virus A/Puerto Rico/8/34 of 3.5 X10^3 CEID50, then polyclonal anti-influenza virus A/Puerto Rico/8/34 rooster antiserum, detected by Alexa Fluor®633 labeled goat anti-chicken IgG. (B) Finger print binding pattern of virus A/Puerto Rico/8/34 of 3.5 X 10^3 CEID50. (C) SC5 binds to virus of different titers. (D) Finger print binding pattern of influenza A/Brisbane/59/2007 of 3.1 X10^3 CEID50. The binding virus was detected by ferret hyperimmune sera to influenza A/Brisbane/59/2007 and rhodamine labeled goat anti-ferret IgG. Error bars represent mean ±standard error of three independent experiments. Statistical analysis using a student t-test was performed comparing the binding ability of each ligand. Ligands were separated into four groups, that includes *,** and *** groups and there were no statistical differences between each group ($P > 0.05$). #, significantly reduced binding compared to * group ($P < 0.0005$); ##, significantly reduced binding of the * group compared to ** group ($P < 0.005$); ###, significantly reduced binding of the ** group compared to *** group ($P < 0.05$).

With 2 strains of influenza viruses showing different binding patterns to our microarray, we wanted to expand our scope of detection. We used active viruses cultured from MDCK cell instead of the BLP inactivated viruses originated from chicken embryo to eliminate the possible interference of BLP in the binding pattern. The virus titer was measured by plaque forming assay, therefore we used plaque-forming unit (PFU) as the titer unit. The six strains we tested include five H1N1 and one H3N2 viruses and the titer of these strains were adjusted to $3X10^4$ PFU/ml before incubation with the printed slide. The binding profiles are shown in Figure 2.8. Even with expanded target range, we still observed unique binding pattern of every strain. This reinforces our previous statement that every virus type should exhibit differences in binding to different sialoside structures glycans leading to a "fingerprint" pattern of recognition for all strains, including emerging strains. Interestingly, we also observed different binding patterns of the same strain from different cultures (chicken embryo vs MDCK cell), which also underwent different treatment (BLP inactivation vs no inactivation)(Figure 2.7B and Figure 2.8A). A detailed study analyzing the impact of different inactivation protocols on the NA and HA activity of influenza viruses have shown that 16h of BLP treatment of a H3N2 strain A/Wisconsin/67/2005 resulted in over 90% loss in the HA titer.(*44*) Since HA is the key element in the binding event, the change in HA titer can lead to alteration of the binding pattern.

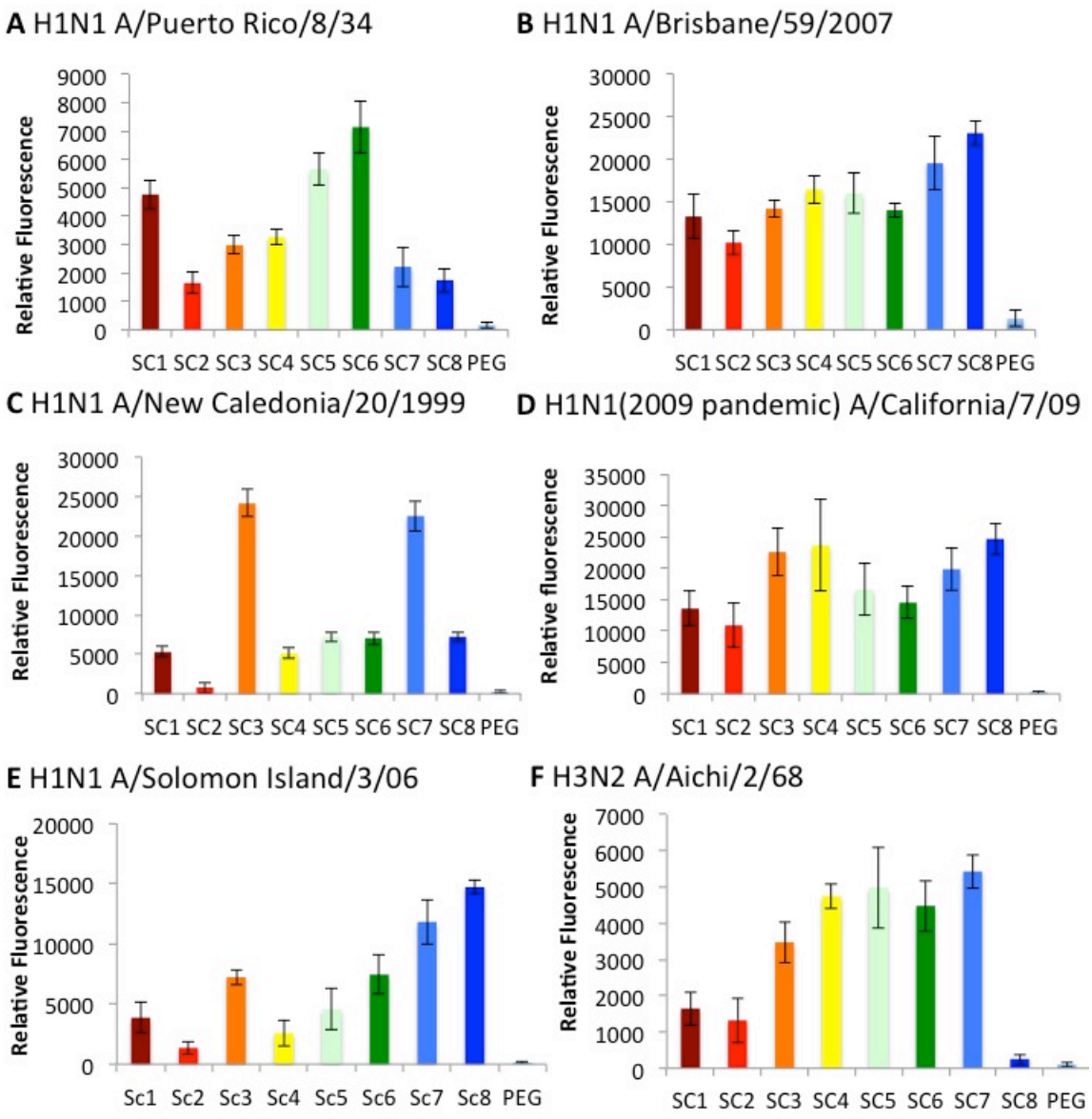

Figure 2.7 Binding profiles of different strains of MDCK cell adapted influenza viruses.

2.3 Experimental section

2.3.1 Materials

All chemical reagents were of analytical grade, used as supplied without further purification unless indicated. The acidic ion-exchange resin used was Dowex-50 and Amberlite (H^+ form). Analytical thin layer chromatography (TLC) was conducted on silica gel 60-F254 (Merck). Plates were visualized

under UV light, and/or by treatment with acidic cerium ammonium molybdate followed by heating. Column chromatography was conducted using silica gel (230-400 mesh) from Qualigens. 1H and 13C NMR spectra were recorded on Bruker AMX 400MHz spectrometer. Chemical shifts are reported in δ (ppm) units using 13C and residual 1H signals from deuterated solvents as references. Spectra were analyzed with Mest-Re-C Lite (Mestrelab Research) and/or iNMR. Electrospray ionization mass spectra were recorded on a Micromass Q Tof 2 (Waters) and data were analyzed with MassLynx 4.0 (Waters) software.

2.3.2 Synthesis procedure and compound characterization

Methyl 5-Acetamido-4,7,8,9-tetra-O-acetyl-3,5-dideoxy-2-[4-(6-chlorohexyl)-1*H*-1,2,3-triazol-1-yl]-D-*glycero*-α-*galacto*-non-2-ulopyranosylonate (5):

In an aluminum foil-rapped flask containing **4**[1] (377mg, 0.73mmol) and 8-chloro-1-octyne (126mg, 1.09mmol, 1.5eq), 10ml of acetonitrile was added, followed by addition of N, N-diisopropylethylamine (361ul, 2.18mmo, 3eq) and copper (I) iodine (277mg, 1.46mmol, 2eq). The reaction mixture was kept stirring overnight at 60^{o}C, concentrated and loaded onto a silica column. Hexane/acetone (2:3) was used as eluent to afford **5** (405mg, 84%).

^{1}H-NMR (400 MHz; $CDCl_3$): δ=7.68 (s, 1H, triazole-H), 5.50 (d, 1H, NH, J=10.0Hz), 5.45-5.43 (m, 1H, H-7), 5.39 (d, 1H, H-8, *J* = 8.8 Hz), 5.19-5.12 (m, 1H, H-4), 4.32-4.27 (m, 2H, H-9a, H-9b), 4.16-4.05 (m, 2H, H-5, H-6), 3.77 (s, 3H, OMe), 3.54 (t, 2H, CH_2Cl, *J* = 6.7 Hz), 2.75-2.71 (m, 2H, linker-H), 2.67 (d, 1H, H-3e, *J* = 12.6 Hz), 2.18 (s, 3H), 2.15 (app d, 1H, H-3a, *J* = 3.3 Hz), 2.12 (s, 3H, OAc), 2.08, 2.06 (s, 6H, OAc), 1.91 (s, 3H, NAc), 1.82-1.68 (m, 4H, linker-H), 1.53-1.37 (m, 4H, linker-H). ^{13}C NMR (400 MHz; $CDCl_3$): δ=170.9, 170.6, 170.3, 170.1, 166.6, 148.9, 119.7, 88.3, 73.7, 68.6, 68.0, 66.9, 62.3, 54.0, 49.2, 45.1, 36.0, 32.5, 28.9, 28.5, 26.5, 25.5, 23.2, 21.3, 20.9, 20.8. HRMS (ESI): m/z calcd for $[C_{28}H_{41}ClN_4O_{12}Na]^+$: 683.2388. Found: 683.2280.

Methyl 5-Acetamido-4,7,8,9-tetra-O-acetyl-3,5-dideoxy-2-[4-(6-azidohexyl)-1*H*-1,2,3-triazol-1-yl]-D-*glycero*-α-*galacto*-non-2-ulopyranosylonate (6):

Compound **5** (405mg, 0.61mmol) was dissolved in 6ml of anhydrous N, N-dimethylformamide and sodium azide (200mg, 3.05mmol, 5eq) was added. The reaction mixture was stirred at 60^{o}C over-night, diluted with ethyl acetate (20ml), washed with water and brine. The organic layer was dried over Na_2SO_4, filtered, concentrated, and purified by silica column using hexane/acetone (2:3) as eluent. White solid 6 was obtained (344mg, 82%).

^{1}H-NMR (400 MHz; $CDCl_3$): δ=7.68 (s, 1H, triazole-H), 5.49-5.44 (m, 1H, H-7), 5.40-5.36 (m, 2H, NH, H-8), 5.21-5.14 (m, 1H, H-4), 4.33-4.28 (m, 2H, H-9a, H-9b), 4.16-4.06 (m, 2H, H-5, H-6), 3.79 (s, 3H, OMe), 3.28 (t, 2H, CH_2N_3, *J* = 6.9 Hz), 2.74 (t, 2H, linker-H, *J* = 7.8 Hz), 2.69 (d, 1H, H-3e, $J_{3e,3a}$ = 12.6 Hz,), 2.20 (s, 3H, OAc), 2.16 (app d, 1H, H-3a, *J* = 4.0 Hz), 2.13 (s, 3H, OAc), 2.09, 2.07 (s, 6H, OAc), 1.92 (s, 3H, NAc), 1.74-1.71 (m, 2H, linker-H), 1.65-1.61 (m, 2H, linker-H), 1.44-1.43 (m, 4H, linker-H). ^{13}C NMR (400 MHz; CDCl3): δ=170.75, 170.58, 170.39, 170.26, 170.0, 166.6, 148.8, 119.7, 88.3, 73.7, 68.7, 68.1, 67.0, 62.4, 53.9, 51.3, 49.0, 36.0, 28.91, 28.72, 28.68, 26.4, 25.5, 23.1, 21.2, 20.81, 20.76, 20.72. HRMS (ESI): m/z calcd for $[C_{28}H_{42}N_7O_{12}]^{+}$: 668.2891. Found: 668.2884.

5-Acetamido-3,5-dideoxy-2-[4-(6-aminohexyl)-1*H*-1,2,3-triazol-1-yl]-D-*glycero*-α-*galacto*-non-2-ulopyranosidic acid (7):

6 (58mg, 0.087mmol) was dissolved in 2ml of methanol and 0.1ml of 0.5M sodium methoxide was added. The reaction mixture was kept stirring overnight at room temperature, neutralized with acidic ion-exchange resin and concentrated. The residue was redissolved in 5ml of 0.25M sodium hydroxide solution. After stirring at room temperature overnight, acidic ion-exchange resin was added to neutralize the base and removed by filtration. Water was evaporated and the residue was dissolved in 10ml of ethanol. Catalytic amount of palladium hydroxide (20% on carbon) was added and the mixture was kept under hydrogen atmosphere (5 atm) for 10h. Palladium hydroxide was removed by filtration and ethanol was evaporated. The residue was purified by Bio gel P-2 column and white powder **7** (25mg, 62%) was obtained after lyophilization.

^{1}H-NMR (400 MHz; D_2O): δ=7.93-7.87 (m, 1H), 4.05-4.04 (m, 1H), 3.96-3.71 (m, 7H), 3.58-3.37 (m, 4H), 3.26-3.21 (m, 1H), 3.18-3.12 (m, 1H), 2.89-2.85 (m, 2H), 2.79-2.79 (m, 1H), 2.69-2.62 (m, 2H), 2.20-2.13 (m, 1H), 1.98 (s, 3H), 1.60-1.53 (m, 4H), 1.29-1.20 (m, 4H). ^{13}C NMR (400MHz; MeOD): δ=21.25, 24.43, 24.56, 25.44, 25.60, 26.89, 26.99, 27.62, 27.94, 28.34, 28.60, 39.24, 39.28, 39.48, 52.45, 53.73, 63.03, 63.22, 65.84, 67.87, 68.71, 70.38, 70.98, 71.66, 74.74, 79.42, 86.53, 90.65, 120.15, 122.18, 147.00, 147.33, 174.19. HRMS (ESI): m/z calcd for $[C_{20}H_{32}ClO_7]^+$: 460.2408 Found: 460.2430.

6-Chlorohexyl 3-O- (4-methoxybenzyl)-β-D-galactopyranoside (9)

Compound **8**[2] (1.78g, 5.9mmol) was dissolved in 40ml of anhydrous methanol and dibutyltin oxide (2.22g, 8.9mmol, 1.5 eq) was added. The reaction mixture was refluxed for ~4 h until the solution became clear. The solvent was evaporated and the residue was redissolved in 40ml of toluene followed by addition of 4-methoxybenzylchloride (1.2ml, 8.9mmol, 1.5 eq) and tetrabutylammonium bromide (953mg, 2.9mmol, 0.5 eq). The reaction mixture was stirred overnight at 60^{o}C, concentrated and purified by column chromatography using hexane/ethyl acetate (1:3) as eluent. White solid **9** was obtained (1.91g, 4.7mmol, 80%).

^{1}H NMR (400MHz, $CDCl_3$): δ=7.32 (d, 2H, ArH, J= 8.8Hz), 6.91 (d, 2H, ArH, J=8.4Hz), 4.70 (app s, 2H), 4.26 (d, 1H, H-1, J=8.0Hz), 4.01-3.91 (m, 3H), 3.87-3.79 (m, 4H, OMe), 3.78-3.75 (m, 1H), 3.57-3.54 (m, 3H, CH_2Cl), 3.52-3.49 (m, 1H), 3.40 (dd, 1H, H-3, $J_{3,4}$=3.6Hz, $J_{3,2}$=9.6Hz), 2.62 (s, 1H, OH), 2.39-2.37 (m, 1H, OH), 2.23-2.18 (m, 1H, OH), 1.83-1.76 (m, 2H, linker-CH_2), 1.70-1.63 (m, 2H, linker-CH_2), 1.52-1.37 (m, 4H, linker-CH_2). ^{13}C NMR (400MHz, $CDCl_3$): δ=159.6, 129.6, 114.1 103.0, 79.8, 76.7, 76.6, 74.3, 71.8, 71.0, 69.8, 67.2, 62.6, 55.3, 45.0, 32.5, 29.4, 26.6, 25.3. HRMS (ESI): m/z calcd for $[C_{20}H_{31}ClO_7Na]^+$: 441.1656. Found: 441.1667.

6-Chlorohexyl 2-O-benzoyl-4, 6-benzylidene-3-O- (4-methoxybenzyl)-β-D-galactopyranoside (10)

Compound **9** (638mg, 1.58mmol) was dissolved in 20ml of anhydrous acetonitrile and benzaldehyde dimethyl acetal (477ul, 3.2mmol, 2 eq) was added. Catalytic amount of p-toluenesulfonic acid was added to adjust the pH to 2. The reaction mixture was stirred at room temperature for 5min and quenched by addition of triethylamine. The solvent was evaporated and the residue was redissolved in 10ml of pyridine. Benzoyl chloride (553ul, 4.74mmol, 3 eq) was added dropwise and the reaction was allowed to proceed overnight at room temperature. 30ml of ethyl acetate was added and pyridine was washed off using 1M HCl. The organic layer was washed one more time with water, dried over Na_2SO_4 and concentrated. Compound **10** (669mg, 1.1mmol, 70%) was obtained after purification by column chromatography (hexane/ethyl acetate=2:1).

^{1}H-NMR (400 MHz; $CDCl_3$): δ=8.05 (d, 2H, Ar, J = 7.1 Hz,), 7.60 (dd, 3H, Ar, J = 7.5, 1.7 Hz), 7.48 (t, 2H, Ar, J = 7.7 Hz), 7.40-7.38 (m, 3H, Ar), 7.18 (d, 2H, Ar, J = 8.6 Hz), 6.74 (d, 2H, Ar, J = 8.7 Hz), 5.62 (dd, H-2, $J_{2,3}$ = 10.1 Hz, $J_{2,1}$ = 8.0 Hz), 5.55 (s, 1H, CHPh), 4.65 (d, 1H, CH_2Ph, J = 12.5 Hz), 4.58-4.54 (m, 2H, H-1, CH_2Ph), 4.36 (dd, 1H, H-6a, $J_{6a,6b}$= 12.2, $J_{6a,5}$= 1.2 Hz), 4.23 (d, 1H, H-4, $J_{4,3}$ = 3.3 Hz), 4.09 (dd, 1H, H-6b, $J_{6b,\,6a}$= 12.3, $J_{6a,5}$= 1.6 Hz), 3.94 (dt, 1H, OCH_2, J = 9.6, 5.9 Hz), 3.77 (s, 3H, OCH_3), 3.74 (dd, 1H, H-3, $J_{3,2}$=10.1, $J_{3,4}$=3.6 Hz), 3.46 (dt, 1H, OCH_2, J = 7.6, 2.0 Hz), 3.43 (s, 1H, H-5), 3.33 (tq, 2H J = 6.7, 3.3 Hz, CH_2Cl), 1.54-1.44 (m, 4H, linker-H), 1.28-1.18 (m, 4H, linker-H). ^{13}C NMR (400MHz; CDCl3): δ=165.1, 159.2, 137.7, 133.0, 130.3, 129.92, 129.77, 129.3, 129.0, 128.3, 128.2, 126.5, 113.7, 101.34, 101.28, 76.5, 73.3, 70.81, 70.63, 69.2, 69.0, 66.7, 55.2, 45.0, 32.4, 29.2, 26.5, 25.2. HRMS (ESI): m/z calcd for $[C_{34}H_{39}ClO_8Na]^+$: 633.2231. Found: 633.2255.

6-Azidohexyl 2-O-benzoyl-4, 6-benzylidene-3-O- (4-methoxybenzyl)-β-D-galactopyranoside (11)

10 (669mg, 1.1mmol) was dissolved in 15ml of N, N-dimethylformamide and sodium azide (712mg, 11mmol, 10 eq) was added. The reaction mixture was stirred overnight at 60°C, diluted with 30ml of ethyl acetate and washed with water (10ml) twice. The organic layer was concentrated, dried

over Na_2SO_4, concentrated and purified by flash chromatography using hexane/ethyl acetate (2:1) as eluent. Compound **11** (676mg, 100%) was obtained.

^{1}H-NMR (400 MHz; $CDCl_3$): δ=8.06-8.04 (m, 2H, Ar), 7.62-7.59 (m, 3H, Ar), 7.49 (t, 2H, Ar, J = 7.7 Hz), 7.41-7.36 (m, 3H, Ar), 7.18 (d, 2H, Ar, J = 8.6 Hz), 6.74 (d, 2H, Ar, J = 8.6 Hz), 5.63 (dd, 1H, H-2, $J_{2,3}$ = 10.0 Hz, $J_{2,1}$ = 8.0 Hz), 5.55 (s, 1H, CHPh), 4.65 (d, 1H, CH_2Ar, J = 12.5 Hz), 4.57-4.54 (m, 2H, H-1, CH_2Ar), 4.36-4.33 (m, 1H), 4.25 (d, 1H, H-4, $J_{4,3}$ = 3.4 Hz), 4.10 (dd, 1H, H-6b, $J_{6b,6a}$ = 12.2, $J_{6a,5}$ = 1.4 Hz), 3.94 (q, 1H, J = 7.7 Hz), 3.76 (s, 3H, OCH_3), 3.73 (d, 1H, H-3, J = 3.5 Hz, 1H), 3.45 (dt, J = 7.6, 1.9 Hz, 1H), 3.42 (s, 1H, H-5), 3.04 (td, 2H, CH_2N_3, J = 7.0, 1.9 Hz), 1.57-1.42 (m, 2H, linker-H), 1.33-1.15 (m, 6H, linker-H). ^{13}C NMR (400 MHz; $CDCl_3$): δ=165.1, 159.2, 137.8, 133.0, 130.3, 129.9, 129.8, 129.3, 128.9, 128.3, 128.1, 126.6, 113.7, 101.36, 101.22, 73.2, 70.8, 70.6, 69.21, 69.03, 66.7, 55.2, 51.2, 29.2, 28.6, 26.3, 25.4. HRMS (ESI): m/z calcd for $[C_{34}H_{39}N_3O_8Na]^+$: 640.2635. Found: 640.2640.

6-Azidohexyl 2-O-benzoyl-4, 6-benzylidene-β-D-galactopyranoside (12)

11 (676mg, 1.1mmol) was dissolved in 30ml of acetonitrile/H_2O (16:1) and cerium (IV) ammonium nitrate (1.8g, 3.3mmol, 3 eq) was added. The reaction mixture was stirred at room temperature for 30min and quenched with saturated sodium thiosulfate solution. The organic layer was washed with water, dried over Na_2SO_4 and concentrated. The residue was purified by flash chromatography using hexane/ethyl acetate (1:1) and afforded compound **12** (371mg, 68%).

^{1}H-NMR (400 MHz; $CDCl_3$): δ=8.10-8.07 (m, 2H, Ar), 7.60-7.55 (m, 3H, Ar), 7.47 (t, 2H, Ar, J = 7.7 Hz), 7.41 (dd, 3H, Ar, J = 5.0, 1.9 Hz), 5.60 (s, 1H, CH_2Ph), 5.38 (dd, 1H, H-2, $J_{2,3}$ = 9.9, $J_{2,1}$ = 8.1 Hz), 4.60 (d, 1H, H-1, J = 8.0 Hz), 4.39 (dd, 1H, H-6a, $J_{6a,6b}$= 12.3 Hz, $J_{6a,5}$=0.9 Hz), 4.29 (d, 1H, H-5, J = 3.7 Hz), 4.13 (dd, 1H, $J_{6b,6a}$ = 12.4 Hz, $J_{6a,5}$=1.6 Hz), 3.99-3.92 (m, 2H, H-3, OCH_2), 3.56 (s, 1H, H-4), 3.53-3.49 (m, 1H, OCH_2), 3.09-3.05 (m, 2H, CH_2N_3), 2.68-2.66 (m, 1H, OH), 1.57-1.52 (m, 2H, linker-H), 1.37-1.33 (m, 2H, linker-H), 1.28-1.22 (m, 4H, linker-H). ^{13}C NMR (400 MHz; $CDCl_3$): δ 166.1, 137.4, 133.2, 129.8, 129.3, 128.4, 128.3, 126.5, 101.6, 101.0, 75.7, 72.9, 71.8, 69.4, 69.1, 66.6, 51.2, 29.3, 28.6, 26.3, 25.5. HRMS (ESI): m/z calcd for $[C_{26}H_{31}N_3O_7Na]^+$: 520.2060. Found: 520.2031.

6-Azidohexyl 2-O-benzoyl-4, 6-benzylidene-β-D-gulopyranoside (13)

12 (206mg, 0.414mmol) was dissolved in 20ml of dichloromethane and pyridine (167ul, 2.07mmol, 5 eq) was added. The mixture was cooled to -25°C and trifluoromethanesulfonic anhydride (1M solution in dichloromethane, 820ul, 2 eq) was added dropwise. The reaction mixture was slowly warmed to room temperature. After stirring for 50min, TLC indicated the reaction was completed. The reaction mixture was diluted with 20ml of dichloromethane and washed sequentially with saturated sodium bicarbonate, 1M HCl and water. The organic layer was dried over Na_2SO_4 and concentrated. The residue was dissolved in 25ml of acetonitrile and tetrabutylammonium nitrite (597mg, 2.07mmol, 5 eq) was added. The reaction mixture was stirred overnight at 50°C, concentrated and loaded onto a silica column and eluted with hexane/ethyl acetate (1:1). Compound **13** was obtained (142mg, 70%).

^{1}H-NMR (400 MHz; $CDCl_3$): δ=8.06 (d, 2H, Ar, J = 7.2 Hz), 7.62-7.55 (m, 3H, Ar), 7.48 (s, 2H, Ar), 7.38-7.36 (m, 3H, Ar), 5.54 (s, 1H, CHPh), 5.37 (dd, 1H, H-2, $J_{2,1}$ = 8.4, $J_{2,3}$ = 3.1 Hz), 5.04 (d, 1H, H-1, J = 8.4 Hz), 4.37-4.30 (m, 2H, H-3, H-6a), 4.08-4.02 (m, 2H, H-6b, H-5), 3.99-3.91 (m, 1H, OCH_2), 3.84 (s, 1H, H-4), 3.52-3.46 (m, 1H, OCH_2), 3.05 (t, 2H, CH_2N_3, J = 6.8 Hz), 1.56-1.44 (m, 2H, linker-H), 1.35-1.31 (m, 2H, linker-H), 1.25-1.19 (m, 4H, linker-H). ^{13}C NMR (400 MHz; $CDCl_3$): δ 165.2, 137.7, 133.4, 129.85, 129.75, 129.1, 128.5, 128.2, 126.4, 101.2, 98.1, 76.4, 71.2, 69.36, 69.3, 69.1, 65.6, 51.2, 29.3, 28.6, 26.3, 25.5. HRMS (ESI): m/z calcd for $[C_{26}H_{31}N_3O_7Na]^+$: 520.2086. Found: 520.2061.

6-Azidohexyl 3-S-acetyl-2-O-benzoyl-4, 6-benzylidene-β-D-galactopyranoside (14)

13 (114mg, 0.29mmol) was dissolved in 10ml of dichloromethane and pyridine (115ul, 1.45mmol, 5 eq) was added. The mixture was cooled to -25°C and trifluoromethanesulfonic anhydride (1M solution in dichloromethane, 820ul, 2 eq) was added dropwise. The reaction mixture was slowly warmed to room temperature. After stirring for 90min, TLC indicated the reaction was completed. The reaction mixture was diluted with 20ml of dichloromethane and washed sequentially with saturated sodium bicarbonate, 1M HCl and water. The organic layer was dried over Na_2SO_4 and concentrated. The

residue was dissolved in 8ml of N, N-dimethylformamide and potassium acetate (196mg, 1.74mmol, 6 eq) was added. The reaction mixture was stirred overnight at 60°C, diluted with 20ml of ethyl acetate and washed with water (3x10ml). The organic layer was dried over Na_2SO_4, concentrated and loaded onto a silica column and eluted with hexane/ethyl acetate (1:1). Compound **14** (83mg, 65%)was obtained.

^{1}H-NMR (400 MHz; $CDCl_3$): δ=8.03-8.01 (m, 2H, Ar), 7.59-7.54 (m, 3H, Ar), 7.46 (t, 2H, Ar, *J* = 7.7 Hz), 7.40 (d, 3H, Ar, *J* = 6.8 Hz), 5.58 (s, 1H, CHPh), 5.46 (dd, 1H, H-2, $J_{2,1}$ = 7.7 Hz, $J_{2,3}$ = 11.5 Hz), 4.71 (d, 1H, H-1, *J* = 7.8 Hz), 4.38 (d, 1H, H-6a, *J* = 12.4 Hz), 4.26 (dd, 1H, H-3, $J_{3,2}$ = 11.5 Hz, $J_{3,4}$ = 3.3 Hz), 4.16-4.10 (d, 1H, H-5, *J* = 2.5 Hz), 4.11 (dd, 1H, H-6b, $J_{6b,\,6a}$= 12.5 Hz, $J_{6b,5}$=1.5 Hz), 3.98-3.92 (m, 1H, OCH_2), 3.72 (s, 1H, H-4), 3.51-3.45 (m, 1H, OCH_2), 3.04 (t, 2H, CH_2N_3, *J* = 6.9 Hz), 2.23 (s, 3H, SAc), 1.56-1.44 (m, 2H, linker-H), 1.33-1.25 (m, 2H, linker-H), 1.19-1.16 (m, 4H, linker-H). ^{13}C NMR (400 MHz; $CDCl_3$): δ=195.0, 165.2, 137.4, 133.1, 129.79, 129.74, 129.0, 128.4, 128.2, 126.3, 102.5, 101.3, 75.9, 69.16, 69.13, 69.04, 68.5, 51.2, 46.9, 30.5, 29.2, 28.6, 26.3, 25.4. HRMS (ESI): m/z calcd for $[C_{28}H_{33}N_3O_7SNa]^+$: 578.1937. Found: 578.1929.

6-Azidohexyl S- (Methyl 5-Acetamido-4, 5, 8, 9-tetra-O-acetyl-3, 5-dideoxy-D-glycero-α-D-galacto-2-nonulopyranosylonate)- (2-3)-2-O-benzoyl-4, 6-benzylidene-3-thio-β-D-galactopyranoside (15)

14 (83mg, 0.15mmol) was dissolved in 4ml of degassed N, N-dimethylformamide. The solution was flushed with argon for 10min and hydrazine acetate (28mg, 0.3mmol, 2 eq) was added. The reaction was stirred under argon at room temperature for 90min, diluted with 10ml of ethyl acetate and washed with water (2x5ml). The organic layer was dried over Na_2SO_4 and concentrated in vacuum.

^{1}H-NMR (400 MHz; $CDCl_3$): δ=8.09-8.07 (m, 2H), 7.60-7.56 (m, 3H), 7.48 (t, *J* = 7.8 Hz, 2H), 7.41-7.39 (m, 3H), 5.61 (s, 1H), 5.34 (dd, *J* = 11.0, 7.9 Hz, 1H), 4.58 (d, *J* = 7.8 Hz, 1H), 4.36 (d, *J* = 12.3 Hz, 1H), 4.17 (d, *J* = 2.6 Hz, 1H), 4.11 (dd, *J* = 12.4, 1.6 Hz, 1H), 3.96-3.91 (m, 1H), 3.62 (s, 1H), 3.49-

3.44 (m, 1H), 3.15 (td, *J* = 10.9, 3.0 Hz, 1H), 3.06-3.02 (m, 2H), 2.24 (d, *J* = 10.8 Hz, 1H), 1.55-1.44 (m, 2H), 1.33-1.16 (m, 8H).

The intermediate thiol was dissolved in 2ml of degassed N, N-dimethylformamide and sodium hydride (24mg of a 60% suspension in mineral oil, 0.6mmol, 4 eq) was added. The mixture was stirred under argon for about 1min and a mixture of **2** (159mg, 0.3mmol, 2 eq) and Kryptofix 21 (7mg, 0.015mmol, 0.1 eq) in 2ml of degassed N, N-dimethylformamide was added. The reaction mixture was stirred overnight under argon at room temperature, diluted with 10ml of ethyl acetate and washed sequentially with 1M HCl, saturated sodium bicarbonate solution and water. The organic layer was dried over Na_2SO_4, concentrated and purified by chromatography using hexane/acetone (3:2) as eluent. A mixture of desired product **15** and unreacted **2** was obtained.

6-Azidohexyl S- (Methyl 5-Acetamido-4, 5, 8, 9-tetra-O-acetyl-3, 5-dideoxy-D-glycero-α-D-galacto-2-nonulopyranosylonate)- (2-3)-2-O-benzoyl-3-thio-β-D-galactopyranoside (16)

The mixture of **15** and unreacted **2** was dissolved in 10ml of 80% acetic acid solution and stirred 24h at 45°C. The solvent was evaporated and the residue was loaded onto a silica column. Hexane/acetone (1:1) was used as eluent to afford white solid **16** (42mg, 32% over 3 steps).

^{1}H-NMR (400 MHz; $CDCl_3$): δ=8.15 (d, 2H, Ar, *J* = 7.1 Hz), 7.59 (t, 1H, Ar, *J* = 7.4 Hz), 7.48 (t, 2H, Ar, *J* = 7.6 Hz), 5.63-5.58 (ddd, 1H, H-8', *J* = 9.8, 5.9, 2.5 Hz), 5.22-5.15 (m, 3H, H-2, H-7', NH), 4.90 (d, 1H, H-1, *J* = 7.7 Hz), 4.83-4.76 (m, 1H, H-4'), 4.39 (dd, 1H, H-9a', $J_{9a', 9b'}$ = 12.3, $J_{9'a, 8}$=2.3 Hz), 4.05 (dd, 1H, H-9b', *J* = 12.5, *J*=5.8 Hz), 3.93-3.85 (m, 5H, H-5', H-4, OCH_2, H-6a, H-6b), 3.79-3.74 (m, 4H, OMe, H-6'), 3.70 (dd, 1H, H-3, $J_{3,2}$ = 11.7, $J_{3,4}$ = 2.6 Hz), 3.62 (s, 1H, H-5), 3.56-3.51 (m, 1H, OCH_2), 3.13 (d, 1H, OH, *J* = 4.4 Hz), 3.04-3.00 (m, 2H, CH_2N_3), 2.61 (dd, 1H, H-3'$_{eq}$, $J_{3eq,3ax}$ = 12.8 Hz, $J_{3eq,4}$ = 4.6 Hz), 2.55 (s, 1H, OH), 2.21 (s, 3H), 2.19 (d, 1H, H-3a', *J* = 2.8 Hz), 2.08 (s, 3H), 1.99 (s, 3H), 1.95-1.89 (m, 2H), 1.84 (s, 3H), 1.69 (s, 3H), 1.50-1.44 (m, 2H), 1.26 (s, 4H), 1.15 (t, *J* = 6.4 Hz, 4H). ^{13}C NMR (400 MHz; CDCl3): δ 170.93, 170.79, 170.23, 170.18, 169.4, 165.8, 133.0, 130.3, 130.1, 128.3, 102.3, 81.4, 75.1, 73.5, 70.4, 69.8, 69.3, 69.2, 67.4, 66.8, 63.0, 62.5, 53.2, 51.2, 49.1, 48.1, 37.4, 29.3,

28.5, 26.3, 25.5, 23.2, 21.5, 20.8, 20.5. HRMS (ESI): m/z calcd for $[C_{39}H_{54}N_4O_{18}SNa]^+$: 921.3052. Found: 921.3062.

6-Aminohexyl S- (5-Acetamido-3, 5-dideoxy-D-glycero-α-D-galacto-2-nonulopyranosylonate)-(2-3)-3-thio-β-D-galactopyranoside (17)

16 (47mg, 0.052mmol) was dissolved in 2ml of methanol and 0.1ml of 0.5M sodium methoxide was added. The reaction mixture was kept stirring overnight at room temperature, neutralized with acidic ion-exchange resin and concentrated. The residue was redissolved in 5ml of 0.25M sodium hydroxide solution. After stirring at room temperature overnight, acidic ion-exchange resin was added to neutralize the base and removed by filtration. Water was evaporated and the residue was dissolved in 10ml of ethanol. Catalytic amount of palladium hydroxide (20% on carbon) was added and the mixture was kept under hydrogen atmosphere (5 atm) for 10h. Palladium hydroxide was removed by filtration and ethanol was evaporated. White powered **17** (21mg, 70%) was obtained after lyophilization.

^{1}H-NMR (400 MHz; MeOD): δ=4.31 (d, *J* = 7.3 Hz, 1H), 3.93-3.88 (m, 3H), 3.86-3.82 (m, 1H), 3.76-3.51 (m, 10H), 3.46 (dd, *J* = 11.4, 2.7 Hz, 1H), 3.37 (dd, *J* = 11.3, 7.3 Hz, 1H), 3.33 (dt, *J* = 3.2, 1.6 Hz, 2H), 3.29 (d, *J* = 6.8 Hz, 2H), 2.92 (dd, *J* = 12.3, 3.4 Hz, 1H), 2.03 (s, 3H), 1.73 (dd, *J* = 11.6, 11.2 Hz, 1H), 1.67-1.60 (m, 4H), 1.43 (t, *J* = 3.5 Hz, 4H). ^{13}C NMR (400 MHz; $CDCl_3$): δ=173.97, 173.87, 131.0, 129.0, 127.6, 104.7, 84.1, 77.6, 75.6, 71.6, 69.01, 68.94, 68.71, 68.59, 68.1, 63.0, 61.6, 52.4, 51.4, 51.0, 41.5, 29.2, 28.5, 26.2, 25.3, 21.3. HRMS (ESI): m/z calcd for $[C_{23}H_{43}N_2O_{13}S]^+$: 587.2486. Found: 587.2365.

6-Chlorohexyl 2,4,6-O-benzyl-3-O- (4-methoxybenzyl)-β-D-galactopyranoside (18)

Compound **9** (900mg, 2.25mmol) was dissolved in 45ml of anhydrous tetrahydrofuran and cooled to 0^{o}C. Sodium hydride (1.35g of a 60% suspension in mineral oil, 33.7mmol, 15 eq) was added in small portions. The suspension was stirred for about 5min and benzyl bromide (1.6ml, 13.5mmol, 6 eq) was added. The reaction mixture was refluxed for 6h and cooled to 0 ^{o}C. 1M HCl was added dropwise to neutralize excessive sodium hydride. The mixture was diluted with 50ml of ethyl acetate. The organic

layer was washed with water (3x20ml), dried over Na_2SO_4, filtered and concentrated. The residue was purified by column chromatography using hexane/ethyl acetate (8:1) as eluent. White solid **18** was obtained (1.29g, 83%).

^{1}H-NMR (400 MHz; $CDCl_3$): δ=7.38-7.30 (m, 17H, Ar), 6.87 (d, 2H, Ar, J = 8.7 Hz), 4.94 (t, 2H, OCH_2Ph, J = 11.3 Hz), 4.79 (d, 1H, H-6a, $J_{6a,\,6b}$ = 11.0 Hz), 4.68 (d, 1H, H-4, J = 3.1 Hz), 4.63 (d, 1H, H-6b, J = 11.7 Hz), 4.44 (q, 2H, OCH_2Ph, J = 9.1 Hz), 4.35 (d, 1H, H-1, J = 7.7 Hz), 3.97-3.91 (m, 1H, OCH_2), 3.87 (dd, 1H, H-4, J = 2.6, 0.3 Hz), 3.82 (s, 3H, OCH_3), 3.80-3.78 (m, 1H, H-2), 3.60-3.58 (m, 2H, OCH_2Ph), 3.56-3.49 (m, 4H, OCH_2, H-3, CH_2Cl), 1.76-1.71 (m, 2H, linker-H), 1.68-1.63 (m, 2H, linker-H), 1.46-1.41 (m, 4H, linker-H). ^{13}C NMR (400 MHz; CDCl3): δ=138.9, 138.7, 138.0, 130.6, 129.2, 128.4, 128.15, 128.01, 127.88, 127.5, 113.8, 104.0, 81.9, 79.6, 75.2, 74.5, 73.55, 73.51, 73.43, 72.7, 69.8, 69.0, 55.3, 45.1, 32.5, 29.6, 26.7, 25.5. HRMS (ESI): m/z calcd for $[C_{41}H_{49}ClO_7Na]^+$: 711.3065. Found: 711.3065.

6-Chlorohexyl 2,4,6-O-benzyl-β-D-galactopyranoside (19)

18 (1.28g, 1.86mmol) was dissolved in 40ml of acetonitrile/H_2O (16:1) and cerium (IV) ammonium nitrate (3.06g, 5.58mmol, 3 eq) was added. The reaction mixture was stirred at room temperature for 2h and quenched with saturated sodium thiosulfate solution. The organic layer was washed with water, dried over Na_2SO_4, filtered and concentrated. The residue was purified by flash chromatography using hexane/ethyl acetate (3:1) and afforded compound **19** (587mg, 55%).

^{1}H-NMR (400 MHz; $CDCl_3$): δ=7.39-7.30 (m, 15H), 4.98 (d, 1H, J = 11.5 Hz, H-6a), 4.80 (d, 1H, H-6b), 4.72-4.65 (m, 2H, OCH_2Ph), 4.54-4.46 (m, 2H, OCH_2Ph), 4.36 (d, 1H, H-1, J = 7.4 Hz), 3.99-3.93 (m, 1H, OCH_2), 3.89 (d, 1H, H-4, J = 3.0 Hz), 3.69-3.64 (m, 4H, OCH_3, OCH_2), 3.58 (dd, 1H, H-2, $J_{2,3}$ = 9.6 Hz, $J_{2,1}$ = 7.6 Hz), 3.54-3.50 (m, 3H, H-3, CH_2N_3), 2.27 (d, 1H, OH, J = 4.8 Hz), 1.78-1.73 (m, 2H, linker-H), 1.69-1.65 (m, 2H, linker-H), 1.47-1.41 (m, 4H, linker-H). ^{13}C NMR (400 MHz; CDCl3): δ=138.52, 138.49, 137.9, 128.50, 128.45, 128.33, 128.22, 128.05, 127.8, 103.8, 79.6, 75.5, 75.0, 74.6,

74.1, 73.59, 73.54, 69.7, 68.8, 45.0, 32.5, 29.6, 26.7, 25.5. HRMS (ESI): m/z calcd for $[C_{33}H_{41}ClO_6Na]^+$: 591.2490. Found: 591.2258.

6-Chlorohexyl 2,4,6-O-benzyl-3-O-propargyl-β-D-galactopyranoside (20)

Compound **19** (116mg, 0.20mmol) was dissolved in 5ml of anhydrous tetrahydrofuran and cooled to 0°C. Sodium hydride (41mg of a 60% suspension in mineral oil, 1mmol, 5 eq) was added. The suspension was stirred for about 2min and propargyl bromide (60ul, 0.4mmol, 2 eq) was added. The reaction mixture was stirred at 50°C for 3h and cooled to 0 °C. 1M HCl was added dropwise to neutralize excessive sodium hydride. The mixture was diluted with 10ml of ethyl acetate. The organic layer was washed with water (3x5ml), dried over Na_2SO_4, filtered and concentrated. The residue was purified by column chromatography using hexane/ethyl acetate (5:1) as eluent. White solid **20** was obtained (93mg, 75%).

^{1}H-NMR (400 MHz; $CDCl_3$): δ=7.43-7.30 (m, 15H, Ar), 4.95 (t, 2H, OCH_2Ph, J = 10.8Hz), 4.77 (d, 1H, H-6a, J = 11.1 Hz), 4.68 (d, H-6b, J = 11.8 Hz), 4.51-4.43 (m, 2H, OCH_2Ph), 4.39-4.36 (m, 3H, H-1, OCH_2Ph), 3.99-3.95 (m, 2H, H-4, OCH_2), 3.78 (dd, 1H, H-2, $J_{2,3}$ = 9.7 Hz, $J_{2,1}$ = 7.7 Hz), 3.64-3.58 (m, 4H, H-5, H-3, OCH_2CCH), 3.54-3.50 (m, 3H, OCH_2, CH_2Cl), 2.47 (t, 1H, alkyn-H, J = 2.4 Hz), 1.78-1.73 (m, 2H, linker-H), 1.70-1.65 (m, 2H, linker-H), 1.47-1.42 (m, 4H, linker-H). ^{13}C NMR (400 MHz; CDCl3): δ= 138.81, 138.65, 138.0, 128.50, 128.45, 128.32, 128.18, 127.96, 127.91, 127.6, 103.9, 81.7, 80.4, 79.6, 75.1, 74.56, 74.40, 74.0, 73.57, 73.46, 69.8, 69.0, 58.7, 45.1, 32.6, 29.6, 26.7, 25.5. HRMS (ESI): m/z calcd for $[C_{36}H_{43}ClO_6Na]^+$: 629.2646. Found: 629.2631.

Chloro-click- (2-3) disaccharide (21)

In a flask containing **20** (93mg, 0.15mmol) and **4** (87mg, 0.16mmol, 1.1 eq), 2ml of acetonitrile was added, followed by addition of N, N-diisopropylethylamine (50ul, 0.3mmol, 2 eq) and copper (I) iodine (29mg, 0.15mmol, 1eq). The reaction mixture was kept stirring overnight at 60°C, concentrated and loaded onto a silica column. Hexane/acetone (2:3) was used as eluent to afford **21** (156mg, 91%).

^{1}H-NMR (400 MHz; $CDCl_3$): δ=8.02 (s, 1H), 7.41-7.24 (m, 18H), 5.47-5.43 (m, 1H), 5.40-5.37 (m, 1H), 5.28 (dd, *J* = 9.9, 0.3 Hz, 1H), 5.19 (td, *J* = 10.9, 3.9 Hz, 1H), 4.93 (t, *J* = 12.7 Hz, 3H), 4.85-4.79 (m, 2H), 4.64 (d, *J* = 11.8 Hz, 1H), 4.48-4.39 (m, 2H), 4.37 (d, *J* = 7.6 Hz, 1H), 4.33 (d, *J* = 1.8 Hz, 1H), 4.19 (dd, *J* = 12.8, 2.5 Hz, 1H), 4.13 (d, *J* = 9.9 Hz, 1H), 4.02 (dd, *J* = 12.3, 5.4 Hz, 1H), 3.97-3.92 (m, 2H), 3.83-3.77 (m, 2H), 3.69 (s, 3H), 3.64-3.61 (m, 1H), 3.61-3.56 (m, 2H), 3.52-3.47 (m, 5H), 3.44-3.43 (m, 1H), 2.70-2.64 (m, 1H), 2.12 (s, 3H), 2.10 (s, 3H), 2.08 (s, 3H), 2.01 (s, 3H), 1.93 (s, 3H), 1.76-1.70 (m, 3H), 1.66-1.64 (m, 2H), 1.44-1.42 (m, 4H). ^{13}C NMR (101 MHz; CDCl3): δ 170.8, 170.5, 170.3, 170.00, 169.96, 166.5, 146.1, 138.90, 138.71, 138.0, 128.54, 128.40, 128.28, 128.09, 128.04, 127.84, 127.72, 127.5, 121.6, 103.9, 88.4, 82.8, 79.6, 75.0, 74.4, 73.71, 73.51, 69.7, 69.1, 68.5, 67.8, 66.8, 64.8, 62.2, 54.0, 49.3, 45.1, 36.1, 32.5, 29.6, 26.7, 25.5, 23.2, 21.2, 20.85, 20.76, 20.71. HRMS (ESI): m/z calcd for $[C_{56}H_{71}ClN_4O_{18}Na]^+$: 1145.4349. Found: 1145.4332.

Azido-click- (2-3) disaccharide (22)

Compound **21** (129mg, 0.11mmol) was dissolved in 2ml of anhydrous N, N-dimethylformamide and sodium azide (37mg, 0.55 mmol, 5eq) was added. The reaction mixture was stirred at 50^{o}C over-night, diluted with ethyl acetate (8ml), washed with water and brine. The organic layer was dried over Na_2SO_4, filtered, concentrated, and purified by silica column using hexane/acetone (2:3) as eluent. White solid **22** was obtained (78mg, 58%).

^{1}H-NMR (400 MHz; $CDCl_3$): δ=8.02 (s, 1H), 7.40-7.25 (m, 20H), 5.45-5.43 (m, 1H), 5.40-5.37 (m, 1H), 5.22-5.15 (m, 1H), 4.93 (dd, *J* = 13.3, 11.5 Hz, 3H), 4.85-4.79 (m, 3H), 4.65-4.62 (m, 1H), 4.48-4.42 (m, 2H), 4.39-4.33 (m, 2H), 4.21-4.17 (m, 1H), 4.15-4.13 (m, 1H), 4.04-3.99 (m, 1H), 3.97-3.91 (m, 2H), 3.82-3.78 (m, 1H), 3.69 (s, 3H), 3.62 (t, *J* = 4.9 Hz, 1H), 3.60-3.56 (m, 3H), 3.54-3.46 (m, 3H), 3.44 (dd, *J* = 4.5, 0.3 Hz, 1H), 3.24-3.21 (m, 2H), 2.69-2.63 (m, 1H), 2.12-2.08 (m, 8H), 2.00 (s, 3H), 1.93 (s, 3H), 1.64-1.55 (m, 4H), 1.41-1.39 (m, 4H). ^{13}C NMR (400 MHz; $CDCl_3$): δ=170.8, 170.5, 170.0, 166.5, 162.5, 146.1, 138.9, 138.7, 128.54, 128.40, 128.28, 128.09, 128.02, 127.83, 127.72, 127.5, 121.6, 103.9, 88.4, 82.8, 79.6, 75.0, 74.4, 73.7, 73.5, 69.7, 69.1, 68.5, 67.80, 67.78, 66.9, 64.8, 62.2, 54.0, 51.4, 36.5,

36.2, 31.4, 29.72, 29.61, 28.8, 26.6, 25.8, 23.2, 21.2, 20.85, 20.76, 20.71. HRMS (ESI): m/z calcd for $[C_{56}H_{71}N_7O_{18}Na]^+$: 1152.4753. Found: 1152.4617.

Amino-click- (2-3) disaccharide (23)

22 (58mg, 0.087mmol) was dissolved in 2ml of methanol and 0.1ml of 0.5M sodium methoxide was added. The reaction mixture was kept stirring overnight at room temperature, neutralized with acidic ion-exchange resin and concentrated. The residue was redissolved in 5ml of 0.25M sodium hydroxide solution. After stirring at room temperature overnight, acidic ion-exchange resin was added to neutralize the base and removed by filtration. Water was evaporated and the residue was dissolved in 10ml of ethanol. Catalytic amount of palladium hydroxide (20% on carbon) was added and the mixture was kept under hydrogen atmosphere (5 atm) for 10h. Palladium hydroxide was removed by filtration and ethanol was evaporated. The residue was purified by Bio gel P-2 column and white powder **23** (25mg, 62%) was obtained after lyophilization.

^{1}H-NMR (400 MHz; D_2O): δ=7.90 (s, 1H), 4.33-4.31 (m, 1H), 4.07 (dd, J = 0.6, 0.2 Hz, 1H), 3.97-3.91 (m, 2H), 3.85-3.67 (m, 8H), 3.58-3.38 (m, 9H), 2.91 (t, J = 7.5 Hz, 1H), 2.19-2.14 (m, 1H), 2.00-1.96 (m, 4H), 1.79-1.67 (m, 2H), 1.57-1.53 (m, 4H), 1.32-1.31 (m, 4H). HRMS (ESI): m/z calcd for $[C_{26}H_{45}N_5O_{14}Na]^+$: 674.2861. Found: 674.2863.

6-Chlorohexyl 6-O- t-butyldimethylsilyl-β-D-galactopyranoside (24)

Compound **8** (370mg, 1.24mmol) was dissolved in 20ml of anhydrous methanol and dibutyltin oxide (462mg, 1.86mmol, 1.5 eq) was added. The reaction mixture was refluxed for ~4 h until the solution became clear. The solvent was evaporated and the residue was redissolved in 10ml of toluene followed by addition of t-butyldimethylchloride (280mg, 1.86mmol, 1.5 eq). The reaction mixture was stirred overnight at 100^{o}C, concentrated and purified by column chromatography using hexane/ethyl acetate (1:1) as eluent. **24** was obtained (324mg, 63%).

^{1}H-NMR (400 MHz; $CDCl_3$): δ=4.23 (d, *J* = 7.6 Hz, 1H), 4.04 (d, *J* = 2.6 Hz, 1H), 3.95-3.85 (m, 3H), 3.66 (d, *J* = 7.8 Hz, 1H), 3.60-3.59 (m, 1H), 3.57-3.54 (m, 3H), 3.50 (dd, *J* = 12.5, 6.3 Hz, 1H), 3.13-3.12 (m, 1H), 3.02 (d, *J* = 3.6 Hz, 1H), 2.87 (d, *J* = 0.4 Hz, 1H), 1.80 (t, *J* = 7.3 Hz, 2H), 1.66 (t, *J* = 7.3 Hz, 2H), 1.48-1.40 (m, 4H), 0.91 (s, 9H), 0.10 (d, *J* = 1.7 Hz, 6H). ^{13}C NMR (400 MHz; CDCl3): δ 103.0, 74.4, 73.7, 72.1, 69.7, 68.9, 62.5, 45.0, 32.5, 29.5, 26.6, 25.8, 25.3, 18.3. HRMS (ESI): m/z calcd for $[C_{18}H_{37}ClO_6SiNa]^+$: 435.1946. Found: 435.1959.

6-Chlorohexyl 2,3,4-O- benzyl-6-O- t-butyldimethylsilyl-β-D-galactopyranoside (25)

24 (314mg, 0.76mmol) was dissolved in 25ml of anhydrous tetrahydrofuran and cooled to 0^{o}C. Sodium hydride (456g of a 60% suspension in mineral oil, 11.4mmol, 15 eq) was added. The suspension was stirred for about 2min and benzyl bromide (542ul, 4.56mmol, 6 eq) was added. The reaction mixture was refluxed overnight and cooled to 0 ^{o}C. 1M HCl was added dropwise to neutralize excessive sodium hydride. The mixture was diluted with 40ml of ethyl acetate. The organic layer was washed with water (3x20ml), dried over Na_2SO_4, filtered and concentrated. The residue was purified by column chromatography using hexane/ethyl acetate (8:1) as eluent. White solid **25** was obtained (420mg, 81%).

^{1}H-NMR (400 MHz; $CDCl_3$): δ=7.34 (dt, *J* = 15.1, 7.6 Hz, 15H), 4.96 (dd, *J* = 16.6, 11.2 Hz, 2H), 4.80 (dd, *J* = 11.4, 4.1 Hz, 2H), 4.69 (dd, *J* = 28.6, 11.8 Hz, 2H), 4.35 (d, *J* = 7.7 Hz, 1H), 3.98-3.92 (m, 1H), 3.88 (d, *J* = 2.7 Hz, 1H), 3.83 (dd, *J* = 9.6, 7.8 Hz, 1H), 3.71 (dd, *J* = 6.5, 2.9 Hz, 2H), 3.54-3.50 (m, 4H), 3.38 (t, *J* = 6.6 Hz, 1H), 1.77-1.72 (m, 2H), 1.69-1.64 (m, 2H), 1.46-1.43 (m, 4H), 0.90 (s, 9H), 0.06 (s, 6H). ^{13}C NMR (400 MHz; CDCl3): δ=138.9, 128.34, 128.27, 128.10, 128.02, 127.6, 104.0, 82.2, 79.7, 75.11, 75.07, 73.7, 73.1, 69.7, 61.8, 32.5, 29.6, 26.7, 25.9, 25.5, 18.2. HRMS (ESI): m/z calcd for $[C_{39}H_{55}ClO_6SiNa]^+$: 705.3354. Found: 705. 705.3333.

6-Chlorohexyl 2,3,4-O- benzyl -β-D-galactopyranoside (26)

25 (656mg**,** 0.96mmol) was dissolved in 20ml of methanol and iodine (200mg, 1% w/v) was added. The reaction mixture was refluxed for 3h and the iodine was neutralized with saturated sodium thiosulfate solution. The mixture was diluted with 20ml of ethyl acetate and the aqueous layer was extract-

ed with 10ml of ethyl acetate. The organics were combined and washed with water (2x10ml), dried over Na_2SO_4, filtered and concentrated. The residue was purified by column chromatography using hexane/ethyl acetate (2:1) as eluent. **26** was obtained (392mg, 72%).

^{1}H-NMR (400 MHz; $CDCl_3$): δ=7.38-7.31 (m, 15H), 4.97 (t, *J* = 11.1 Hz, 2H), 4.86-4.75 (m, 3H), 4.69 (d, *J* = 11.8 Hz, 1H), 4.38 (d, *J* = 7.8 Hz, 1H), 3.99-3.93 (m, 1H), 3.88-3.83 (m, 1H), 3.80-3.75 (m, 2H), 3.57-3.47 (m, 5H), 3.40-3.37 (m, 1H). ^{13}C NMR (101 MHz; CDCl3): δ 138.7, 138.43, 138.24, 128.7, 128.46, 128.32, 128.0, 127.6, 104.1, 82.3, 79.7, 75.2, 74.5, 74.1, 73.4, 72.8, 69.9, 62.0, 45.0, 32.5, 29.6, 26.7, 25.5. HRMS (ESI): m/z calcd for $[C_{33}H_{41}ClO_6Na]^+$: 591.2489. Found: 591.2484.

6-Chlorohexyl 2,3,4-O-benzyl-6-O-propargyl-β-D-galactopyranoside (27)

Compound **26** (381mg, 0.67mmol) was dissolved in 10ml of anhydrous tetrahydrofuran and cooled to 0^{o}C. Sodium hydride (134mg of a 60% suspension in mineral oil, 3.34mmol, 5 eq) was added. The suspension was stirred for about 2min and propargyl bromide (200ul, 1.34mmol, 2 eq) was added. The reaction mixture was stirred at 50^{o}C for 17h and cooled to 0^{o}C. 1M HCl was added dropwise to neutralize excessive sodium hydride. The mixture was diluted with 20ml of ethyl acetate. The organic layer was washed with water (3x10ml), dried over Na_2SO_4, filtered and concentrated. The residue was purified by column chromatography using hexane/ethyl acetate (3:1) as eluent. White solid **20** was obtained (336mg, 83%).

^{1}H NMR (400 MHz; $CDCl_3$): δ=7.39-7.29 (m, 15H), 4.96 (dd, *J* = 17.5, 11.3 Hz, 2H), 4.81-4.68 (m, 4H), 4.37 (d, *J* = 7.7 Hz, 1H), 4.05 (t, *J* = 2.3 Hz, 2H), 3.98-3.93 (m, 1H), 3.90 (s, 1H), 3.83 (dd, *J* = 9.6, 7.8 Hz, 1H), 3.66-3.58 (m, 2H), 3.53 (td, *J* = 8.6, 4.5 Hz, 5H). ^{13}C NMR (400 MHz; $CDCl_3$): δ 138.80, 138.61, 138.51, 128.47, 128.39, 128.29, 128.19, 128.03, 127.6, 104.0, 82.1, 79.6, 75.2, 74.7, 74.5, 73.28, 73.24, 73.08, 69.8, 68.7, 58.6, 45.1, 32.5, 29.6, 26.7, 25.5. HRMS (ESI): m/z calcd for $[C_{36}H_{43}ClO_6Na]^+$: 629.2646. Found: 629.2629.

Chloro-click- (2-6) disaccharide (28)

In a flask containing **27** (97mg, 0.19mmol) and **4** (114mg, 0.19mmol, 1 eq), 2ml of acetonitrile was added, followed by addition of N, N-diisopropylethylamine (62ul, 0.38mmol, 2eq) and copper (I) iodine (54mg, 0.28mmol, 1.5eq). The reaction mixture was kept stirring overnight at 60^{o}C, concentrated and loaded onto a silica column. Hexane/acetone (2:3) was used as eluent to afford **21** (192mg, 91%).

^{1}HNMR (400 MHz; $CDCl_3$): δ=7.93 (s, 1H, triazole-H), 7.37-7.26 (m, 15H, Ar), 5.53-5.38 (m, 4H, NH, H-7', H-8'), 5.22-5.15 (m, 1H, H-4'), 4.94 (dd, 2H, OCH_2Ph, J = 16.9, 11.3 Hz), 4.79-4.67 (m, 4H, OCH_2Ph), 4.60 (d, 1H, H-6a, $J_{6b,6a}$ = 12.1 Hz), 4.49 (d, 1H, H-6b, $J_{6b,6a}$ = 12.1 Hz), 4.37-4.32 (m, 2H, H-1, H-9a'), 4.23 (dd, 1H, H-9b', $J_{9b',9a'}$ = 12.4Hz, $J_{9b',8'}$=2.3 Hz), 4.14-4.03 (m, 2H, H-5'), 3.97-3.89 (m, 2H, H-4, OCH_2), 3.84-3.79 (m, 2H, H-6', H-2), 3.76 (s, 3H, OMe), 3.69-3.63 (m, 2H, H-5, H-3), 3.59-3.47 (m, 6H, OCH_2-Triazole, OCH_2Ar, CH_2Cl), 2.65 (t, 1H, H-3e', J = 12.6 Hz), 2.17-2.13 (m, 4H, OAc, H-3a'), 2.10, 2.09 (s, 2x3H, OAc), 2.03 (s, 3H, OAc), 1.92 (s, 3H, OAc), 1.75-1.71 (m, 2H, linker-H), 1.66-1.63 (m, 2H, linker-H), 1.43-1.42 (m, 4H, linker-H). ^{13}C NMR (400 MHz; CDCl3): δ=170.8, 170.5, 170.32, 170.19, 170.0, 166.5, 145.2, 138.81, 138.67, 138.52, 128.47, 128.35, 128.26, 128.19, 128.01, 127.5, 121.8, 103.9, 88.4, 82.2, 79.5, 75.1, 74.5, 73.7, 73.3, 72.9, 69.8, 69.5, 68.5, 67.9, 66.8, 64.4, 62.3, 54.1, 49.2, 45.0, 36.2, 32.5, 29.6, 26.7, 25.5, 23.2, 21.3, 20.85, 20.75. HRMS (ESI): m/z calcd for $[C_{56}H_{71}ClN_4O_{18}Na]^+$: 1145.4349. Found: 1145.4371.

Azido-click- (2-6) disaccharide (29)

29 was synthesized from **28** (182mg, 0.16mmol) and in an analogues manner described in the synthesis of **23**. Purification by Bio gel P-2 column followed by lyophilization yielded white powder **30** (25mg, 62%). Compound **28** (182mg, 0.16mmol) was dissolved in 3ml of anhydrous N, N-dimethylformamide and sodium azide (105mg, 1.6 mmol, 10eq) was added. The reaction mixture was stirred at 55^{o}C overnight, diluted with ethyl acetate (8ml), washed with water and brine. The organic layer was dried over Na_2SO_4, filtered, concentrated, and purified by silica column using hexane/acetone (2:3) as eluent. White solid **29** was obtained (91mg, 50%).

^{1}H NMR (400 MHz; $CDCl_3$): δ=7.93 (s, 1H, triazole-H), 7.35-7.28 (m, 15H, Ar), 5.57-5.35 (m, 4H, NH, H-7', H-8'), 5.22-5.15 (m, 1H, H-4'), 4.94 (dd, 2H, OCH_2Ar, J = 16.6, 11.4 Hz), 4.80-4.67 (m, 4H, OCH_2Ph), 4.60 (d, 1H, H-6a, $J_{6b,6a}$ = 12.1 Hz), 4.50 (d, 1H, H-6b, $J_{6b,6a}$ = 12.0 Hz), 4.37-4.32 (m, 2H, H-1, H-9a'), 4.23 (dd, 1H, H-9b', $J_{9b',9a'}$ = 12.3Hz, $J_{9b',8'}$=1.8), 4.13-4.04 (m, 3H, H-5'), 3.95-3.90 (m, 2H, H-4, OCH_2), 3.84-3.73 (m, 5H, H-6', H-2, OMe), 3.67 (t, J = 5.7 Hz, 2H), 3.59-3.46 (m, 4H), 3.22 (t, J = 6.9 Hz, 2H), 2.65 (t, 1H, H-3e', J = 12.6 Hz), 2.18-2.13 (m, 4H, OAc, H-3a'), 2.11, 2.09 (s, 6H, 2xOAc), 2.04 (s, 3H, OAc), 1.92 (s, 3H, OAc), 1.65-1.54 (m, 4H, linker-H), 1.42-1.36 (m, 4H, linker-H). ^{13}C NMR (400 MHz; CDCl3): δ=170.8, 170.55, 170.37, 170.21, 170.0, 166.4, 145.2, 138.84, 138.68, 138.53, 128.46, 128.34, 128.25, 128.20, 128.0, 127.5, 121.8, 103.9, 88.4, 82.2, 79.5, 75.1, 74.5, 73.7, 73.36, 73.33, 72.9, 69.8, 69.4, 68.5, 67.9, 66.9, 64.4, 62.3, 54.0, 51.4, 49.2, 29.6, 28.8, 26.6, 25.8, 23.2, 21.3, 20.84, 20.77, 20.74. HRMS (ESI): m/z calcd for $[C_{56}H_{71}N_7O_{18}Na]^+$: 1152.4753. Found: 1152.4744.

Amino-click- (2-6) disaccharide (30)

30 was synthesized from **29** (58mg, 0.087mmol) in an analogues manner describe in the synthesis of **23**. Purification by Bio gel P-2 column followed by lyophilization yielded white powder **30** (25mg, 62%). HRMS (ESI): m/z calcd for $[C_{26}H_{45}N_5O_{14}Na]^+$: 674.2861. Found: 674.3046.

2.3.3 Glycan microarray fabrication

Microarrays were printed using a OmniGrid Micro system. About 0.6 nl of 200 uM of amine containing glycans in printing buffer (300 mM phosphate containing 0.005% Tween-20, pH 8.5) was deposited onto NHS-activated glass slides by robotic pin. Each compound was printed in a replicate of eight. For the conjugation to be completed, the printed slides were kept in an atmosphere of 55% humidity for 30 min and dried in desiccator at least overnight before use. Next, the unreacted NHS groups were quenched by blocking buffer (50mM ethylamine in 50mM borate buffer, pH 8.6) and the slides were dried under continuous airflow before assays with proteins/viruses.

2.3.4 Lectin and HA binding study

50μl of rhodamine labeled wheat germ agglutinin (WGA, Vector Laboratories) or precomplexed HA (Protein Sciences, HA protein: primary antibody: secondary antibody=4:2:1, 30 min on ice) was applied directly onto printed slide at the concentration of 100ug/ml in PBST buffer (PBS containing 0.005% Tween-20) and covered with a microscope slide. The printed slide was incubated at rt for 1h. Unbound proteins were washed away in the wash step, in which the printed slide was immersed into 3 X 50ml of PBST buffer, 1 X 50ml of PBS buffer and 4 X 50ml of DI water successively. Slides were dried under continuous airflow and stored in a dark environment before image analysis.

2.3.5 NA treatment

Printed slides were incubated with either one of NAs: H1N1 and H5N1 NA (Sino Biotechnology Inc.) at rt for 2h and then washed with 3X50ml of PBST buffer, 1X50ml of PBS buffer and 4X50ml of DI water successively.

2.3.6 Inactivated influenza virus binding assay

BPL-inactivated influenza virus A/Puerto Rico/8/1934 stock solution (BEI Resources) was serially diluted in PBST buffer to make the final concentration of $3.5X10^4$, $3.5X10^3$, $3.5X10^2$, respectively. 50 μl of the diluted virus containing solutions were applied onto printed slides and covered with a microscope slide. The slides were incubated at rt for 1h, washed with several times with buffer and dried. 50 μl of anti sera (1:100 dilution) was applied and incubated for 1h followed by wash step. 50 μl of secondary antibody (1:250 dilution) was applied onto the surface and incubated in dark for 1h. The slides were washed, dried and kept in dark before image analysis.

2.3.7 Active influenza virus binding assay

The active influenza viruses were propagated in MDCK cell in our lab. The detailed procedure can be found in the experimental section of Chapter III. The titer of different viral strains was adjusted to

$3X10^4$ PFU/ml before incubation. One printed slide was divided into 8 separated wells by a plastic 8-well divider. All 10 sialosides were printed in each well. 200 µl of virus suspension in PBST buffer was added to each well and the slide was incubated at rt for 1h, followed by several wash. 200 µl of anti sera (1:1000 dilution) was applied and incubated for 1h followed by wash step. 200 µl of secondary antibody (1:1000 dilution) was applied onto the surface and incubated in dark for 1h. The slides were washed, dried and kept in dark before image analysis.

2.3.8 Image acquisition and analysis

Fluorescence intensities were detected by GenePix 4000B scanner and image analyses were carried out by using Adobe Photoshop CS6. Data were plotted by using Microsoft EXCEL software.

2.4 Conclusion and future direction

To summarize, I have synthesized five S- and N-linked sialosides, together with the three C-linked sialosides synthesized by Dr. Yang Yang and two commercial available O-linked sialosides, we were able to fabricate a small robust sialoside microarray. We were able to probe sialic acid binding proteins such as lectins and viral HA. We also demonstrated the stability of these sialosides towards viral NA and intact influenza viruses. In addition, we demonstrated the ability of these sialosides to capture viral particles, presumably through binding to both HA and NA, at ambient temperature and without addition of inhibitors. Previously, we have demonstrated that glycans are highly robust(*12*) and therefore these could be readily translated to a field deployable device. We are currently involved in expanding the scope of this work by synthesizing a larger library of robust sialosides and developing a 'fingerprint pattern of recognition" for different influenza virus types.

REFERENCE

1. M. von Itzstein, The war against influenza: discovery and development of sialidase inhibitors. *Nat Rev Drug Discov* **6**, 967 (Dec, 2007).
2. A. E. Fiore *et al.*, Prevention and control of influenza: recommendations of the Advisory Committee on Immunization Practices (ACIP), 2008. *MMWR Recomm Rep* **57**, 1 (Aug 8, 2008).
3. A. O'Dowd, WHO raises level of alert on flu pandemic. *Bmj* **338**, b1777 (2009).
4. New influenza A (H1N1) virus: WHO guidance on public health measures, 11 June 2009. *Wkly Epidemiol Rec* **84**, 261 (Jun 26, 2009).
5. M. R. Sills *et al.*, Resource burden at children's hospitals experiencing surge volumes during the spring 2009 H1N1 influenza pandemic. *Acad Emerg Med* **18**, 158 (Feb).
6. W. J. Rodriguez, H. R. Schwartz, M. M. Thorne, Evaluation of diagnostic tests for influenza in a pediatric practice. *The Pediatric Infectious Disease Journal* **21**, 193 (2002).
7. A. Balish *et al.*, Evaluation of rapid influenza diagnostic tests for detection of novel influenza A (H1N1) Virus - United States, 2009. *MMWR Wkly Rep* **58**, 826 (Aug 7, 2009).
8. R. R. Kale *et al.*, Detection of intact influenza viruses using biotinylated biantennary S-sialosides. *J Am Chem Soc* **130**, 8169 (Jul 2, 2008).
9. J. H. Kim, F. Huang, M. Ly, R. J. Linhardt, Stereoselective synthesis of a C-linked neuraminic acid disaccharide: potential building block for the synthesis of C-analogues of polysialic acids. *J Org Chem* **73**, 9497 (Dec 5, 2008).
10. R. R. Kale, C. M. Clancy, R. M. Vermillion, E. A. Johnson, S. S. Iyer, Synthesis of soluble multivalent glycoconjugates that target the Hc region of botulinum neurotoxin A. *Bioorg Med Chem Lett* **17**, 2459 (May 1, 2007).
11. A. K. Adak *et al.*, Bishydrazide glycoconjugates for lectin recognition and capture of bacterial pathogens. *Bioconjug Chem* **21**, 2065 (Nov 17, 2010).

12. D. M. Hatch, A. A. Weiss, R. R. Kale, S. S. Iyer, Biotinylated Bi- and Tetra-antennary Glycoconjugates for Escherichia coli Detection. *ChemBioChem* **9**, 2433 (Oct 13, 2008).

13. A. A. Kulkarni, A. A. Weiss, S. S. Iyer, Detection of carbohydrate binding proteins using magnetic relaxation switches. *Anal Chem* **82**, 7430 (Sep 1, 2010).

14. S. Fukui, T. Feizi, C. Galustian, A. M. Lawson, W. Chai, Oligosaccharide microarrays for high-throughput detection and specificity assignments of carbohydrate-protein interactions. *Nat Biotechnol* **20**, 1011 (Oct, 2002).

15. T. Feizi, F. Fazio, W. Chai, C. H. Wong, Carbohydrate microarrays - a new set of technologies at the frontiers of glycomics. *Curr Opin Struct Biol* **13**, 637 (Oct, 2003).

16. T. Horlacher, P. H. Seeberger, Carbohydrate arrays as tools for research and diagnostics. *Chem Soc Rev* **37**, 1414 (Jul, 2008).

17. J. Stevens *et al.*, Glycan microarray analysis of the hemagglutinins from modern and pandemic influenza viruses reveals different receptor specificities. *J Mol Biol* **355**, 1143 (Feb 3, 2006).

18. J. Stevens, O. Blixt, J. C. Paulson, I. A. Wilson, Glycan microarray technologies: tools to survey host specificity of influenza viruses. *Nat Rev Microbiol* **4**, 857 (Nov, 2006).

19. J. Stevens *et al.*, Structure and receptor specificity of the hemagglutinin from an H5N1 influenza virus. *Science* **312**, 404 (Apr 21, 2006).

20. A. Chandrasekaran *et al.*, Glycan topology determines human adaptation of avian H5N1 virus hemagglutinin. *Nat Biotechnol* **26**, 107 (Jan, 2008).

21. J. C. Wilson, M. J. Kiefel, D. I. Angus, M. von Itzstein, Investigation of the stability of thiosialosides toward hydrolysis by sialidases using NMR spectroscopy. *Org Lett* **1**, 443 (Aug 12, 1999).

22. K. C. Bradley *et al.*, Analysis of influenza virus hemagglutinin receptor binding mutants with limited receptor recognition properties and conditional replication characteristics. *J Virol* **85**, 12387 (Dec, 2011).

23. H. Y. Liao *et al.*, Differential receptor binding affinities of influenza hemagglutinins on glycan arrays. *J Am Chem Soc* **132**, 14849 (Oct 27, 2010).

24. J. Heimburg-Molinaro *et al.*, Probing virus-glycan interactions using glycan microarrays. *Methods Mol Biol* **808**, 251 (2012).

25. A. K. Adak, C.-C. Yu, C.-F. Liang, C.-C. Lin, Synthesis of sialic acid-containing saccharides. *Curr. Opin. Chem. Biol.* **17**, 1030 (2013).

26. Z. J. Witczak, R. Chhabra, H. Chen, X.-Q. Xie, Thiosugars II. A novel approach to thiodisaccharides; the synthesis of 3-deoxy-4-thiocellobiose from levoglucosenone. *Carbohydr. Res.* **301**, 167 (1997).

27. Y. Suzuki, K. Sato, M. Kiso, A. Hasegawa, New ganglioside analogs that inhibit influenza virus sialidase. *Glycoconjugate J.* **7**, 349 (1990).

28. J. C. Wilson, M. J. Kiefel, D. I. Angus, I. M. von, Investigation of the Stability of Thiosialosides toward Hydrolysis by Sialidases Using NMR Spectroscopy. *Org. Lett.* **1**, 443 (1999).

29. G. Sulzenbacher, H. Driguez, B. Henrissat, M. Schuelein, G. J. Davies, Structure of the Fusarium oxysporum endoglucanase I with a nonhydrolyzable substrate analog: Substrate distortion gives rise to the preferred axial orientation for the leaving group. *Biochemistry* **35**, 15280 (1996).

30. D. Horton, D. H. Hutson, M. L. Wolfrom, Developments in the chemistry of thio sugars. *Advan. Carbohydrate Chem.* **18**, 123 (1963).

31. D. Carriere, S. J. Meunier, F. D. Tropper, S. Cao, R. Roy, Phase transfer catalysis toward the synthesis of O-, S-, Se- and C-glycosides. *J. Mol. Catal. A: Chem.* **154**, 9 (2000).

32. S. Cao, R. Roy, Phase transfer catalyzed anomeric nucleophilic substitutions occur by an SN2-type mechanism. *Carbohydr. Lett.* **2**, 27 (1996).

33. J. R. Rich, D. R. Bundle, S-linked ganglioside analogues for use in conjugate vaccines. *Org Lett* **6**, 897 (Mar 18, 2004).

34. J. R. Rich, W. W. Wakarchuk, D. R. Bundle, Chemical and chemoenzymatic synthesis of S-linked ganglioside analogues and their protein conjugates for use as immunogens. *Chemistry* **12**, 845 (Jan 11, 2006).

35. D. M. Lewallen, D. Siler, S. S. Iyer, Factors Affecting Protein-Glycan Specificity: Effect of Spacers and Incubation Time. *ChemBioChem* **10**, 1486 (May 26, 2009).

36. D. M. Lewallen, D. Siler, S. S. Iyer, Factors Affecting Protein-Glycan Specificity: Effect of Spacers and Incubation Time. *ChemBioChem* **10**, 1486 (2009).

37. P.-H. Liang, S.-K. Wang, C.-H. Wong, Quantitative Analysis of Carbohydrate-Protein Interactions Using Glycan Microarrays: Determination of Surface and Solution Dissociation Constants. *J. Am. Chem. Soc.* **129**, 11177 (2007).

38. E. A. Smith, W. D. Thomas, L. L. Kiessling, R. M. Corn, Surface Plasmon Resonance Imaging Studies of Protein-Carbohydrate Interactions. *J. Am. Chem. Soc.* **125**, 6140 (2003).

39. G. J. Wegner, H. J. Lee, R. M. Corn, Characterization and Optimization of Peptide Arrays for the Study of Epitope-Antibody Interactions Using Surface Plasmon Resonance Imaging. *Anal. Chem.* **74**, 5161 (2002).

40. K. A. Kronis, J. P. Carver, Specificity of isolectins of wheat germ agglutinin for sialyloligosaccharides: a 360-MHz proton NMR binding study. *Biochemistry* **21**, 3050 (1982).

41. Y. Nagata, M. M. Burger, Wheat germ agglutinin. Molecular characteristics and specificity for sugar binding. *J. Biol. Chem.* **249**, 3116 (1974).

42. N. Shibuya *et al.*, The elderberry (Sambucus nigra L.) bark lectin recognizes the Neu5Ac(α2-6)Gal/GalNAc sequence. *J. Biol. Chem.* **262**, 1596 (1987).

43. Y. Li *et al.*, High-throughput neuraminidase substrate specificity study of human and avian influenza A viruses. *Virology* **415**, 12 (2011).

44. M. Jonges *et al.*, Influenza virus inactivation for studies of antigenicity and phenotypic neuraminidase inhibitor resistance profiling. *J. Clin. Microbiol.* **48**, 928 (2010).

3 INHIBITION OF INFLUENZA VIRUSES USING BIVALENT THIOSIALOSIDES

*The work presented in this chapter has been published in Bioorganic & Medicinal Chemistry Letters. Volume 24, Issue 2, P636-643. Figures and tables are adapted from the published paper with permission.

ABSTRACT

The circulating influenza viruses have started to develop resistance to currently available antiviral drugs such as Oseltamivir® and Zanamivir®, therefore novel influenza inhibitors are in high demand. In this chapter, we describe the design and inhibitory activity evaluation of a new class of NA inhibitors. Combining the robustness of thiosialosides, increased intrinsic affinity by C-4 modification and valency, these compounds show IC50 values ranging from low micromolar to high nanomolar in enzyme inhibition and plaque reduction assays with two intact viruses, Influenza H1N1 (A/California/07/2009) and H3N2 (A/Hongkong/8/68)

3.1 Introduction

NA inhibitors including Oseltamivir®, Zanamivir®, and Peramivir® (Figure 3.1**B-D**) are the first-line defense drugs used to treat influenza infection. (*1*) These FDA approved anti-influenza drugs are sialic acid analogs that mimic the transition state of sialic acid in the binding pocket of NA. Due to the structural similarity, they fit well in the NA active site and can compete with natural sialylated receptors and prevent NA from cleaving the terminal sialic acid (Figure 3.1**A**) from cell surface. As a result, the newly synthesized viral particles can not detach from the cell surface due to HA binding thus can not effectively infect other host cells. However, in recent years, some strains of influenza viruses have developed resistance to these inhibitors. In a 2009 surveillance study in northern Vietnam, all 19 clinical samples containing seasonal H1N1 isolate showed resistance to Oseltamivir®.(2) Another study identified a mutated pandemic A (H1N1)2009 strain that was resistant to both Zanamivir® and Oseltamivir®.(3) The emerging of drug resistant strain raises the need for development of novel anti-influenza drugs. Recently, Wither group reported a new class of mechanism based NA inhibitors, which showed broad spectrum activity against influenza virus including oseltamivir resistant strains in vitro and in animal models. (4, 5)(Figure 1E, F) Compared to transition state analogs, these compounds don't possess double bond and are more similar to natural substrate, with fluorine at the 3 position and amine or guanidine group at the 4 positions. The design of almost all NA inhibitors is based on the structure of natural substrate, sialic acid with modifications that lead to increased and highly specific inhibition.

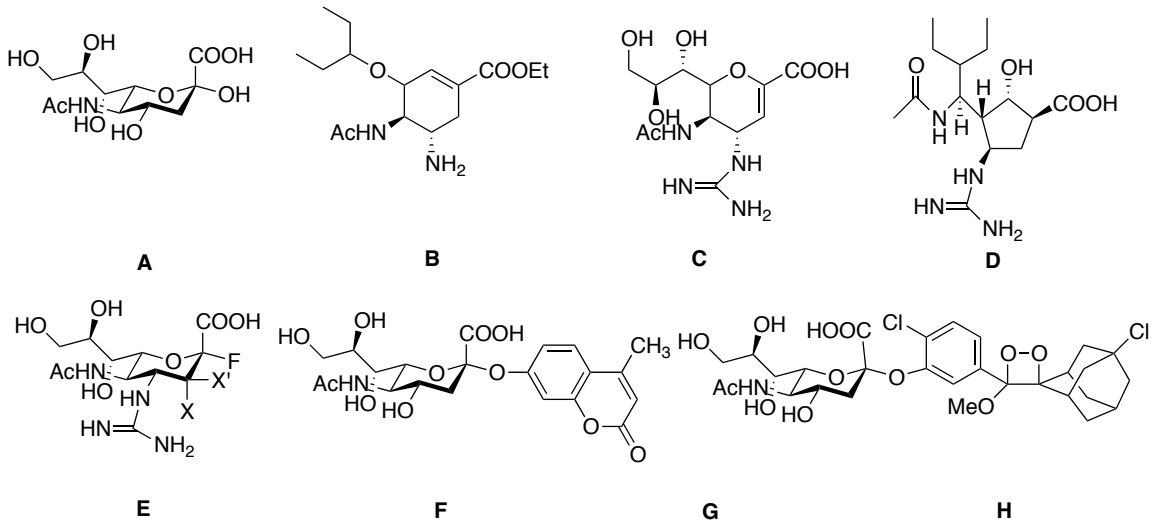

Figure 0.1 Structures of sialic acid (A), analogues as NA inhibitors (B: Oseltamivir; C:Zanamivir; D: Penamivir) and NA substrate (G: 2-O-(4-methylumbelliferyl)-N-acetylneuraminic acid substrate; H: NA STAR 1,2-dioxetane substrate).

3.1.1 Multivalent NA inhibitor

Along with the modification of sialic acid at the 3 or 4 position, a different strategy that adopts multivalency can also be used to develop novel NA inhibitors. Immunoelectron microscopy studies of labeled influenza virus reveal that an individual viral particle possesses 200-300 copies of trimeric HA and 50-100 copies of tetrameric NA. HAs distribute uniformly on the virion while NAs cluster in discrete area.(*6, 7*) Due to the oligomeric nature of NA and clustered distribution, polyvalent sialic acid may be good candidate as NA inhibitor. In fact, our innate defense system has demonstrated the value of polyvalent sialic acid. For instance, respiratory epithelial cells can release endogenous sialylated proteins called mucins to capture viral particles. Similarly, a highly sialylated salivary mucin protein MUC5B shows inhibition to influenza viruses. (*8-10*) There are several studies showing the anti-viral activity of multivalent sialic acid bound to linear polymer backbone and dendrimers. Compared to the monomeric sialic acid, these sialylated polymers show greater inhibitory effect, with IC50 value in the micromolar/submicromolar range. (*11-13*)

Our design of novel NA inhibitors is to combine the C-4 modification of sialic acid and increased valency. We introduced amine/guanidine group at the 4 position of sialic acid, because under physiological pH, these two groups are positively charged and can interact with the trio of negatively-charged amino acids present in the binding pocket of NA. (*14, 15*)We introduced sulfur at the anomeric position (C-2), because we have demonstrated the robustness of thiosialosides in the microarray studies and other groups have also confirmed that influenza virus does not readily cleave thiosialosides in solution. (*16, 17*) In addition, thiol group is good nucleophile, which can readily react with triflates and/or bromides present on multivalent scaffolds and yield multivalent molecules. The structures of our synthetic bivalent thiosialosides are shown in figure 3.2.

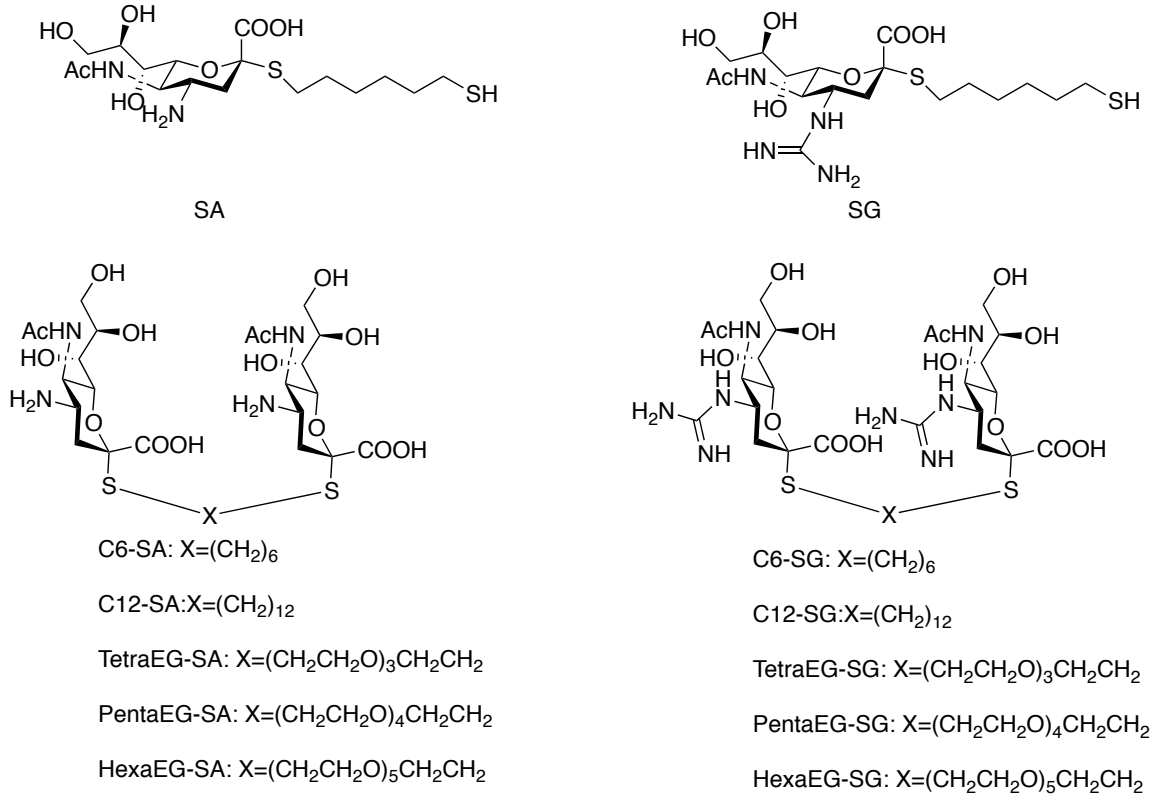

Figure 0.2 Structures of monovalent and bivalent thiosialosides

3.1.2 Method of assessing influenza virus susceptibility to NA inhibitors

Currently, cell-based assays and functional NA inhibition assays are the two major types of methods in assessing influenza virus susceptibility to NA inhibitors. The cell-based assay was first introduced by Hayden *et al.* to determine 50% inhibition of M2 inhibitors amantadine and rimantadine. This method utilizeds Madin-Darby canine kidney cell monolayers and a plaque inhibition assay. Similar to bacteria, virus can form "colony" on the cell monolayer when a single viral particle propagates and lyses adjacent cells, leaving round shape plaque on the cell layer. Depending on the way of introducing the virus inhibitors (premix with virus before incubation or introduce after virus inoculation), the number or size of plaques will be reduced. The IC50 is expressed by 50% reduction of plaque number or sizes.

The functional NA inhibition assays rely on the enzymatic nature of viral NA, which can hydrolyze terminal neuraminic acid. The substrates used in this type of assay are all sialic acid analogues, with a small fluorescent of chemiluminescent molecule conjugated to the anomeric position of sialic acid. (Figure 3.1 **G, H**) Upon cleavage by the NA enzyme, a luminescent or a fluorescent signal will be produced. The fluorescent (FL) assay employs 2-O- (4-methylumbelliferyl)-N-acetylneuraminic acid substrate (MUNANA) and chemiluminescent (CL) assay uses the 1,2-dioxetane derivative of neuraminic acid substrate in the influenza neuraminidase inhibitor resistance detection (NA-Star) kit.(*18*) The formation of the fluorescent or luminescent molecules can be detected in real time and the NA hydrolysis kinetic can be determined. The NA activity is usually expressed as amount of substrate formation/min. The results of the NI assays are expressed as the 50% inhibitory concentration (IC50), which represents the NAI concentration that inhibits 50% of the enzyme activity of the virus in a way that the initial hydrolysis speed is reduced by 50%. Compared to the cell-based assay, NA inhibition assay dose not involve the HA-receptor binding, thus reflect the actual sensitivity to NA inhibitors. In order to obtain thorough evaluation of inhibitory activity of our synthetic compounds, we performed both functional NA inhibition and cell-based assay.

3.2 Results and discussion

3.2.1 Inhibition assay with recombinant NA

We evaluated the inhibitory activity of our monovalent and bivalent thiosialosides using commercially available fluorescent substrate 2'-(4-Methylumbelliferyl)-α-D-N-acetylneuraminic acid (MU-NANA) (Figure 1**G**). We first tested two recombinant soluble viral NAs (N1 and N2) as the enzyme. We premixed the compounds with NA before adding to the substrate solution to allow adequate binding. The hydrolysis of substrate was monitored during a time course of 2h to ensure maximum cleavage and the fluorescent signal was measured and recorded every one minute to obtain kinetic curve, which can be used to calculate the velocity of the enzymatic reaction. We defined the IC50 as the concentration of compounds required to decrease the initial hydrolysis velocity (V_0) by 50%. At lower concentration of inhibitors, although the initial velocity decreases, the substrate can still be fully hydrolyzed. In this case, we observe the kinetic curve reach a plateau at certain time point. Therefore, we used only the linear slope between 0-35 min to calculate V_0 . (Figure 3.3) The IC50 values were obtained from three independent experiments for each compound and are given in Table 1. We included commercial drugs Zanamivir® and Ostelimivir® with IC50 at the nanomolar range as positive controls. Introduction of amine group at the 4 position (**SA**) decreases the IC50 to micromolar levels for both N1 (127±29) and N2 (178±20) compared to unmodified sialic acid (Data not shown). Generally, the bivalent sialosides (**C6-SA**, **C12-SA**, **TetraEG-SA**, **PentaEG-SA** and **HexaEG-SA**) exhibit higher inhibitory activity compared to the monomer, with approximately 1.5 to 5 fold decrease in IC50. The decrease is more significant for N1. However, the two compounds with longer spacers (**PentaEG-SA** and **HexaEG-SA**) were less efficacious compared to the **SA** against the N2 enzyme. Introduction of the guanidine group increase inhibition more than the amine group, with IC50 values at high nanomolar to micromolar range. The monomer **SG** shows higher inhibition towards H1 than H2 (0.1±0.02 vs 1±0.1). The IC50 values for the bivalent com-

pounds (**C6-SG**, **C12-SG**, **TetraEG-SG**, **PentaEG-SG** and **HexaEG-SG**), irrespective of the spacers, fall into the submicromolar range, which are similar to **SG** for both enzymes. In summary, compounds with guanidine group at the 4-position show better inhibitory activity toward soluble NAs than amino compounds. In addition, the N1 NA with the more open binding pocket and a flexible loop is more susceptible to our synthetic compounds, compared to N2 NA, which has a preset binding pocket, (*20*).

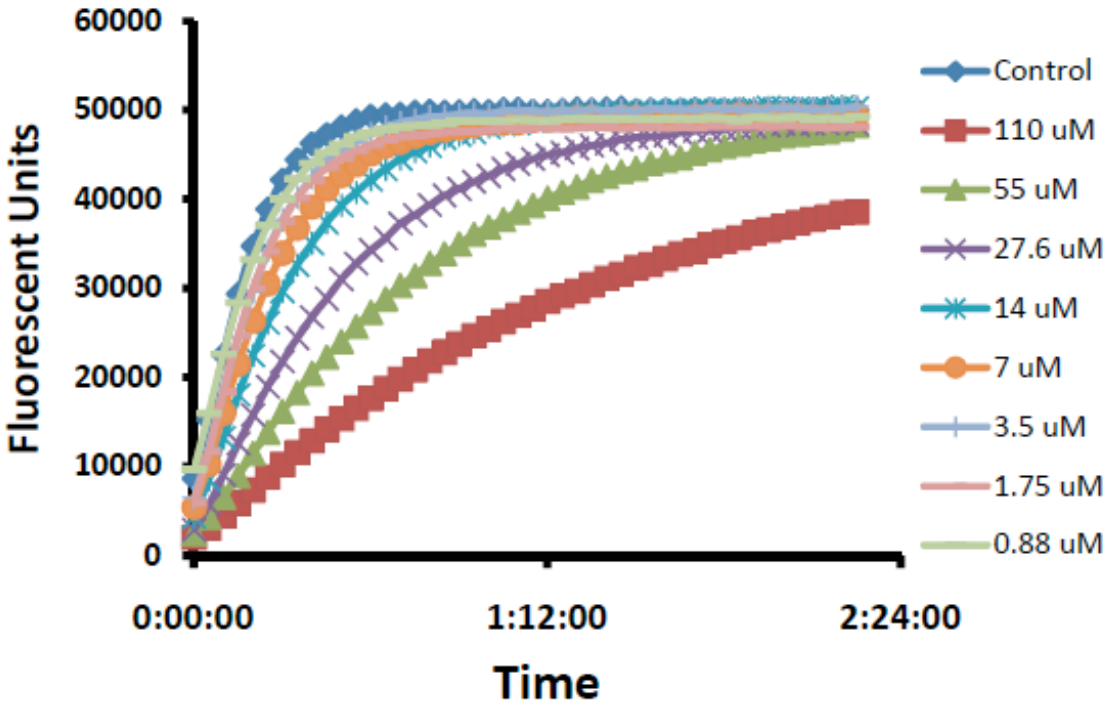

Figure 0.3 NA inhibition assays with H3N2 recombinant NA for C6-SA

3.2.2 Inhibition assay with intact influenza viruses

Next, we performed the same assay with two strains of intact viruses, H1N1 (A/California/07/2009) and H3N2 (Influenza A/Hongkong/8/68) to test the inhibitory activity of these compounds toward the transmembrane NAs present on the viral membrane. We observe a similar trend as the soluble NAs. The monomeric amino compound **SA** exhibits an IC50 value of 60 μM for both strains while the bivalent molecules exhibit decreased IC50 values up to 5 fold. Similar to the inhibition

of soluble NAs, the amino compounds with longer spacers (**PentaEG-SA** and **HexaEG-SA)** show lower inhibition to both strains of viruses, presumably because the spacer is too long and floppy to exhibit a bidentate effect. The guanidine monomer **SG** has an IC50 value of about 1 μM for both strains, which is 50-fold lower than **SA**. The bivalent compounds (**C6-SG**, **C12-SG**, **TetraEG-SG**, **PentaEG-SG** and **HexaEG-SG**) show lower IC50 compared to the monomer, ranging from 250 nm to 2.4 μM for both viruses. Among these bivalent compounds, **C6-SG** with the shortest carbon linker shows the best inhibitory activity. With these results, we confirm our hypothesis that using the combination of 4-position modification and increased valency can significantly decreases the IC50 values from the millimolar range (unmodified monomeric sialic acid) to the nanomolar range.

A cross comparison of the inhibitory towards soluble NAs and intact influenza viruses by the same compound reveals that most compounds show lower IC50 (higher inhibition) toward intact influenza viruses compared to soluble NA of the same type. (e.g. **C12-SA** IC50 H3N2 virus: 15±9; soluble NA from H3N2 virus: 40±1) This result indicates that multivalent effect plays an important role in the inhibition activity of our bivalent compounds. The NAs present on the membrane of intact influenza viruses are homotetramers with four sialic acid binding sites on each copy of NA, while the soluble NAs are present as a mixture of monomers, dimers, trimers and some tetramers. The bivalent compounds can possibly bind to two binding sites of the same viral NA with less entropy cost(*21*) therefore the binding is more favorable.

Name	Virus		NA from Virus	
	H3N2(μM)	H1N1(μM)	H5N1(μM)	H3N2(μM)
SA	64±14	56±6	127±29	178±20
C6-SA	11.6±3.5	9.9±1.8	20±5	32±5
C12-SA	15±9	11±1	31±7	40±1
TetraEG-SA	11±5	9.8±2.4	28±3	39±14
PentaEG-SA	21±3	36±4	64±14	178±20
HexaEG-SA	33±15	45±1	85±12	216±56
SG	0.55±0.02	0.8±0.1	0.1±0.02	1±0.1
C6-SG	0.25±0.05	0.26±0.03	0.2±0.02	4.2±1.2
C12-SG	0.5±0.3	0.8±0.06	0.73±0.03	12±2
TetraEG-SG	1.78±1.3	2.4±0.4	2.5±0.1	10±1
PentaEG-SA	1±0.6	1.2±0.2	1.1±0.1	10±2
HexaEG-SA	0.5±0.2	0.9±0.1	0.57±0.06	11±2
Zanamivir®	~0.001	~0.01	~0.04	~0.04
Oseltamivir ®	~0.008	~0.01	~0.05	~0.05

Table 0.1 IC50 values for the inhibition of soluble NAs and intact virus by the gemini sialoside analogs. The influenza strains used in these studies were Influenza H1N1 (A/California/07/2009) and H3N2 (A/Hongkong/8/68)

3.2.3 Plaque size reduction assay

We also tested the efficacy of these compounds to inhibit the virus in cell-based systems. We performed a plaque size reduction assay for all compounds. Briefly, we inoculate the cell monolayer with viruses for 30 minutes and removed the viral suspension. The compounds were introduced along with agarose plug, which was used to cover the cell, and arrest the spread of the viruses. The images of plaque size reduction assays using two different strains of influenza viruses (H1N1 and H3N2) are shown in Figure 3.4 and Figure 3.5. The IC50 values based on 50% decrease in plaque size are summarized in Table 2. We observe a similar trend of inhibition for all compounds as was seen with the cell free system. The bivalent amino compounds show a 1o-fold lower IC50 compared to the monomer **SA** for both H1N1 and H3N2 strains. The guanidine monomer **SG** has similar IC50 to amino dimers.. The bivalent

guanidine derivatives (**C6-SG**, **C12-SG**, **TetraEG-SG**, **PentaEG-SG** and **HexaEG-SG**) further lower the IC50 value to 10-1000 nM range.

The two strains of influenza viruses exhibit different susceptibilities to zanamivir as well as the bivalent thiosialosides on the cell-based assay. The plaque size reduction assay shows that the H3N2 strain is more susceptible than H1N1 strain, with a 10-fold lower of IC50 of all the compounds. However, the trend is not observed on the NA inhibition assay. One possible reason is that the pandemic H1N1 strain has much lower NA activity as well as HA avidity to the sialylated receptors compared the H3N2 strain.(*22*) As previously mentioned, nascent viruses remain attached to the cell surface via HA binding during budding until NA removes sialic acids to release the progeny. A balanced HA/NA activity is important for efficient transmission of influenza viruses. In the case of the pandemic H1N1 strain, the low NA activity is compensate with low HA avidity, therefore, even though NA is inhibited and less efficient in cleaving terminal sialic acid, the progeny viral particle can still move to seek other uninfected host cells. (*23*)In the NA inhibition assay, since HA binding is not involved, the result only reflects the actual inhibition effect of these compounds.

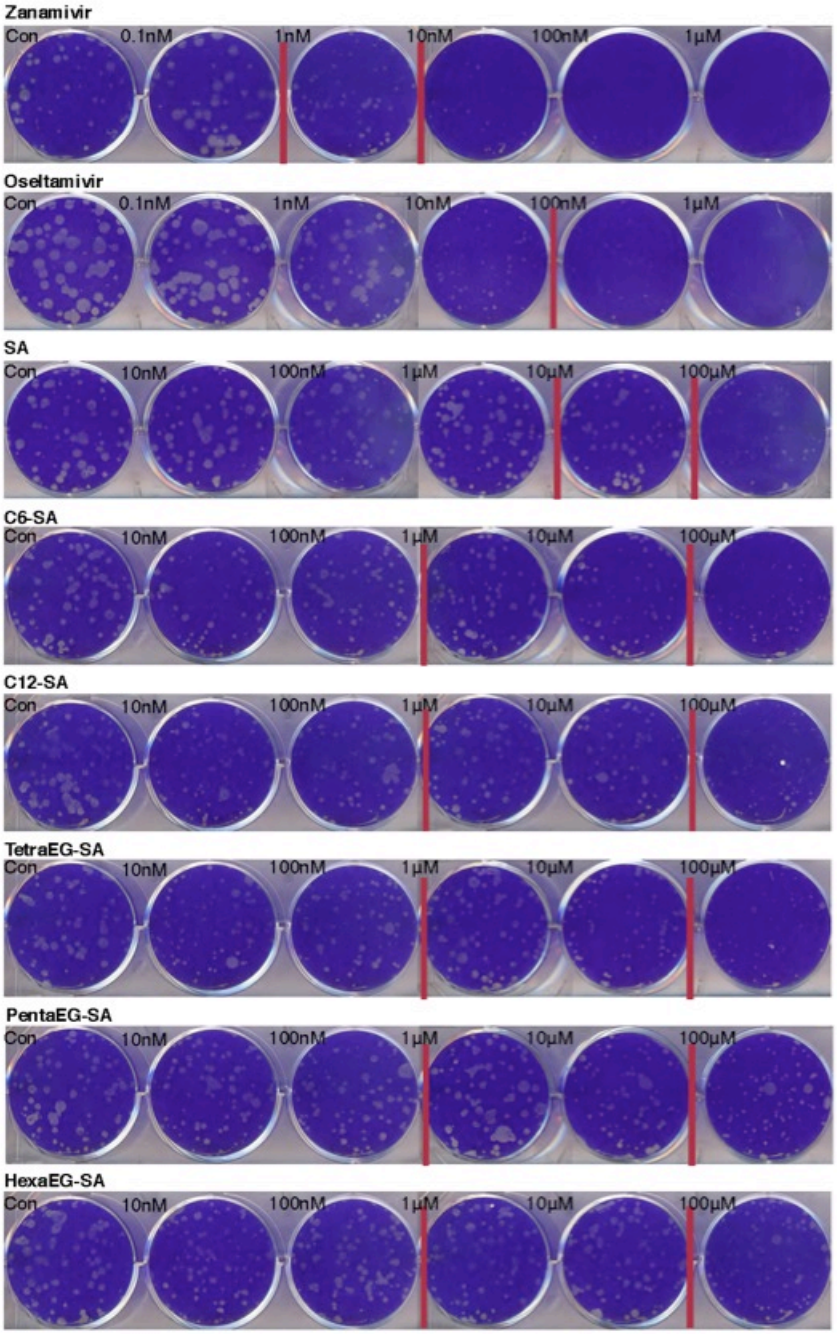
Zanamivir
Con
0.1nM
1nM
10nM
100nM
1μM
Oseltamivir
Con
0.1nM
1nM
10nM
100nM
1μM
SA
Con
10nM
100nM
1μM
10μM
100μM
C6-SA
Con
10nM
100nM
1μM
10μM
100μM
C12-SA
Con
10nM
100nM
1μM
10μM
100μM
TetraEG-SA
Con
10nM
100nM
1μM
10μM
100μM
PentaEG-SA
Con
10nM
100nM
1μM
10μM
100μM
HexaEG-SA
Con
10nM
100nM
1μM
10μM
100μM

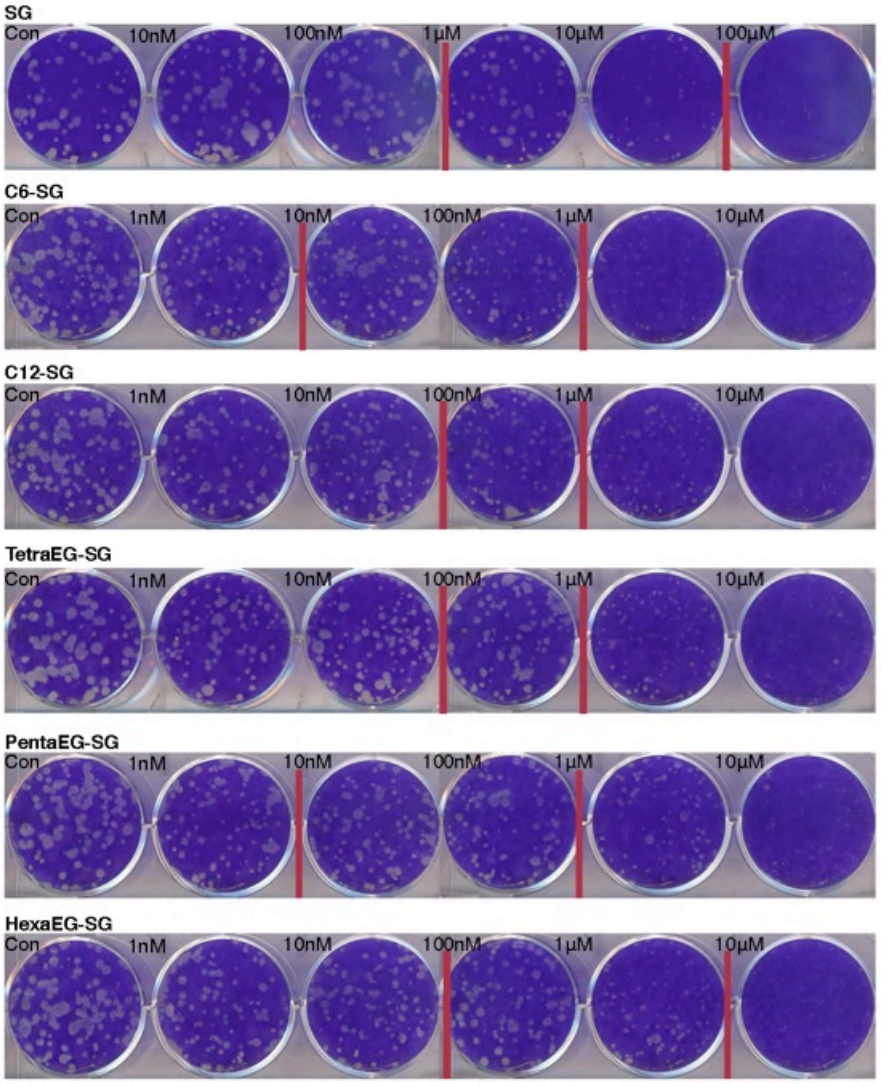

Figure 0.4 Images of the plaque size reduction assay by the sialosides synthesized in this report and current antivirals using A/Hongkong/8/1968 (H3N2) virus

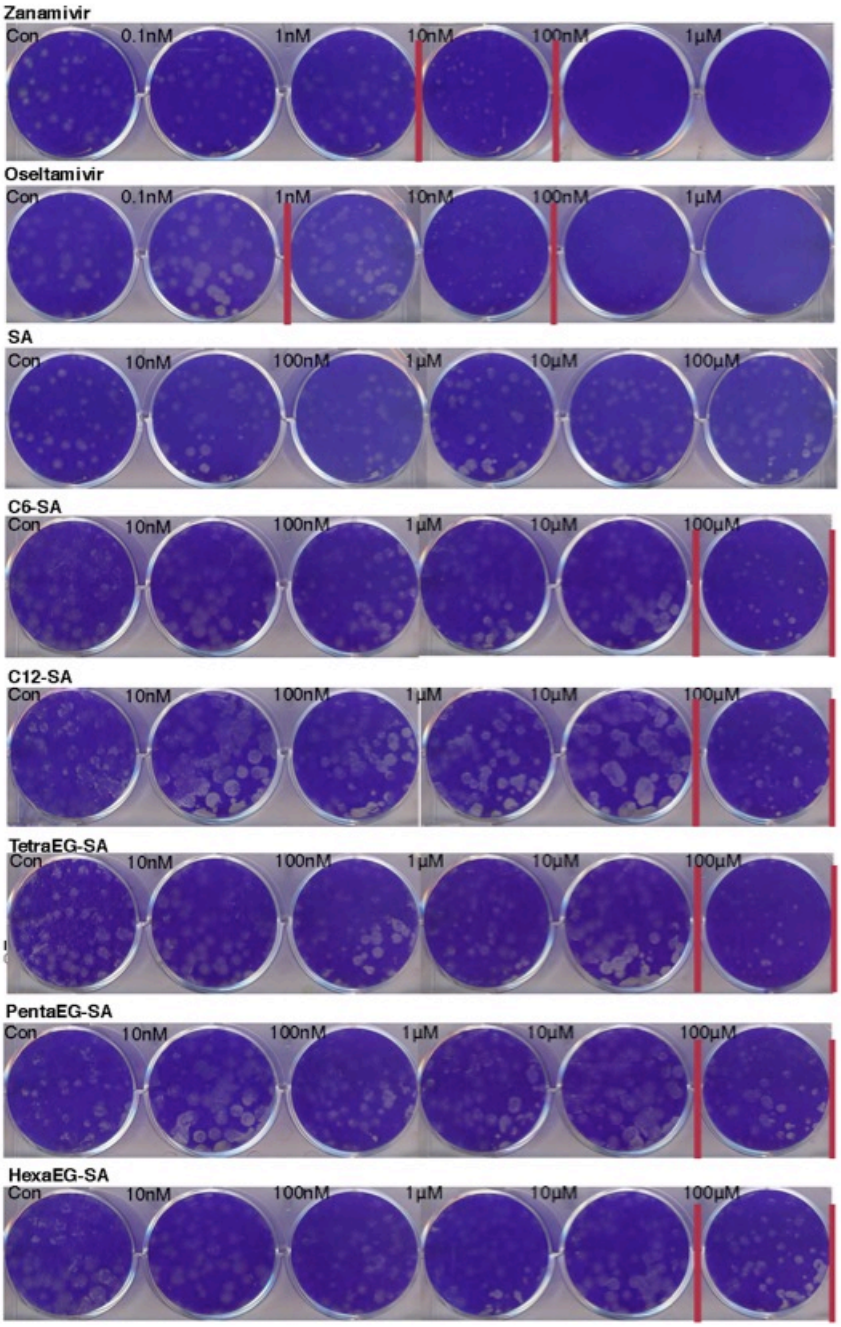
Zanamivir
Con
0.1nM
1nM
10nM
100nM
1μM
Oseltamivir
Con
0.1nM
1nM
10nM
100nM
1μM
SA
Con
10nM
100nM
1μM
10μM
100μM
C6-SA
Con
10nM
100nM
1μM
10μM
100μM
C12-SA
Con
10nM
100nM
1μM
10μM
100μM
TetraEG-SA
Con
10nM
100nM
1μM
10μM
100μM
PentaEG-SA
Con
10nM
100nM
1μM
10μM
100μM
HexaEG-SA
Con
10nM
100nM
1μM
10μM
100μM

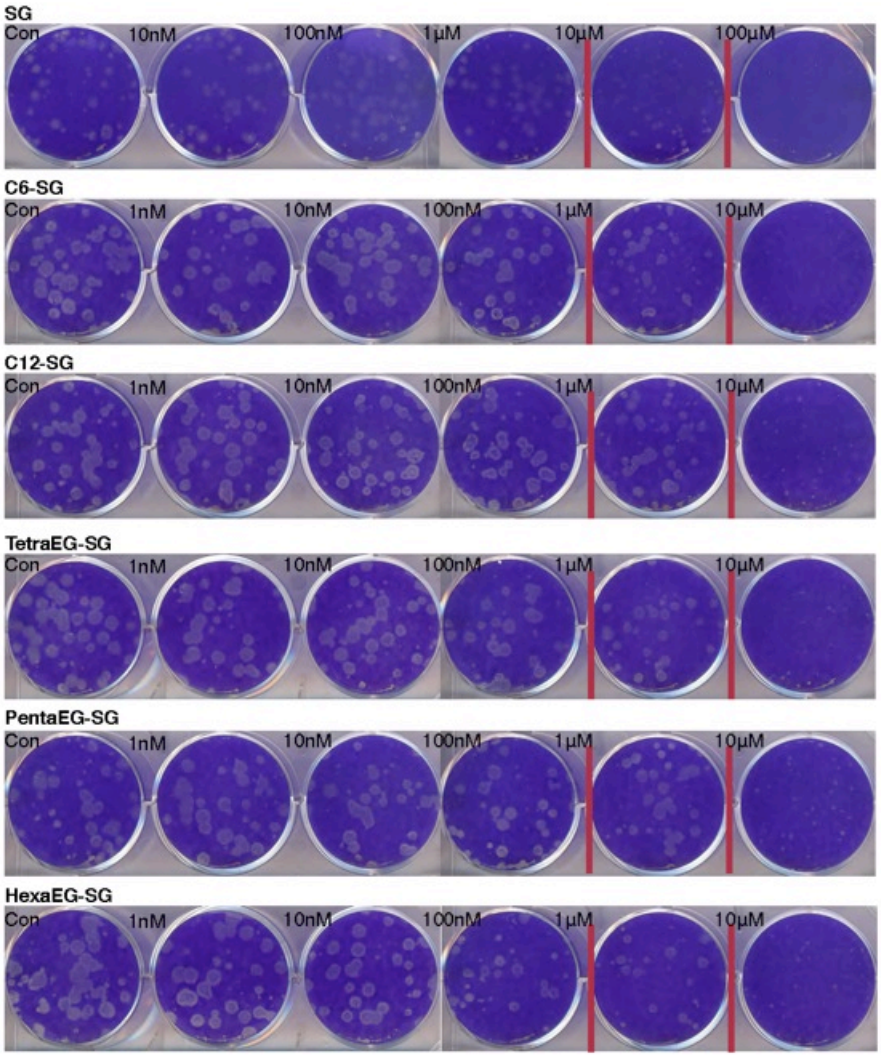

Figure 0.5 Images of the plaque size reduction assay by the sialosides synthesized in this report and current antivirals using A/California/07/2009 (H1N1) virus

Name	Virus	
	H3N2 (μM)	H1N1 (μM)
SA	10-100	>100
C6-SA	10-100	100
C12-SA	10-100	100
TetraEG-SA	10-100	100
PentaEG-SA	10-100	100
HexaEG-SA	10-100	100
SG	10-100	10
C6-SG	0.01-0.1	1
C12-SG	0.1	1
TetraEG-SG	0.1	1
PentaEG-SG	.01-0.1	1
HexaEG-SG	0.1-1.0	1
Zanamivir®	0.001	0.01
Oseltamivir ®	0.001-0.01	0.001-0.01

Table 0.2 IC50 values of influenza strains by the gemini sialosides based on 50% decrease in plaque size. The strains used in these studies were Influenza H1N1 (A/California/07/2009) and H3N2 (A/Hongkong/8/68)

3.3 Experimental section

3.3.1 Synthesis of bivalent thiosialosides

* The synthesis was performed by Dr. Yang Yang, a postdoctoral fellow in our laboratories. The detailed procesures and characterization are not shown in this dissertation.

3.3.2 Cell and viruses

MDCK (NBL2) (ATCC® CCL34™) cells were cultured in DMEM medium (Life Technologies, USA) with 10% fetal bovine serum and 1% antibiotic-antimycotic. The viruses were obtained through the NIH

Biodefense and Emerging Infections Research Resources Repository, NIAID including Influenza A Virus, A/Hong Kong/8/1968 (H3N2) egg isolate (produced in eggs), NR-346 and Influenza A/California/07/2009 (H1N1) egg isolate (produced in eggs), NR-13663.

3.3.3 Virus propagation

The viruses used in the plaque reduction assay and the MUNANA based enzyme inhibition assay were propagated from the initial virus stocks. MDCK cells were grown to 100% confluent and then infected with a 1:10,000 dilution of the initial stock of virus isolates. The cells were subsequently grown in DMEM with 0.3% BSA and 1% antibiotic-antimycotic for three days. Supernatants of the cultures were collected and followed by ultracentrifugation at 70,000g for 3 hours to purify and concentrate the viruses. Viruses had their plaque forming units (pfu) determined by plaque assay in MDCK cells as previously described (*19*) and were stored in Phosphate Buffered Saline (PBS) at -80 degrees until using.

3.3.4 NA inhibition assay

* The inhibition assay was performed by Dr. Yang Yang, a postdoctoral fellow in our laboratories.

Assays were conducted in 0.1 M sodium acetate buffer pH 5.5 containing 10 mM CaCl2. MUNANA (Sigma) was used as the fluorescent substrate. Serial dilutions of inhibitors were premixed with the protein or virus for 30 min. The fluorescence was monitored at 3 min intervals for 2 h after addition of the substrate. The IC50 was calculated as the concentration of the inhibitor resulting in a 50% decrease of the rate compared to the control.

3.3.5 Plaque size reduction assay

Plaque reduction assays (PRA) in MDCK cells were performed by the addition of serial ten-fold dilutions of inhibitors in the overlay of serum-free DMEM with 0.6% molecular biology grade agarose (Fisher, USA) containing 1 µg/mL of L-1-tosylamido-2-phenylethyl chloromethyl ketone ('TPCK')-treated

trypsin (Sigma, USA). The agarose overlays were removed after 5 days; cells were fixed with 70% ethanol and then stained with 0.2% crystal violet. The IC50 is the concentration of inhibitor causing a 50% decrease in plaque sizes. A range was used when the 50% reduction in plaque size fell between two inhibitor concentrations.

3.4 Conclusion and future direction

In summary, we have designed and synthesized a panel of bivalent thiosialosides with C-4 modifications. By incorporating the robustness of *S*-sialosides, increased intrinsic affinity of a single unit and bivalency, we were able to demonstrate the inhibitory activity toward two different strains of influenza virus using these compounds. The IC50 values range from the low micromolar to a high nanomolar ranges. In addition, we have identified the appropriate spacer resulted in higher inhibitory effect, which is the carbon linker C6G and C12G. Finally, we note that these compounds are not as efficacious as Zanamivir® or Oseltamivir®. As part of the future work, the Iyer group is currently making structural modifications base on sialic acid, e.g. introducing a fluorine at the 3 position and tethering the molecules polymeric/dendrimeric scaffold to develop second generation inhibitors.

REFERENCE

1. I. M. von, The war against influenza: discovery and development of sialidase inhibitors. *Nat. Rev. Drug Discovery* 6, 967 (2007).

2. V. M.-P. Hoang, C. T. Nguyen, L. K. H. Nguyen, T. K. P. Nguyen, Q. M. Le, Oseltamivir resistance among influenza viruses: surveillance in northern Viet Nam, 2009-2012. *Western Pac Surveill Response J* 4, 25 (2013).

3. J. LeGoff *et al.*, I223R mutation in influenza A(H1N1)pdm09 neuraminidase confers reduced susceptibility to oseltamivir and zanamivir and enhanced resistance with H275Y. *PLoS One* 7, e37095 (2012).

4. C. J. Vavricka *et al.*, Influenza neuraminidase operates via a nucleophilic mechanism and can be targeted by covalent inhibitors. *Nat Commun* 4, 1491 (2013).

5. J.-H. Kim *et al.*, Mechanism-Based Covalent Neuraminidase Inhibitors with Broad-Spectrum Influenza Antiviral Activity. *Science (Washington, DC, U. S.)* 340, 71 (2013).

6. K. G. Murti, R. G. Webster, Distribution of hemagglutinin and neuraminidase on influenza virions as revealed by immunoelectron microscopy. *Virology* 149, 36 (1986).

7. H. Amano, H. Uemoto, K. Kuroda, Y. Hosaka, Immunoelectron microscopy of influenza A virus neuraminidase glycoprotein topography. *J. Gen. Virol.* 73, 1969 (1992).

8. M. R. White *et al.*, Multiple components contribute to ability of saliva to inhibit influenza viruses. *Oral Microbiol Immunol* 24, 18 (2009).

9. M. R. White *et al.*, Cooperative anti-influenza activities of respiratory innate immune proteins and neuraminidase inhibitor. *Am J Physiol Lung Cell Mol Physiol* 288, L831 (2005).

10. O. Lieleg, C. Lieleg, J. Bloom, C. B. Buck, K. Ribbeck, Mucin Biopolymers As Broad-Spectrum Antiviral Agents. *Biomacromolecules* 13, 1724 (2012).

11. K. I. P. J. Hidari *et al.*, Chemoenzymatic synthesis, characterization, and application of glycopolymers carrying lactosamine repeats as entry inhibitors against influenza virus infection. *Glycobiology* 18, 779 (2008).

12. J.-i. Sakamoto *et al.*, Systematic syntheses of influenza neuraminidase inhibitors: A series of carbosilane dendrimers uniformly functionalized with thioglycoside-type sialic acid moieties. *Bioorg. Med. Chem.* 17, 5451 (2009).

13. J.-I. Sakamoto *et al.*, Thiosialoside clusters using carbosilane dendrimer core scaffolds as a new class of influenza neuraminidase inhibitors. *Bioorg. Med. Chem. Lett.* 17, 717 (2007).

14. I. M. von *et al.*, Rational design of potent sialidase-based inhibitors of influenza virus replication. *Nature (London)* 363, 418 (1993).

15. J. C. Wilson, M. J. Kiefel, D. I. Angus, I. M. von, Investigation of the Stability of Thiosialosides toward Hydrolysis by Sialidases Using NMR Spectroscopy. *Org. Lett.* 1, 443 (1999).

16. R. R. Kale *et al.*, Detection of Intact Influenza Viruses using Biotinylated Biantennary S-Sialosides. *J. Am. Chem. Soc.* 130, 8169 (2008).

17. M. Chandler *et al.*, Synthesis of the potent influenza neuraminidase inhibitor 4-guanidino Neu5Ac2en. X-ray molecular structure of 5-acetamido-4-amino-2,6-anhydro-3,4,5-trideoxy-D-erythro-L-gluco-nonionic acid. *J. Chem. Soc., Perkin Trans. 1*, 1173 (1995).

18. H. T. Nguyen, T. G. Sheu, V. P. Mishin, A. I. Klimov, L. V. Gubareva, Assessment of pandemic and seasonal influenza A (H1N1) virus susceptibility to neuraminidase inhibitors in three enzyme activity inhibition assays. *Antimicrob. Agents Chemother.* 54, 3671 (2010).

19. S. J. F. Macdonald *et al.*, Potent and long-acting dimeric inhibitors of influenza virus neuraminidase are effective at a once-weekly dosing regimen. *Antimicrob. Agents Chemother.* 48, 4542 (2004).

20. R. J. Russell *et al.*, The structure of H5N1 avian influenza neuraminidase suggests new opportunities for drug design. *Nature (London, U. K.)* 443, 45 (2006).

21. L. L. Kiessling, J. E. Gestwicki, L. E. Strong, Synthetic multivalent ligands in the exploration of cell-surface interactions. *Curr. Opin. Chem. Biol.* 4, 696 (2000).

22. R. Xu *et al.*, Functional balance of the hemagglutinin and neuraminidase activities accompanies the emergence of the 2009 H1N1 influenza pandemic. *J. Virol.* 86, 9221 (2012).

23. J. McKimm-Breschkin *et al.*, Neuraminidase sequence analysis and susceptibilities of Influenza virus clinical isolates to zanamivir and oseltamivir. *Antimicrob. Agents Chemother.* 47, 2264 (2003).

4 ELECTROCHEMICAL BIOSENSOR FOR DETECTION OF INFLUENZA VIRUSES

ABSTRACT

In this chapter, we report a novel electrochemical biosensor for the detection of influenza viruses. Neuraminidase (NA) is one of the two abundant glycoproteins on the surface of influenza viruses. NA functions an enzyme that hydrolyzes terminal sialic acid from glycans, glycoproteins or glycolipids. We exploited the enzymatic property of NA to develop the biosensor. Specifically, we synthesized α-2, 6-sialylglucose, a substrate that can be recognized and hydrolyzed by viral NA. The hydrolysis product D-glucose can be detected electrochemically.

ABBREVIATION

Glassy carbon electrode, GCE; Cyclic voltammetry, CV; Deionized water, DI H_2O; Nitric acid, HNO_3; Hydrochloric acid, HCl; Prussian blue, PB; Potassium ferricyanide, $K_3Fe(CN)_6$; Potassium chloride, KCl; Glucose oxidase, GOD; Chitosan, CS; Bismuth selenide, Bi_2Se_3; Bismuth nitrate, $Bi(NO)_3$; Selenium oxide, SeO_2; Neuraminidase, NA.

4.1 Introduction

A summary of existing techniques for detection of influenza viruses was mentioned in chapter I. One very well-established technique that measures neuraminidase (NA) activity, thereby quantifying influenza viruses is a fluorometric enzyme assay.(*1*) This assay utilizes a fluorogenic reagent 2'-(4-methylumberlliferyl)-α-D-N-acetylneuraminic acid (4-MUNANA) as a NA substrate. The enzyme cleaves the sialic acid from this substrate and releases the enzymatic hydrolysis product 4-methylumberlliferone, which can be readily measured using by measuring the fluorescence intensity as a function of time and concentration.The excitation and emission of 4-methylumberlliferone are 365nm and 450nm respectively, which are significantly different compared to the excitation and emission of MUNANA, which is 315nm and 374nm, respectively. Therefore, the fluorescent interference of MU-NANA can be ignored and the fluorescent intensity at 450nm can be used to determine the concentration of 4-methylumberlliferone resulted from the hydrolysis of MUNANA. (Figure 4.1)

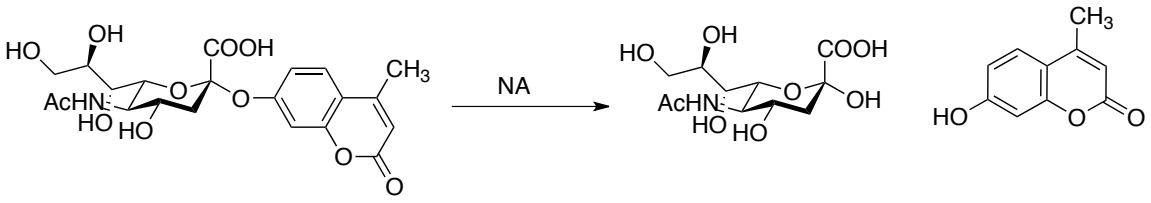

Figure 4.1 Cleavage of 4-MUNANA by neuraminidase

While fluorescence can readily be measured in a laboratory setting, it is very difficult, if not impossible, to use this compound in a primary care setting, where access to a flourometer might not be feasible. Furthermore, optical detection can be subject to misinterpretation if not performed by trained personnel and appropriate laboratory skills using instruments. Therefore, we decided to develop a novel non-optical method that could potentially be used to detect influenza viruses using the unique properties of the hydrolase.

We developed molecules, which could lead to a measurable electrical signal upon exposure to influenza virus. The principle is that NA will cleave sialic acid from a “masked” sialic acid containing electrochemicallly inactive compound, releasing a molecule that can generate an electrochemical signal that can easily be measured. Since we intend to use electrochemical detection as our technique of choice, a brief primer of electrochemical biosensors is described in the following sections.

4.1.1 Electrochemical biosensor

Electrochemical biosensors offer several advantages, which make them attractive candidates for real world applications, especially in low resource settings. Its a label free system, which greatly simplifies assay development, avoids possible change in target binding profile caused by labeling and eliminates variations in labeling efficiency. Sensitivity can be very high with small amount of analytes (*2*) Electrochemical settings are easy to miniaturize and can be engineered into a portable device, . Unlike fluorescent settings, turbid media can be used, thus eliminate the sample preparation step and therefore, clinical samples including urine, saliva and blood can be tested directly.(*3-5*)Integration of enzymes to react with the released compound can greatly increase selectivity , especially when the sample is very complex and has multiple analytes. The response time of electrochemical biosensor is usually very short. For example, seconds of wait time is sufficient using commercial glucose monitors. Low cost and long-term stability also make electrochemical biosensor are further advantages of an electrochemical biosensor.

The basic principle of electrochemical biosensor is utilizing chemical reaction between immobilized biomolecules, usually enzymes, or consumption of electrons to produce measurable electrical property change, such as current, conductance, potential and ionic strength. A basic electrochemical setting consists of three electrodes: working electrode, reference electrode and counter electrode (Figure 4.2). Typicalelectrodes are platinum, gold and carbon, since they are inert, biocompatible, highly conductive and readily modified.

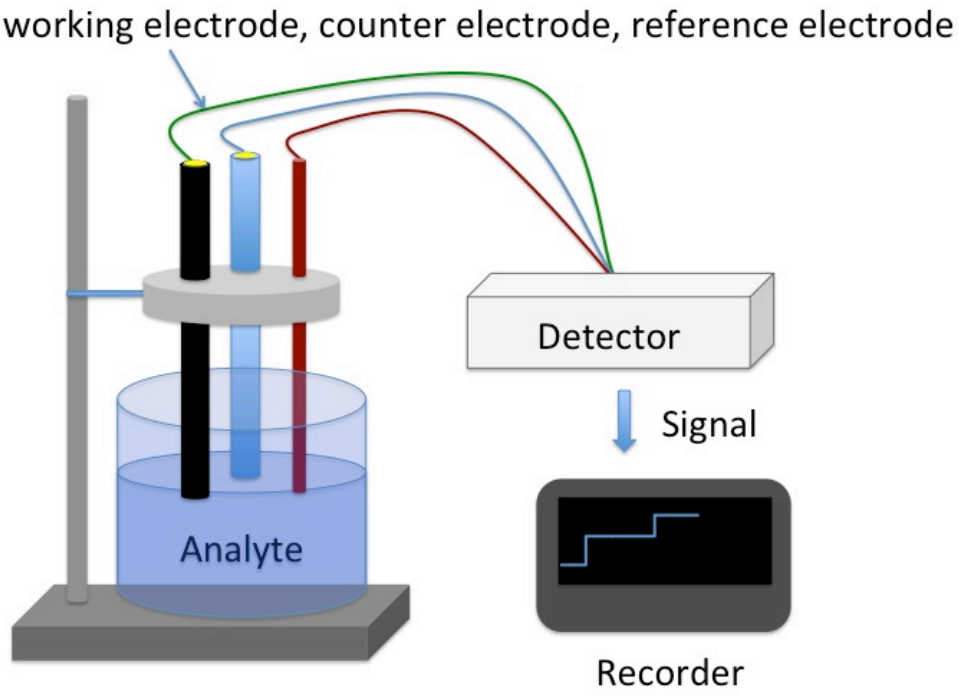

Figure 4.2 Schematic of a three-electrode system. The working electrode measures current change produced by the interaction of immobilized enzymes and analytes.

Electrochemical biosensors have broad applications in clinical diagnosis, covering a variety of metabolites such as glucose, lactate, cholesterol and urea, etc.(*4, 6-8*) Other targets include antigens, antibodies and cancer markers.(*9-11*)In recent years, electrochemical sensing has been extended to more complex targets: pathogens, e.g., E. coli and HIV virus, by targeting at DNA or RNA.(*12, 13*) Among these applications, electrochemical sensing of glucose biosensor is the most successful example as it is currently being used by pre-diabetic and diabetic patients to monitor blood glucose concentration. In the following sections, we describe the principles, methods and applications of electrochemical sensing of glucose as our detection system as our novel assay is directly related to glucose sensing.

4.1.2 Electrochemical sensing of glucose in diabetic patients. Principles, methods and applications

Diabetes is one of the most common threats of human health. According to American Diabetes Association, there're 25.8 million people who have diabetes in the United States, along with 79 million people with pre-diabetes. Blood glucose level is the indicator of diabetes and needs to be monitored closely. If blood glucose is between 70 -120 mg/dl, patients are not diabetic. If the glucose level is above 126mg/dl from the fasting plasma glucose test, or 200mg/dl from the oral glucose tolerance test, patients are considered diabetic.(*14*) Therefore a lot of progress has been made towards the development of a user friendly, portable glucose biosensor and these sensors are commercially available. The principle of most glucose biosensors is that glucose oxidase (GOD) converts D-glucose into D-gluconic acid with the presence of oxygen and also produces hydrogen peroxide,(*15*) as shown in the following reaction:

$$\text{D-Glucose} + H_2O + O_2 \xrightarrow[\text{Oxidase}]{\text{Glucose}} \text{D-Gluconic Acid} + H_2O_2$$

The enzyme provides the specificity needed for eliminating false positives or negatives.

While hydrogen peroxide can be readily detected using an electrochemical setup illustrated in Figure 4.2, the oxidation of hydrogen peroxide is usually over +600mV with standard electrodes, which is high enough to oxidize many other electroactive compounds present in biological samples. Moreover, the response of the biosensor is highly susceptible to oxygen concentration in the media thus affect the reproducibility of the assays a great deal.(*16*) Therefore, redox mediators such as ferrocene, Prussian blue (PB), potassium hexacyanoferrate are widely used due to the ability of significantly decreasing the large overvoltage required for the oxidation or reduction of hydrogen peroxide. An alternative reaction is shown below:

$$\text{D-Glucose} + [\text{Med}]_{ox} \xrightarrow[\text{Oxidase}]{\text{Glucose}} \text{D-Gluconic Acid} + [\text{Med}]_{red}$$

Where [Med] represents a mediator. Among several available mediators, ferrocene and its derivatives are the most widely used class of mediators in the development of chemically modified electrodes due to the following features: relatively low molecular mass, rapid responses to many electroactive substances, being pH-independent, stability in both oxidized and reduced forms at low potential and having fast electron transfer.(*17*) However, ferrocene usually has to be covalently linked to chitosan in order to prevent leakage, a common problem seen in low molecular weight materials.

Ferrocene functions as artificial electron acceptor/donor or mediator by taking place of oxygen in the enzymatic reaction. In the case of glucose oxidase, two electrons are first transferred from glucose to FAD to form $FADH_2$, and then to ferrocene and convert it to the reduced form, which can be oxidized at the electrode surface and produce a current. The current is directly proportional to the glucose concentration in solution. The reaction is shown below.(*18*)

$$\text{Glucose} + \text{GOD (FAD)} \longrightarrow \text{gluconolactone} + \text{GOD (FADH}_2\text{)}$$

$$\text{GOD(FADH}_2\text{)} + 2Fc^{+} \longrightarrow \text{GOD (FAD)} + 2Fc + 2H^{+}$$

$$2Fc \longrightarrow 2e^{-} + 2Fc^{+}$$

GOD: Glucose oxidase; FAD: Flavin adenine dinucleotide; $FADH_2$: reduced form of FAD; Fc: Ferrocene. Fc^{+}: oxidized form of ferrocene.

Prussian blue is also called “artificial peroxidase”, which can catalyze hydrogen peroxide electrochemical reaction at lower potential, thus chosen as another candidate of mediators. The catalytic mechanism of PB is shown as following: (*19*)

$$\underset{\text{Prussian blue}}{KFe^{(III)}[Fe^{(II)}CN_6]} + e^{-} + K^{+} \longleftrightarrow \underset{\text{Prussian white}}{K_2Fe^{(II)}[Fe^{(II)}CN_6]} \quad (1)$$

$$\underset{\text{Prussian white}}{2K_2Fe^{(II)}[Fe^{(II)}CN_6]} + H_2O_2 + 2H^{+} \longleftrightarrow \underset{\text{Prussian blue}}{2KFe^{(III)}[Fe^{(II)}CN_6]} + 2H_2O + 2K^{+} \quad (2)$$

4.1.3 GOD immobilization

Since the first enzyme-based commercial glucose biosensor came to the market (use reference numbers), enormous effort has been devoted to develop enzyme immobilization technique. There're three major techniques including adsorption, covalently cross-linking and entrapment.(*20*) Adsorption is the simplest method but least stable due to the fast desorption of the enzyme. Cross-linking enzyme to a membrane or coating layer greatly increases stability but on the cost of possible enzymatic activity loss due to the change of enzyme conformation. Moreover, when utilizing Shiff's base formation, leaching of enzyme can still occur due to reversibility of the reaction.(*21*) Entrapment using carbon paste or polymers increases the lifetime of enzyme-modified electrode, however, utilization of the entrapped enzyme is very limited.

We look for optimal enzyme immobilization method, which can be easily handled and also help maintain enzyme activity in long term. Trough extensive literature survey and preliminary experiments conducted in our laboratories, we found that sol-gel coating technique is the best technique that can readily produce the desired immobilization and coating of the electrodes.. This coating technique utilizes sol-gel-derived materials to embed enzyme onto electrodes, which possesses the following features: physically rigid, chemically inert and thermally stable in both aqueous and organic solution.

For the polymer, we choose a complex polysaccharide, chitosan, comprising of repeating units of randomly distributed β- (1,4)-linked D-glucoseamine and N-acetyl-D-glucoseamine. Chitosan is a widely used material in enzyme immobilization due to its excellent film-forming ability, biocompatibility, well mechanical strength, cheapness and susceptibility to chemical modification.(*22*) Chitosan becomes insoluble when the pH is above 6.3, which greatly increases the stability of immobilized enzyme layer, thus the assay for detecting glucose should be done under neutral or weak basic condition.

4.1.4 Principle of detection of influenza virus by measuring glucose released by cleavage of sialic acid-glucose conjugates

The design of our probe for detecting influenza viruses shares similarity to the 4-MUNANA. The a-2, 6-sialylglucose contains terminal sialic acid, which can be recognized and hydrolyzed by neuraminidase or intact influenza viruses. The intact probe itself will not result in electrochemical signal, however, the hydrolysis product β-D-glucose can be detected electrochemically. The presence of absence of electrochemical signal indicates whether or not a unknown sample contains influenza viruses. Moreover, when the glucose concentration in the hydrolysis sample falls in the linear range of detection, the amount of glucose can be quantified. Thus, the NA unit, defined as the ability of hydrolyzing α-2, 6-sialylglucose in given time can be measured.

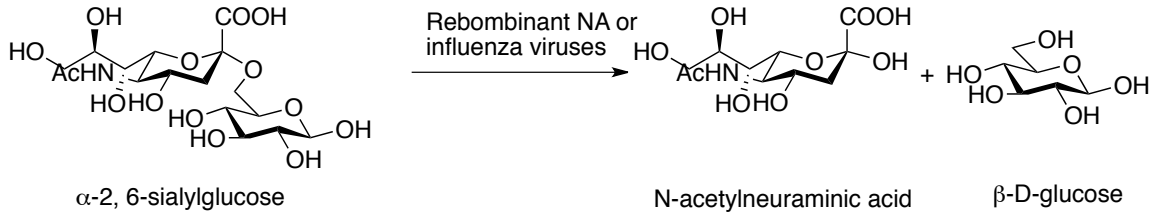

Figure 4.3 Cleavage of α-2, 6-sialylglucose by neuraminidase or influenza viruses.

4.1.5 Differences between commercial glucose biosensors and our assay

All commercial glucose sensors are designed to monitor human blood sugar range, which lies between 70-180mg/dL or 3.9-10mM (non-diabetics: 70-130mg/dL; diabetics: less than 180mg/dL), Also, glucose is already present in the blood for detection. In our system, we are interested in detecting influenza virus from nasal/throat swabs, which doesn't has any glucose. Introduction of the substrate to a sample containing the virus is expected to lead to the production of glucose; however, the concentration of the glucose will be dependent on the amount of substrate, the concentration of the virus, the nature and activity/catalytic turnover of the NA (eg. N1 vs N2 vs N7) present on the viral surface, etc. Therefore, we need to develop glucose biosensors that have a wider range and potentially lower limit of

detection than commercial systems. As a starting point, the conventional fluorescence based assay utilizing fluorogenic reagent 2'-(4-methyllumbelliferyl)-a-D-*N*-acetylneuraminic acid (MUNANA) can detect hydrolyzed substrate in the range of 30-1,000 uM. Most clinical isolates that demonstrate normal to high NA activity can be detected using this method.[12] Thus, we are seeking glucose-sensing techniques with the detection limit of micromolar level or lower. After an extensive literature survey, we decided to follow a procedure that coelectrodeposits a PB/Bi_2Se_3 hybrid film onto electrode surface and corporates GOD by CS immobilization. The reported detection limit of glucose using this method was 3.8 µM. (reference) Also, the modified surface was stable at mild acidic condition, which was required for maximum activity of viral NA.

4.2 Experimental section

4.2.1 Synthesis of "masked" electrochemical substrates The synthesis was performed by Dr. Abasaheb Dhawane, a postdoctoral fellow in our laboratories.

4.2.2 Fabrication of PB/Bi_2Se_3 mediat ed glucose biosensor (22)

Glassy carbon electrode (GCE) was polished and cleaned thoroughly prior to the modification following standard procedures. Briefly, GCE was polished on a nylon-polishing pad using alumina micropolish powder of different particle size, following the sequence of 1.0 µm, 0.3 µm and 0.05 µm with rinses in between. The polished GCE then was washed ultrasonically in HNO_3 (50% in H_2O), ethanol (50% in H_2O) and DI H_2O. The clean surface of GCE was dried under continuous airflow.

PB solution was prepared by dissolving $K_3Fe(CN)_6$ and $FeCl_3$ in 10mM HCl containing 0.1M KCl, reaching a final concentration of 2mM. Electrodepositing Bi_2Se_3 solution was a mixture of 2mM $Bi(NO)_3$ and 3mM SeO_2 in diluted nitric acid (14% in H_2O). Co-electrodepositing solution was obtained by mixing PB solution and Bi_2Se_3 solution in the ratio of 2:1. Activation solution was 0.1M KCl in 10mM HCl. 0.5% CS solution was prepared by dissolving 50mg CS in 10ml of 2% acetic acid with sonication. 2mg of Glu-

cose oxidase was mixed with 50ul of CS solution and pipetted gently to obtain a homogenous mixture. All solutions were prepared fresh daily.

The hybrid film of PB/Bi_2Se_3 was electrodeposited on the GCE surface by cyclic voltammetry (CV) with a scan range of -0.2V to +0.6V and scan rate of 20mV/s for 30 cycles. The modified electrode was rinsed with DI H_2O and activated in activation solution by CV with a scan range of -0.05V to +0.35V and scan rate of 50mV/s for 30 cycles, followed by rinse and air-dry procedure. The electrode was further modified with glucose oxidase by dropping 10µl of GOD-CS mixture onto the electrode surface and then dried with airflow. Modified electrode was soaked in PBS buffer (pH=6.86) and stored at 4^{o}C when not in use.

4.2.3 Amperometric measurement of glucose standard solution

A serial 2-fold dilution of D-(+)-glucose solution in 25mM PBS containing 0.1M KCl (pH=6.8), from 800 µM to 6.25 µM, was prepared to determine the linear measurement range of GOD modified PB/Bi_2Se_3/GCE. Current was measured continuously in 200 seconds with applied potential of 0.0V. The end point current was recorded to establish the standard curve.

4.2.4 Hydrolysis of sialylglucose by recombinant NA or intact influenza virus

A 10mM sialylglucose stock solution was diluted in 10mM of NH_4OAc buffer (pH=5.68) and re-combinant NA or live influenza virus suspension was added. The final concentration of sialylglucose was adjusted to 1mM. The substrate/NA or virus mixture was incubated at 37^{o}C. NA or influenza virus was removed by filtration using Amicon-ultra centrifugal filter with a 300K cut-off membrane. The glucose concentration then was measured amperometrically following the same procedure as the glucose standard solution.

4.3 Results and discussion

4.3.1 Co-electrodeposition of PB/Bi2Se3 hybrid film by cyclic voltammograms (CV)

The method of employing cyclic voltammograms to obtain stable PB/Bi_2Se_3 hybrid film was reported by Wu *et al.* In comparison to pure PB film, the nanostructure of PB particles that are co-deposited on the electrode surface was more compact and smaller in size. Under scanning electron microscope (SEM), the pure PB film showed serious aggregation, which enlarged the effective particle size furthermore; on the contrary, a much smoother surface without obvious defect was observed when PB was co-electrodeposited. In addition, the alkaline-resistant Bi_2Se_3 particles can prevent PB from leaching under mild basic condition, thus expand the pH range of running assays. The CV technique allows dissolution and electrodeposition film occur alternatively during the oxidation and reduction process, as a result, the deposited film is compact and can firmly adherent to the electrode surface.

The cyclic voltammograms of PB/Bi_2Se_3 hybrid film co-depostion are shown in figure 4.4 (A). Two pairs of redox peaks and one irreversible peak are observed, in accordance with the previous report. The redox pair at around +0.21V correspond to PB while the pair at 0.40V may be attributed to nitric acid in the coating solution. The peak at -0.11V is attributed to the formation of Bi_2Se_3, resulting from reduction of H_2SeO_3. The reaction equation is shown below.

$$3H_2SeO_3 + 2Bi^{3+} + 12H^+ + 18e^- = Bi_2Se_3 + 9H_2O$$

The PB redox peak pair increases gradually as the cycle of scan increases, indicating the continuous growth of PB layer. 30 cycles of scan has been found to be optimal, resulting in a PB layer with optimal thickness that provides sufficient stability as well as sensitivity. 50 cycles or more of scan (data not shown) lead to a much thicker PB layer but greatly reduce the sensitivity in detecting hydrogen peroxide. The scan rate is also a key factor in the co-electrodeposition process. Although a higher scan rate accelerates the coating process, the resulting deposited PB layer is less compact and unstable. The PB layer formed at a scan rate of 100mV/s decomposes with only a few assays in KCl solution. On the con-

trary, a scan rate of 20mV/s results in a much more stable PB layer, which lasts for more than 30 assays. The activation step helps stabilize the current in cyclic voltammotric run in KCl solution. The cyclic voltammogram is shown in figure 4.4B.

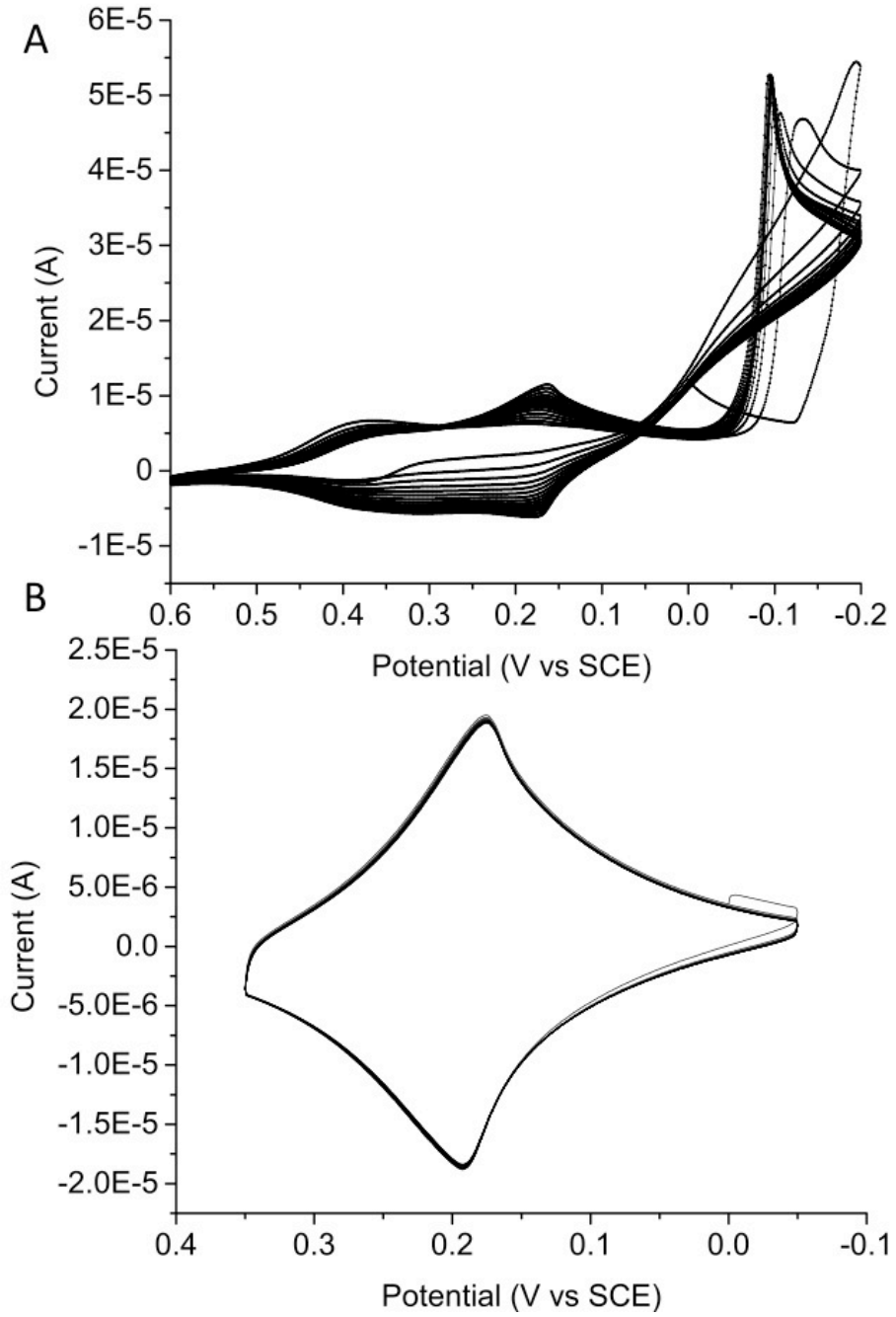

Figure 4.4 (A) Cyclic voltammograms of PB/Bi_2Se_3 coating on GCE: 30 cycles in a range of -0.2V to +0.6V at a scan rate of 20mV/s. (B) Cyclic voltammograms of PB/Bi_2Se_3 coated GCE in activation buffer: 30 cycles in a range of -0.05V to +0.35V at a scan rate of 50mV/s.

4.3.2 Amperometric detection of glucose

GODs from different sources have various optimal pH ranges. Generally, GOD from fungi and yeast, such as Aspergillus niger GOD which was used in fabricating our glucose biosensor, requires acidic to neutral pH range.[13] On the other hand, CS stays insoluble when pH is above 6.3, which is crucial to the stability of the glucose biosensor. Considering both factors, a buffer with the pH of 6.9 was chosen. The amperometric response of PB/Bi_2Se_3 coated GCE at different concentration of glucose is shown in figure 4.5A. Excellent linear response with a correlation coefficient of 0.998 is observed in the range of 12.5 μM to 800 μM. The detection limit is sufficient for our application of detecting glucose from influenza virus hydrolysis samples.

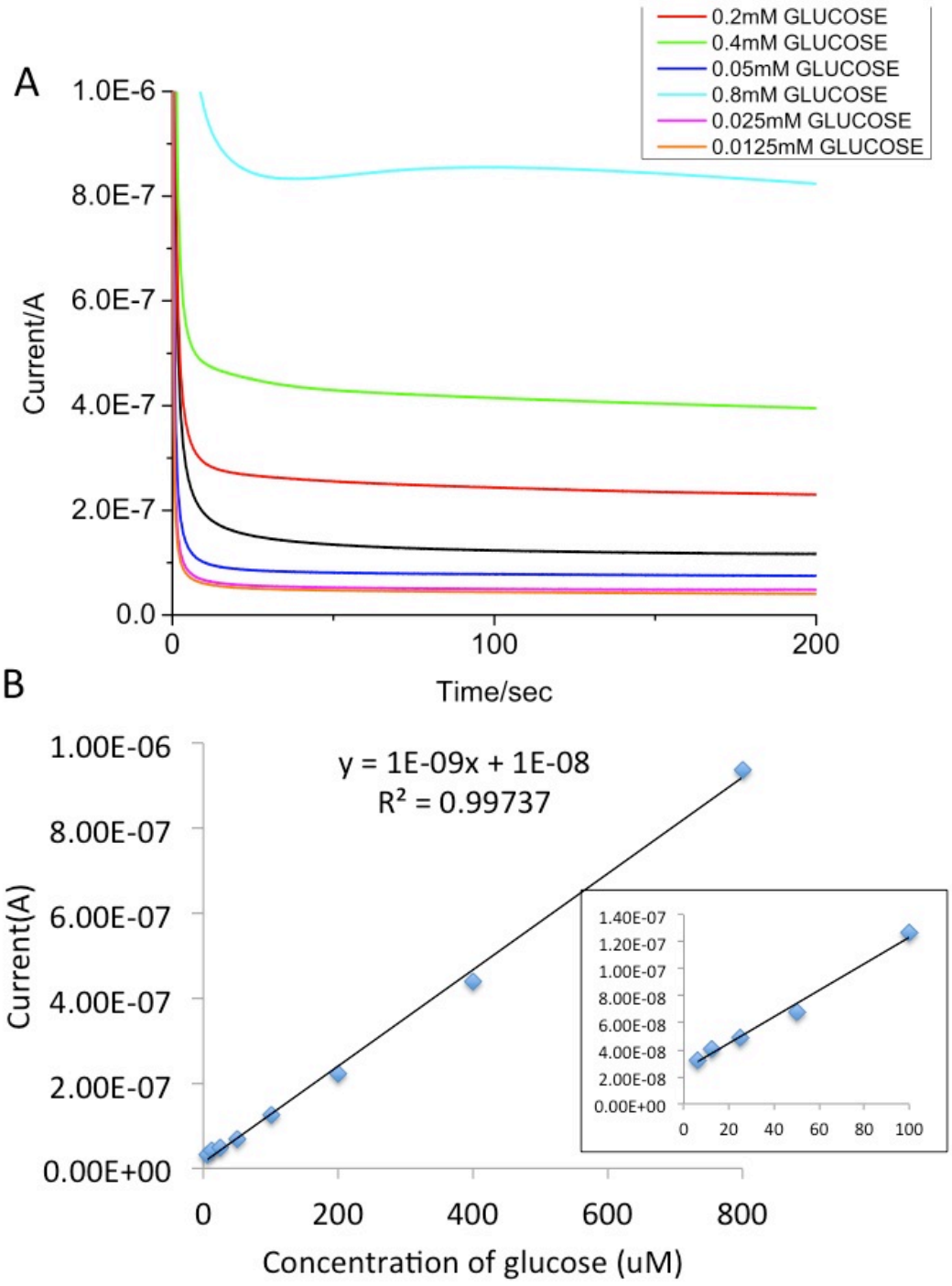

Figure 4.5 (A) Amperometric response of PB/Bi_2Se_3 coated GCE at different concentration of D-(+)-glucose. Applied potential: 0.00V. (B) Standard curve generated by linear regression. The insert is a zoomed region from 0-100uM.

4.3.3 Hydrolysis of sialylglucose by recombinant NA or influenza viruses

Influenza neuraminidases are enzymes that can hydrolyze terminal sialic acid from glycoproteins or glycolipids. In the previous chapter, we have shown that influenza NA hydrolyzes α-2,3-sialyllactose faster than α-2,6-sialyllactose. However, to the best of our knowledge, no study has been done to determine the hydrolysis of α-sialylglucose by NA. We first examined if our novel synthetic substrate α-2,6-sialylglucose could be hydrolyzed by influenza NA by mass spectroscopy. To ensure a complete hydrolysis, the substrate was incubated with NA overnight. At a physiological pH 7.40 and room temperature at overnight incubation , both substrate peak and hydrolysis product sialic acid peak could be seen, indicating an incomplete hydrolysis (Figure 4.6A). However, when the pH was adjusted to 5.68 and temperature was increased to 37 ^{o}C which was optimal for NA, the substrate peak could no longer be observed (Figure 4.6B). The same condition was applied for intact influenza virus hydrolysis and the mass spectrum showed complete hydrolysis for both H1N1 and H3N2 viruses (Figure 4.6C and D).

The molecular ion peak of both α-2,6-sialylglucose and sialic acid could be clearly seen in the mass spectrum, however, the glucose peak was hardly observed. The reason is that glucose lacks functional groups such as carboxyl group or amine group, which can be easily ionized. The mass spectrum obtained from a sample containing equal amount of sialic acid and glucose showed strong peak of sialic acid but very tiny peak of glucose (data not shown). In our study, we use the sialic acid peak and the disappearance of α-2,6-sialylglucose peak as indication of the hydrolysis completion.

A

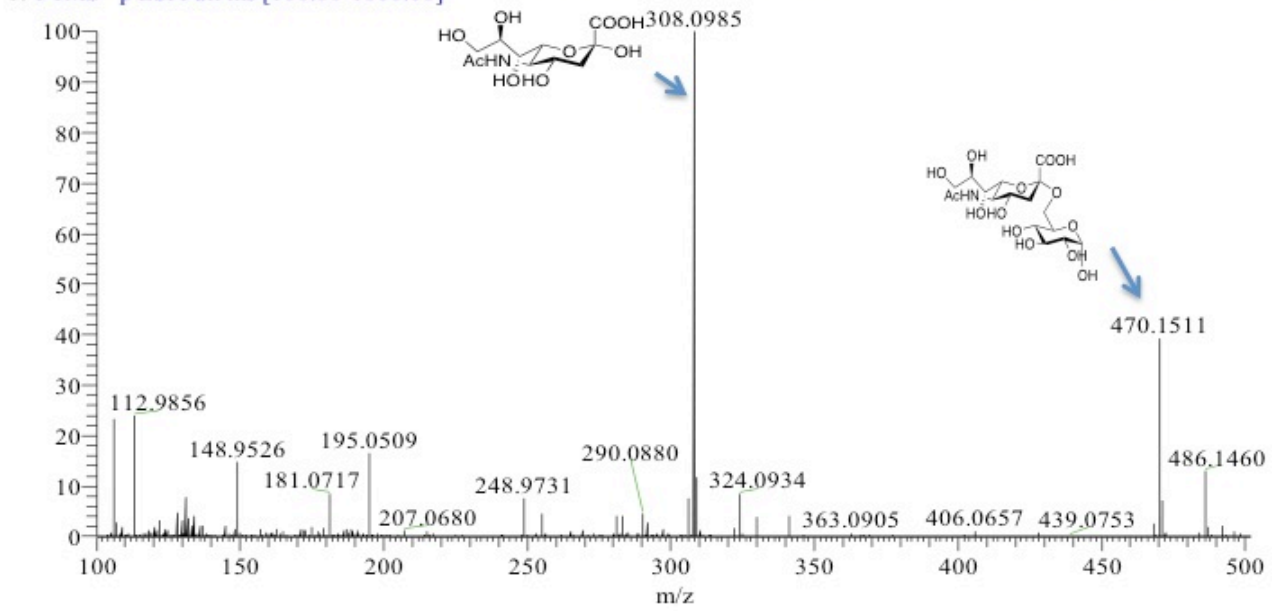
Yun_102813-glucose-reaction-dialysis_Iyer _10272013_ESINEG-02 #181 RT: 2.59 AV: 1 NL: 3.70E6
T: FTMS - p ESI Full ms [100.00-1000.00]
308.0985
470.1511
112.9856
148.9526
195.0509
181.0717
290.0880
248.9731
324.0934
207.0680
363.0905
406.0657
439.0753
486.1460
m/z

B

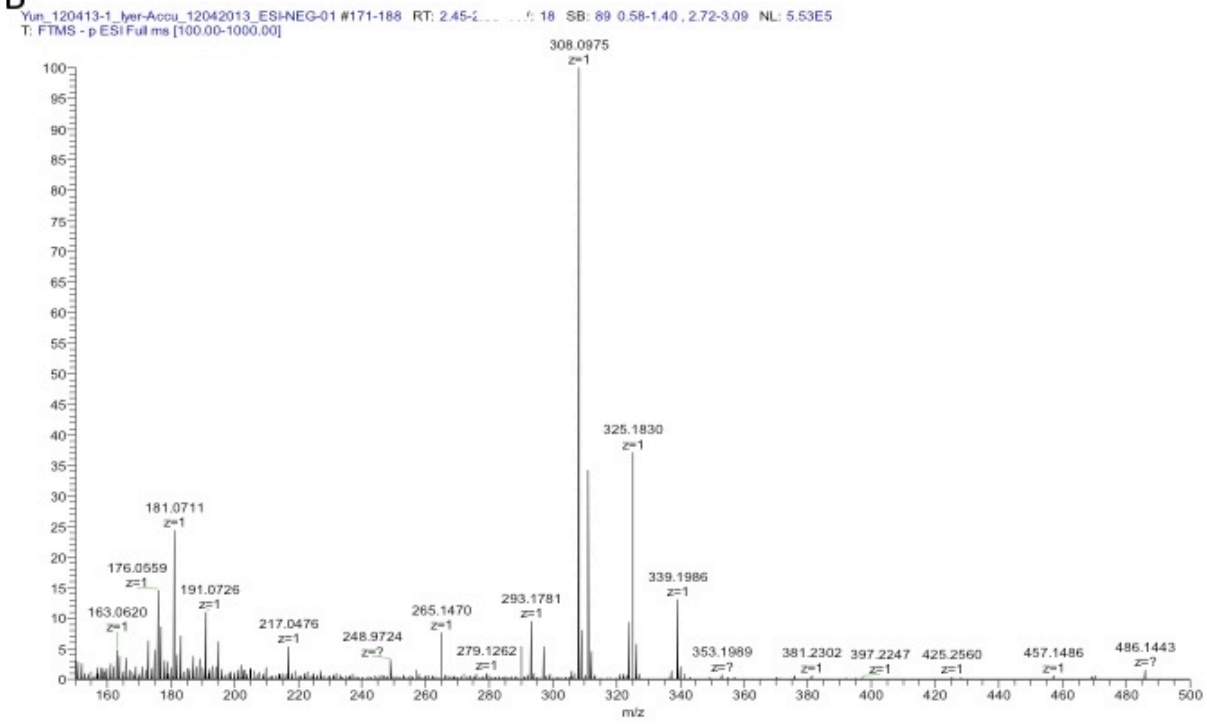
Yun_120413-1_Iyer-Accu_12042013_ESI-NEG-01 #171-188 RT: 2.45-2 18 SB: 89 0.58-1.40 , 2.72-3.09 NL: 5.53E5
T: FTMS - p ESI Full ms [100.00-1000.00]
308.0975 z=1
325.1830 z=1
181.0711 z=1
176.0559 z=1
191.0726 z=1
339.1986 z=1
163.0620 z=1
217.0476 z=1
265.1470 z=1
293.1781 z=1
248.9724 z=?
279.1262 z=1
353.1989 z=?
381.2302 z=1
397.2247 z=1
425.2560 z=1
457.1486 z=1
486.1443 z=?
m/z

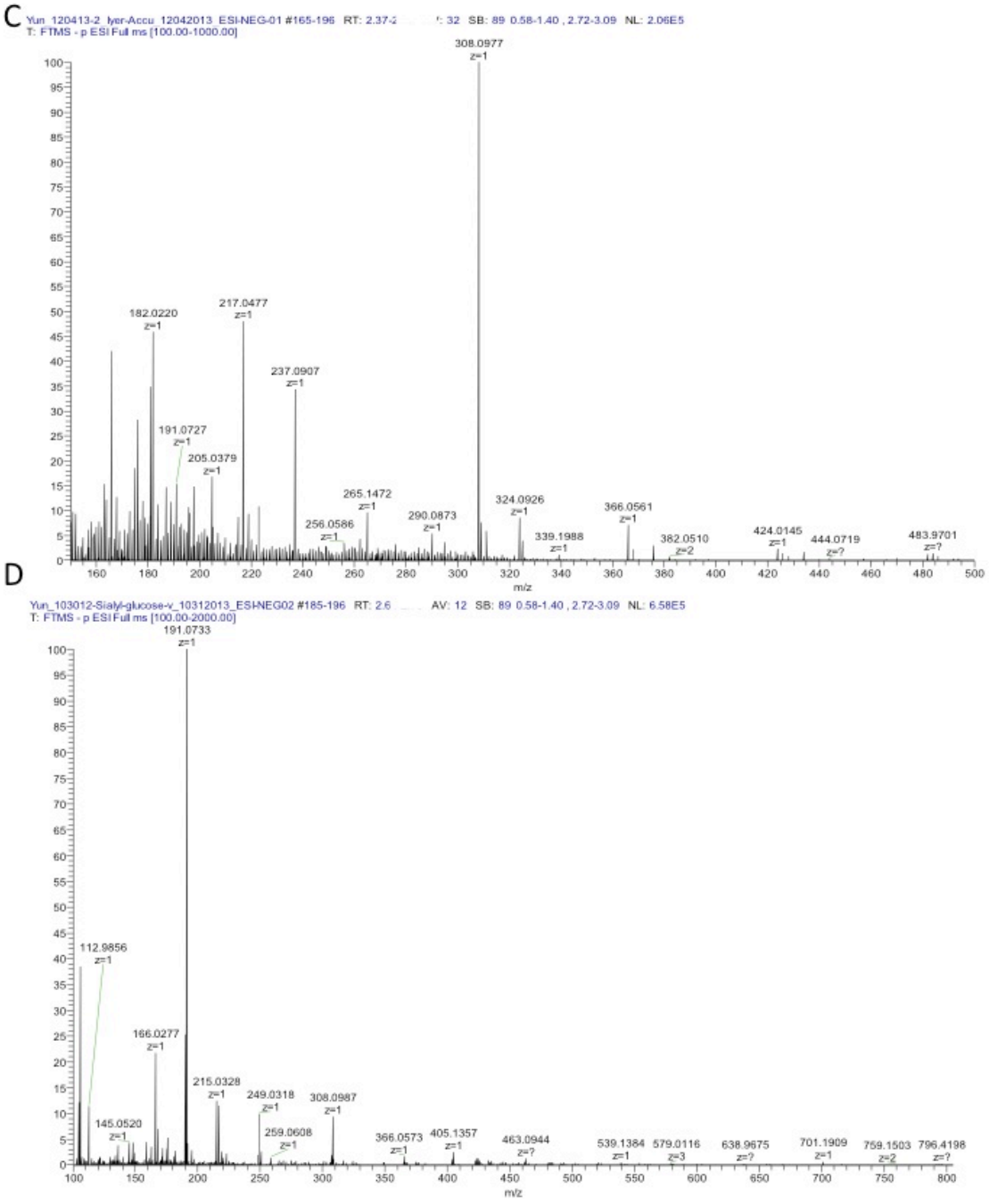

Figure 4.6 Mass spectrums of α-2,6-sialylglucose samples after hydrolysis by recombinant NA or influenza viruses. (A) Hydrolysis of α-2,6-sialylglucose by H5N1 NA at pH 7.40 and room temperature. (B) Hydrolysis of α-2,6-sialylglucose by H3N2 NA at pH 5.68 and 37^{o}C. (C) Hydrolysis of α-2,6-sialylglucose by influenza virus A/Solomon Island/59/07 (H1N1) at pH 5.68 and 37^{o}C. (D) Hydrolysis of α-2,6-sialylglucose by influenza virus A/Honkong/8/68 at pH 5.68 and 37^{o}C.

4.3.4 Electrochemical sensing of glucose in NA or influenza virus hydrolysis samples

The concentration of glucose from the hydrolysis of α-2,6-sialylglucose by recombinant NA or intact influenza viruses were measured amperometrically. The hydrolysis reaction was carried out in 10mM NH_4OAc buffer with a pH of 5.68 and the reaction mixture then was diluted in PBS buffer containing 0.1 KCl as support electrolyte for electrochemical sensing using 1 mM of the substrate. Amperometric responses of overnight hydrolysis samples by NA or influenza viruses are shown in figure 4.7A.. The concentrations of glucose in these hydrolysis samples were calculated by applying the current value into the linear regression equation obtained from the glucose standard curve.. We also performed a time course of the reaction. The hydrolysis of α-2,6-sialylglucose by H1N1 virus was stopped at 1h, 5h and overnight respectively and the current was recorded. The 1h and 5h samples showed currents comparable to the 100 μM glucose standard solution while the overnight sample showed significantly lower current. This result indicated that the hydrolysis reaction was completed in 1h, however, elongation of incubation time decreased the glucose concentration, presumably because the released glucose is consumed by the virus or is degraded by an unknown mechanism if left overnight. Summary of current and calculated glucose concentration in all hydrolysis samples is shown in table 4.1. Include one more column where the % of glucose released in given. Is it 100%, or 50%.

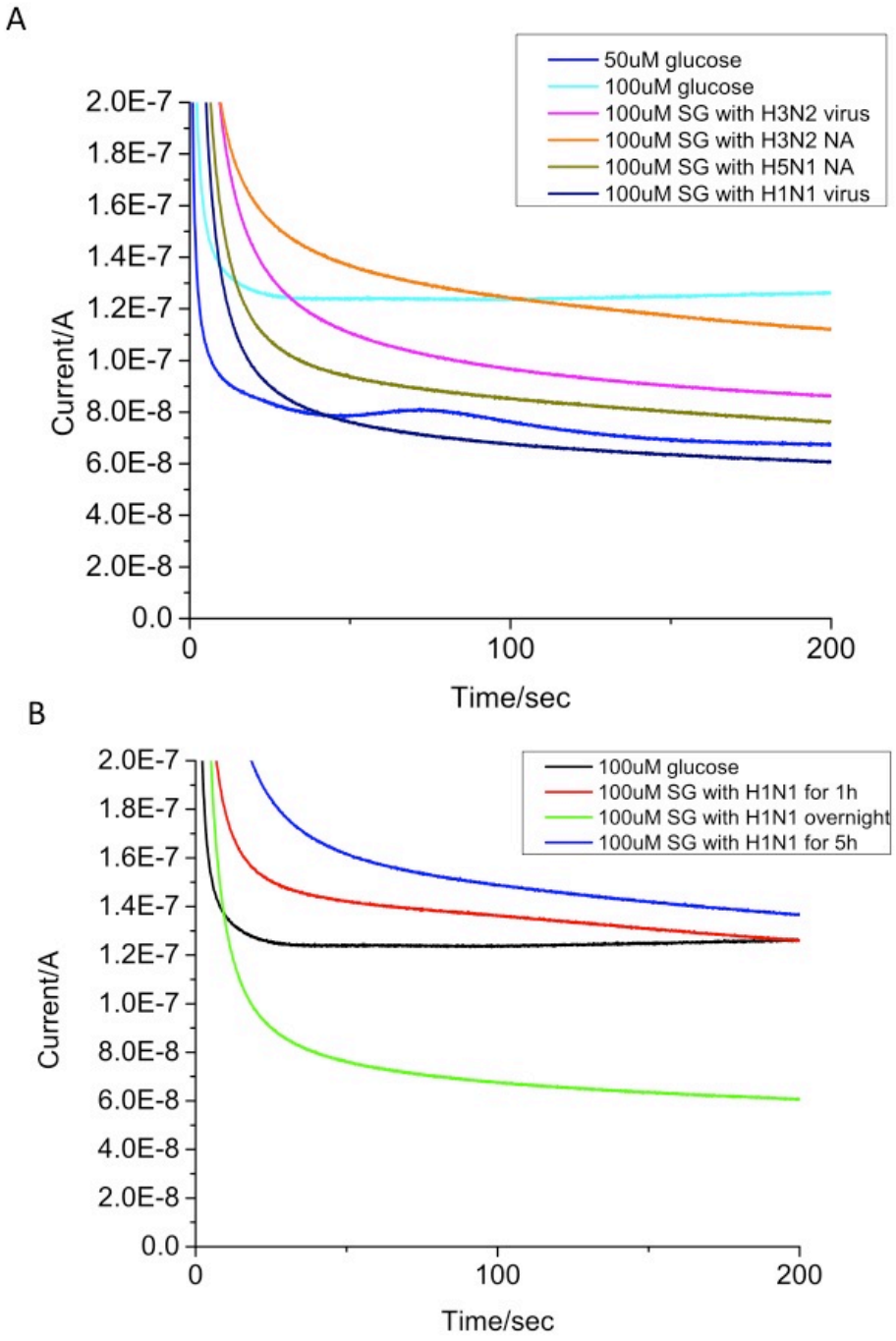

Figure 4.7 (A) Amperometric response of overnight hydrolysis samples by NA or influenza viruses. Applied potential: 0.00V. (B) Amperometric response of hydrolysis samples by H1N1 virus for different time courses.

Sample	Current(A)	Calculated conc. of glucose(μM)
H1N1 virus 1h	1.262E-07	116.2
H1N1 virus 5h	1.366E-07	126.6
H1N1 virus overnight	6.066E-08	50.66
H3N2 NA overnight	1.123E-07	102.3
H5N1 NA overnight	7.647E-08	66.47
H3N2 virus overnight	8.609E-08	76.09

Table 4.1 Summary of amperometric current and calculated concentration of glucose in sialyl-glucose hydrolysis samples by NA or influenza viruses.

4.4 Conclusion and future direction

In this chapter, we established proof of concept of detecting influenza viruses using a novel compound α-2, 6-sialylglucose as substrate. The mass spectrums clearly showed that α-2, 6-sialylglucose was hydrolyzed by both recombinant NA and intact influenza viruses. The hydrolysis product β-D-glucose can be detected quantified using electrochemical methods,. The next steps to further develop this novel method to a commercial biosensor, we have to optimize conditions and test clinical samples.

REFERENCE

1. M. Potier, L. Mameli, M. Belisle, L. Dallaire, S. B. Melancon, Fluorometric assay of neuraminidase with a sodium (4-methylumbelliferyl- α -D-N-acetylneuraminate) substrate. *Anal. Biochem.* **94**, 287 (1979).

2. C. Liao, M. Zhang, L. Niu, Z. Zheng, F. Yan, Highly selective and sensitive glucose sensors based on organic electrochemical transistors with graphene-modified gate electrodes. *J. Mater. Chem. B* **1**, 3820 (2013).

3. A. Safavi, F. Farjami, Electrodeposition of gold-platinum alloy nanoparticles on ionic liquid-chitosan composite film and its application in fabricating an amperometric cholesterol biosensor. *Biosens. Bioelectron.* **26**, 2547 (2011).

4. R. Singhal, A. Gambhir, M. K. Pandey, S. Annapoorni, B. D. Malhotra, Immobilization of urease on poly(N-vinyl carbazole)/stearic acid Langmuir-Blodgett films for application to urea biosensor. *Biosens. Bioelectron.* **17**, 697 (2002).

5. C. J. Ballesta, M. M. C. Valencia, L. F. Capitan-Vallvey, Disposable electrochemiluminescent biosensor for lactate determination in saliva. *Analyst (Cambridge, U. K.)* **134**, 1423 (2009).

6. J. Ballesta-Claver *et al.*, Electrochemiluminescent disposable cholesterol biosensor based on avidin-biotin assembling with the electroformed luminescent conducting polymer poly(luminol-biotinylated pyrrole). *Anal. Chim. Acta* **754**, 91 (2012).

7. L. Cheng, S. Deng, J. Lei, H. Ju, Disposable electrochemiluminescent biosensor using bidentate-chelated CdTe quantum dots as emitters for sensitive detection of glucose. *Analyst (Cambridge, U. K.)* **137**, 140 (2012).

8. A. Martinez-Olmos, J. Ballesta-Claver, A. J. Palma, M. d. C. Valencia-Miron, L. F. Capitan-Vallvey, A portable luminometer with a disposable electrochemiluminescent biosensor for lactate determination. *Sensors* **9**, 7694 (2009).

9. H. Shu, W. Wen, H. Xiong, X. Zhang, S. Wang, Novel electrochemical aptamer biosensor based on gold nanoparticles signal amplification for the detection of carcinoembryonic antigen. *Electrochem. Commun.* **37**, 15 (2013).

10. M. S. Chiriaco *et al.*, On-chip screening for prostate cancer: an EIS microfluidic platform for contemporary detection of free and total PSA. *Analyst (Cambridge, U. K.)* **138**, 5404 (2013).

11. R. L. Rubin, D. Wall, K. N. Konstantinov, Electrochemical biosensor for quantitation of anti-DNA autoantibodies in human serum. *Biosens. Bioelectron.* **51**, 177 (2014).

12. B. Elsholz *et al.*, Electrical microarrays for highly sensitive detection of multiplex PCR products from biological agents. *Biosens. Bioelectron.* **24**, 1737 (2009).

13. H. Shafiee *et al.*, Acute On-Chip HIV Detection Through Label-Free Electrical Sensing of Viral Nano-Lysate. *Small* **9**, 2553 (2013).

14. S. Bhatt, R. Mahesh, G. Gampa, An overview on recent advances in diabetes mellitus therapy. *Int. J. Pharm. Front. Res.* **1**, 84 (2011).

15. Q. Wu, L. Wang, H.-J. Yu, J.-J. Wang, Z.-F. Chen, Organization of Glucose-Responsive Systems and Their Properties. *Chem. Rev. (Washington, DC, U. S.)* **111**, 7855 (2011).

16. R. Monosik, M. Stred'ansky, E. Sturdik, Application of electrochemical biosensors in clinical diagnosis. *J. Clin. Lab. Anal.* **26**, 22 (2012).

17. O. Yilmaz *et al.*, Chitosan-ferrocene film as a platform for flow injection analysis applications of glucose oxidase and Gluconobacter oxydans biosensors. *Colloids Surf., B* **100**, 62 (2012).

18. K. Sirkar, M. V. Pishko, Amperometric Biosensors Based on Oxidoreductases Immobilized in Photopolymerized Poly(ethylene glycol) Redox Polymer Hydrogels. *Anal. Chem.* **70**, 2888 (1998).

19. J.-Z. Tao *et al.*, Poly(m-phenylenediamine)-Prussian blue hybrid film formed by one-step electrochemical deposition for glucose biosensor. *J. Electroanal. Chem.* **689**, 96 (2013).

20. X.-C. Tan, Y.-X. Tian, P.-X. Cai, X.-Y. Zou, Glucose biosensor based on glucose oxidase immobilized in sol-gel chitosan/silica hybrid composite film on Prussian blue modified glass carbon electrode. *Anal. Bioanal. Chem.* **381**, 500 (2005).

21. K. Peters, F. M. Richards, Chemical cross-linking: reagents and problems in studies of membrane structure. *Annu. Rev. Biochem.* **46**, 523 (1977).

22. S. Wu, G. Liu, P. Li, H. Liu, H. Xu, A high-sensitive and fast-fabricated glucose biosensor based on Prussian blue/topological insulator Bi2Se3 hybrid film. *Biosens. Bioelectron.* **38**, 289 (2012).

APPENDIX

Compound 5, CDCl3, 1H

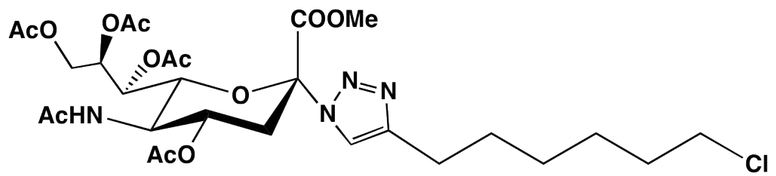

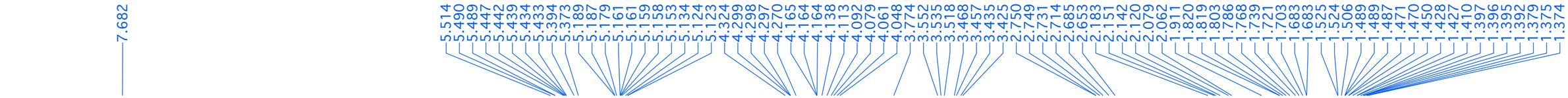

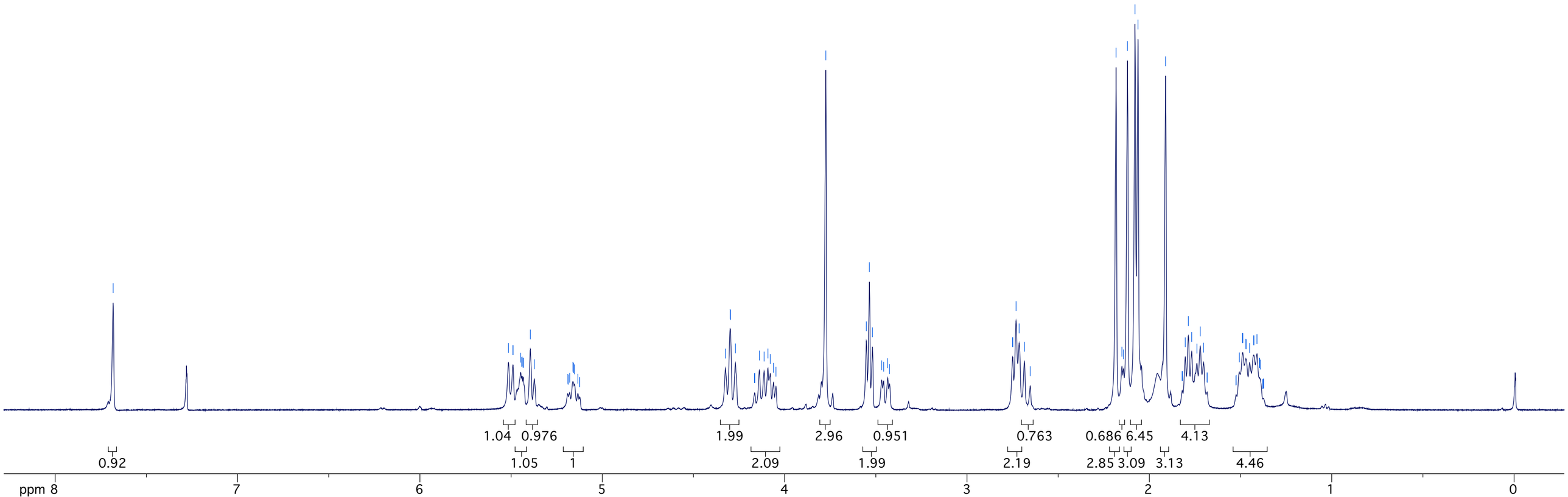

Compound 5, CDCl3, 13C

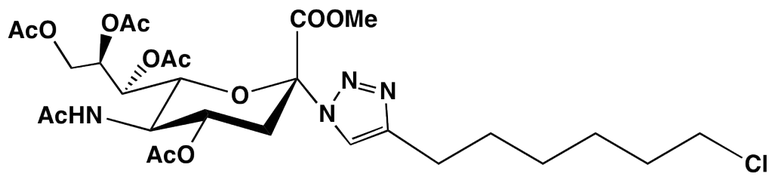

Compound 6, CDCl3, 1H

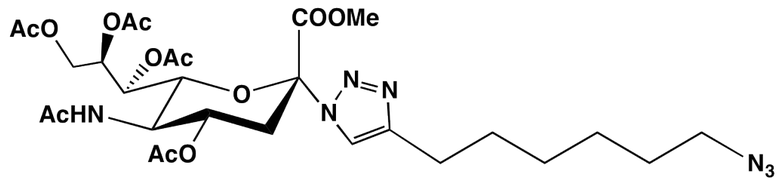

170.75
170.58
170.39
170.26
170.00
166.62
148.77
119.69
88.28
73.70
68.69
68.12
66.97
62.36
53.89
51.35
49.02
35.96
28.91
28.72
28.68
26.38
25.48
23.10
21.18
20.81
20.76
20.72

Compound 6, CDCl3, 13C

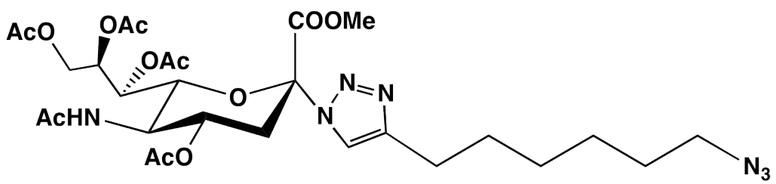

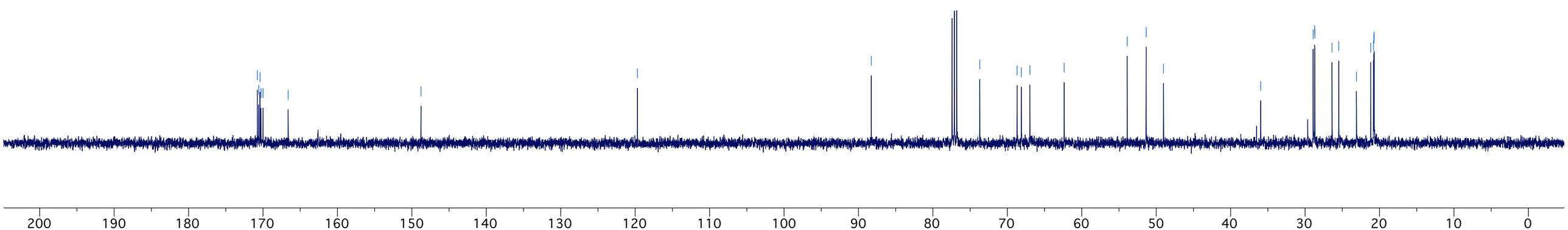

Compound 7, D2O, 1H

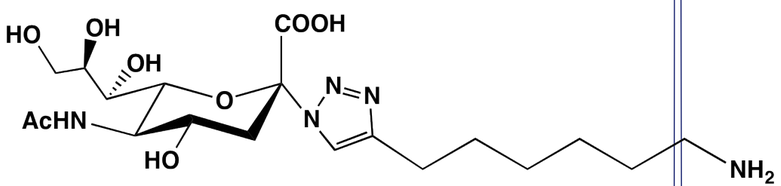

7.932
7.865

4.051 4.043 3.960 3.884 3.882 3.845 3.798 3.797 3.796 3.771 3.770 3.769 3.738 3.737 3.736 3.735 3.576 3.555 3.532 3.451 3.450 3.449 3.406 3.404 3.373 3.372 3.261 3.210 3.208 3.180 3.176 3.176 3.175 3.146 3.144 3.143 3.120 2.888 2.887 2.870 2.852 2.851 2.639 2.196 2.194 2.193 2.192 2.191 2.166 2.165 2.164 2.163 2.162 2.161 2.157 2.154 1.978 1.583 1.582 1.564 1.545 1.544 1.269 1.259 1.258 1.257 1.254 1.251

Compound 7, MeOD, 13C

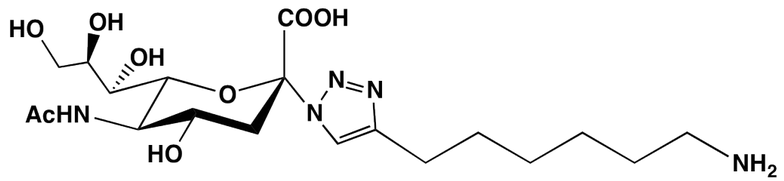

174.19
147.33
147.00
122.18
120.15
90.65
86.53
79.42
74.74
71.66
70.98
70.38
68.71
67.87
65.84
63.22
63.03
53.73
52.45
39.48
39.28
39.24
28.60
28.34
27.94
27.62
26.99
26.89
25.60
25.44
24.56
24.43
21.25

200 190 180 170 160 150 140 130 120 110 100 90 80 70 60 50 40 30 20 10 0

Compound 9, CDCl3, 1H

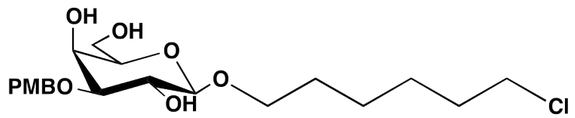

159.55
129.60
114.06
103.03
79.79
74.31
71.85
71.03
69.81
67.15
62.57
55.31
45.05
32.47
29.45
26.63
25.30

Compound 9, CDCl3, 13C

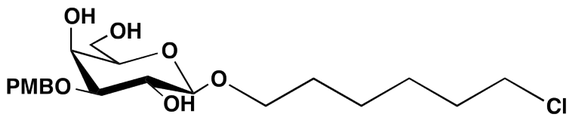

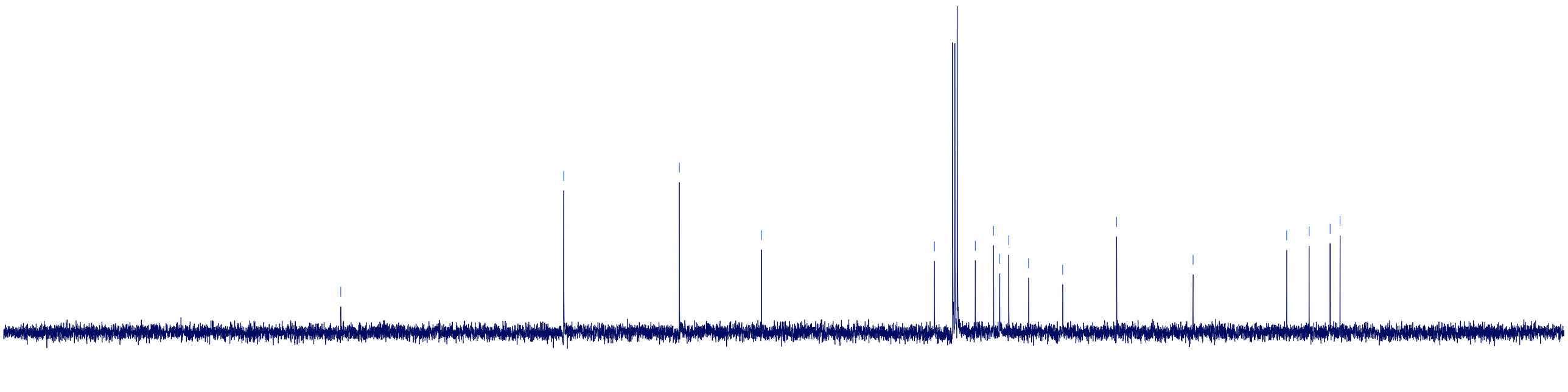

Compound 10, CDCl3, 1H

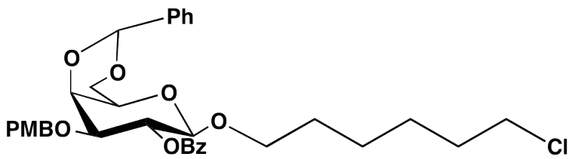

Compound 10 CDCl3, 13C

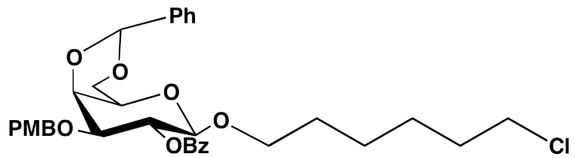

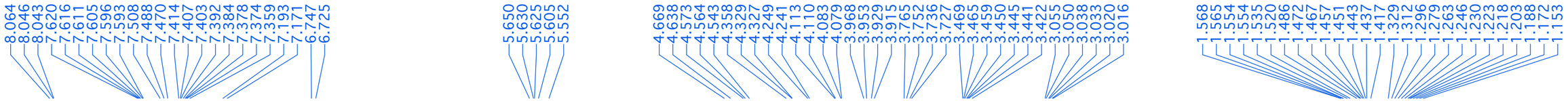

Compound 11, CDCl3, 1H

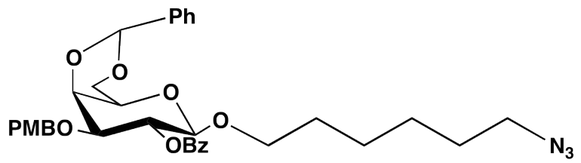

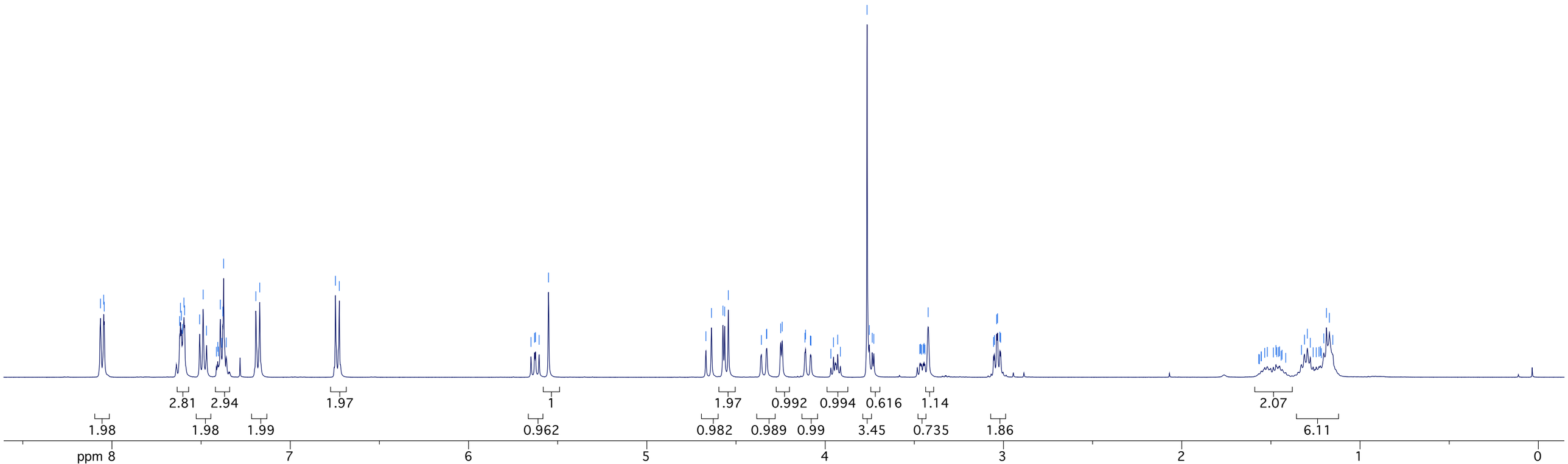

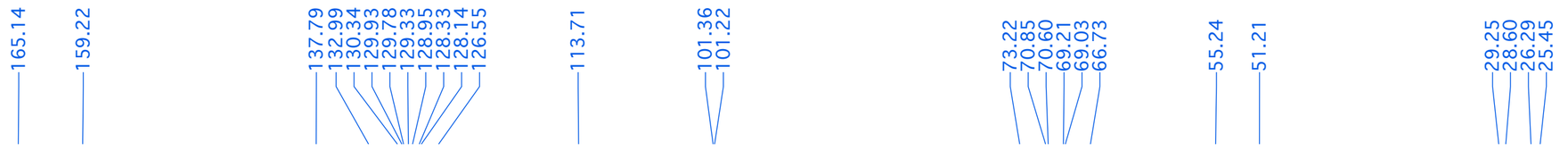

Compound 11, CDCl3, 13C

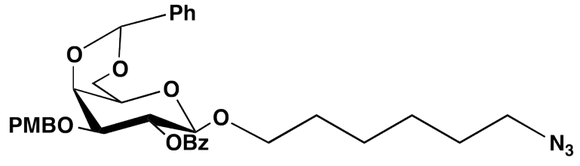

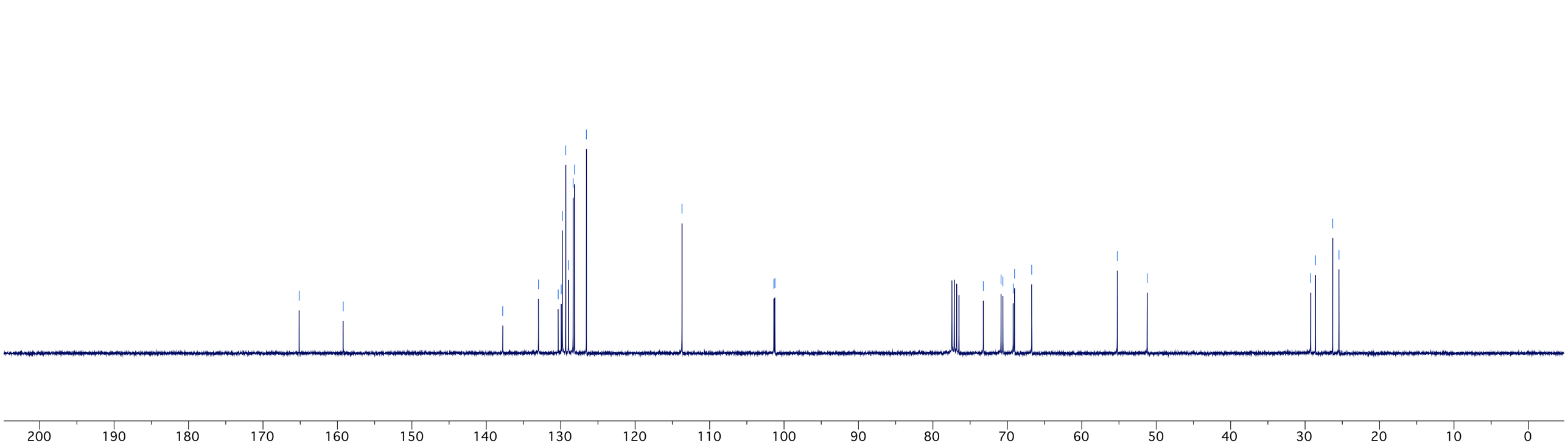

Compound 12, CDCl3, 1H

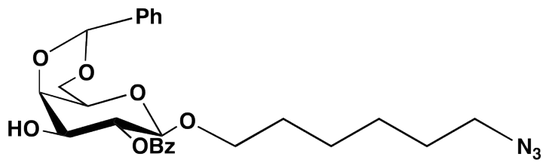

166.15
137.37
133.17
129.80
129.33
128.36
128.29
126.48
101.55
101.00
75.70
72.91
71.78
69.39
69.06
66.64
51.21
29.28
28.62
26.33
25.50

Compound 12, CDCl3, 13C

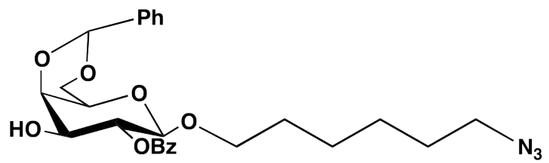

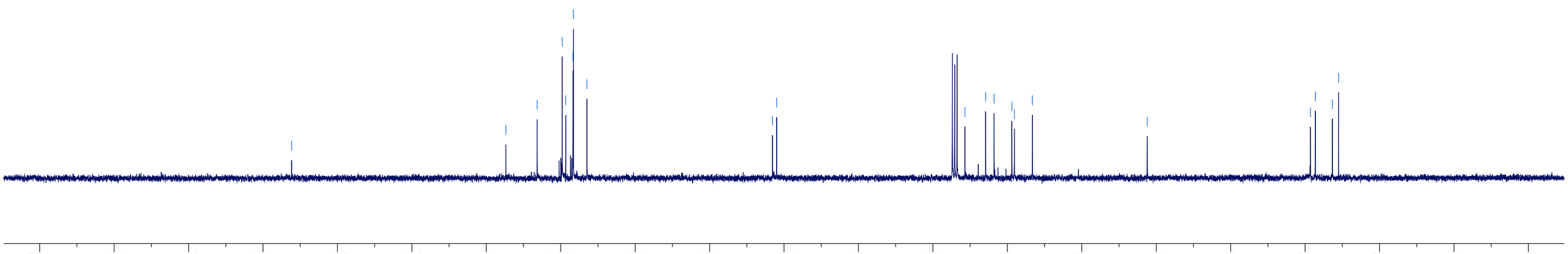

8.073
8.055
7.617
7.579
7.577
7.570
7.564
7.551
7.547
7.477
7.380
7.366
7.362
5.538
5.381
5.373
5.360
5.352
5.052
5.031
4.374
4.366
4.358
4.333
4.302
4.084
4.077
4.053
4.025
4.022
3.982
3.967
3.958
3.953
3.943
3.928
3.845
3.516
3.500
3.498
3.493
3.482
3.477
3.459
3.069
3.052
3.035
1.563
1.562
1.547
1.532
1.529
1.519
1.512
1.505
1.497
1.482
1.476
1.462
1.442
1.346
1.329
1.317
1.313
1.250
1.242
1.238
1.238
1.236
1.222
1.221
1.208
1.196
1.192

Compound 13] CDCl3, 1H

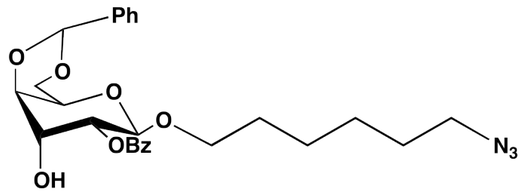

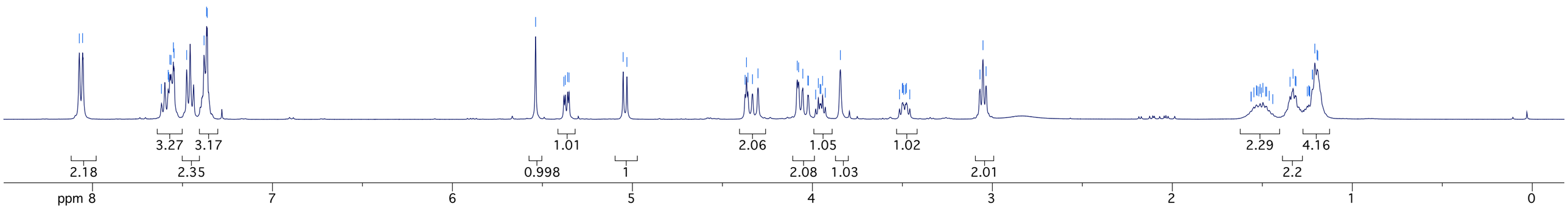

165.18
137.69
133.37
129.85
129.75
129.09
128.50
128.19
126.43
101.15
98.11
76.37
71.23
69.36
69.29
69.12
65.65
51.22
29.35
28.63
26.34
25.55

Compound 13, CDCl3, 13C

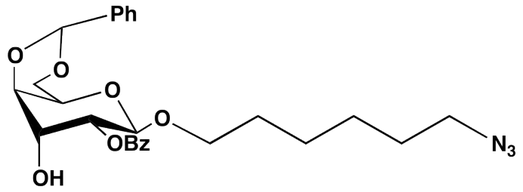

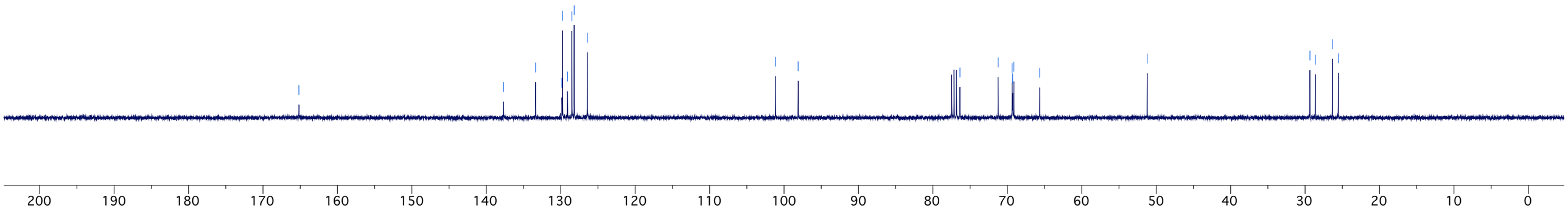

Compound 14, CDCl3, 1H

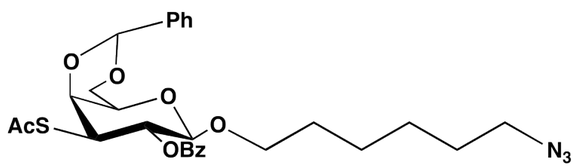

195.00
165.16
137.39
133.15
129.79
129.74
129.04
128.41
128.18
126.27
102.51
101.26
75.88
69.16
69.13
69.04
68.51
51.20
46.85
30.53
29.21
28.59
26.28
25.42

Compound 14, CDCl3, 13C

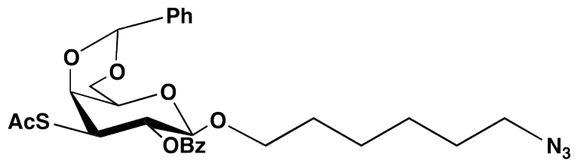

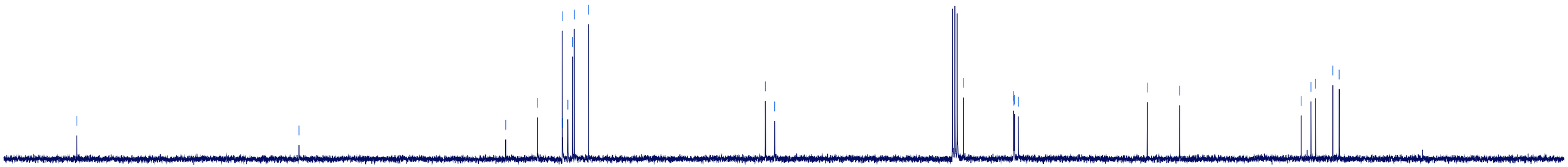

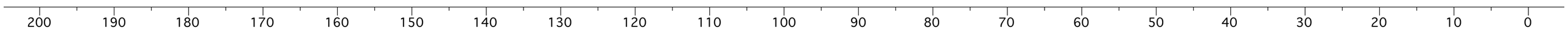

Intermediate thiol, CDCl3, 1H

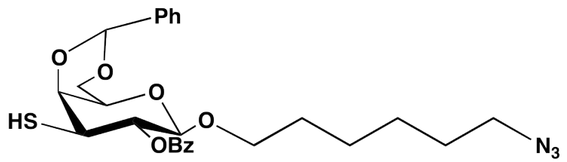

Compound 16, CDCl3, 1H

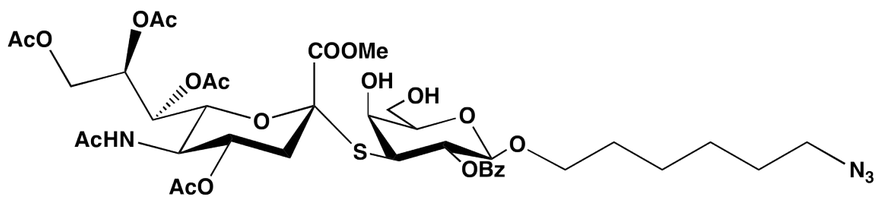

170.93
170.79
170.38
170.23
170.18
169.38
165.78
133.04
130.31
130.08
128.32
102.32
81.43
75.15
73.55
70.43
69.82
69.31
69.24
67.41
66.84
62.98
62.50
53.23
51.17
49.09
48.11
37.39
29.35
28.54
26.27
25.50
23.17
21.49
20.82
20.52

Compound 16, CDCl3, 13C

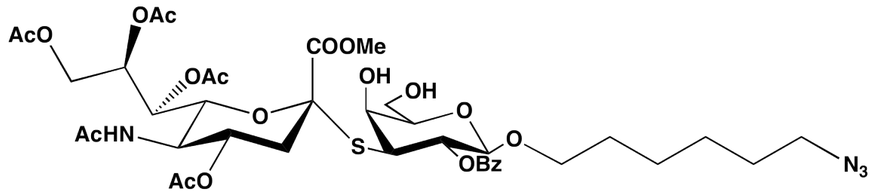

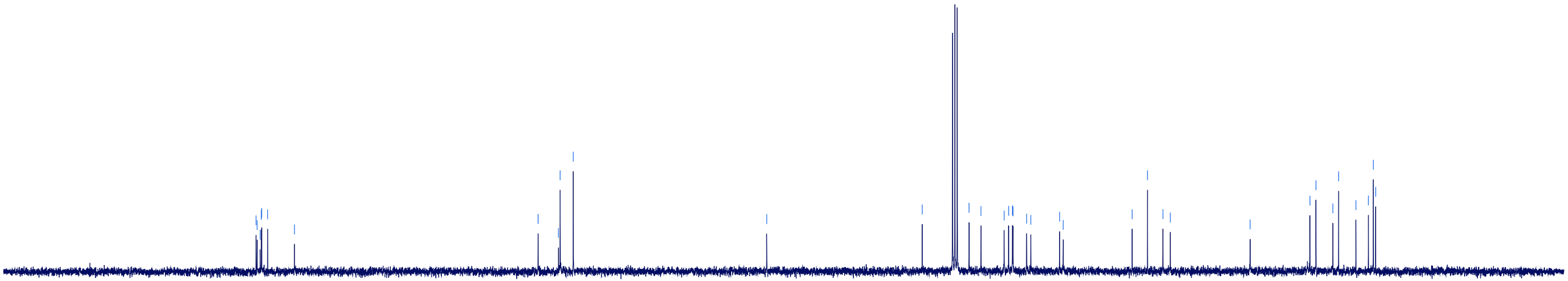

200 190 180 170 160 150 140 130 120 110 100 90 80 70 60 50 40 30 20 10 0

Compound 17, D2O, 1H

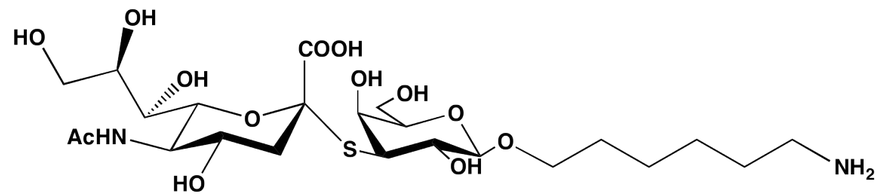

Compound 17, MeOD, 13C

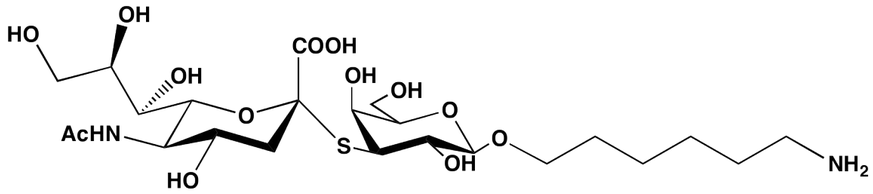

173.97
173.87
131.04
129.04
127.63
104.72
84.13
77.63
75.59
71.64
69.01
68.94
68.71
68.59
68.11
62.99
61.61
52.44
51.41
51.02
41.53
29.25
28.48
26.25
25.27
21.30

200 190 180 170 160 150 140 130 120 110 100 90 80 70 60 50 40 30 20 10 0

Compound 18, CDCl3, 1H

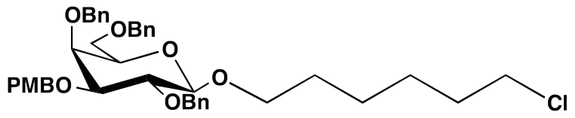

Compound 18, CDCl3, 13C

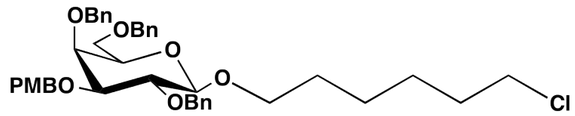

Compound 19, CDCl3, 1H

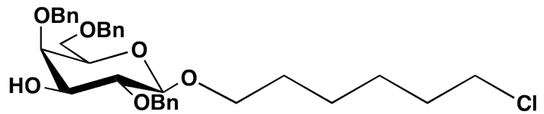

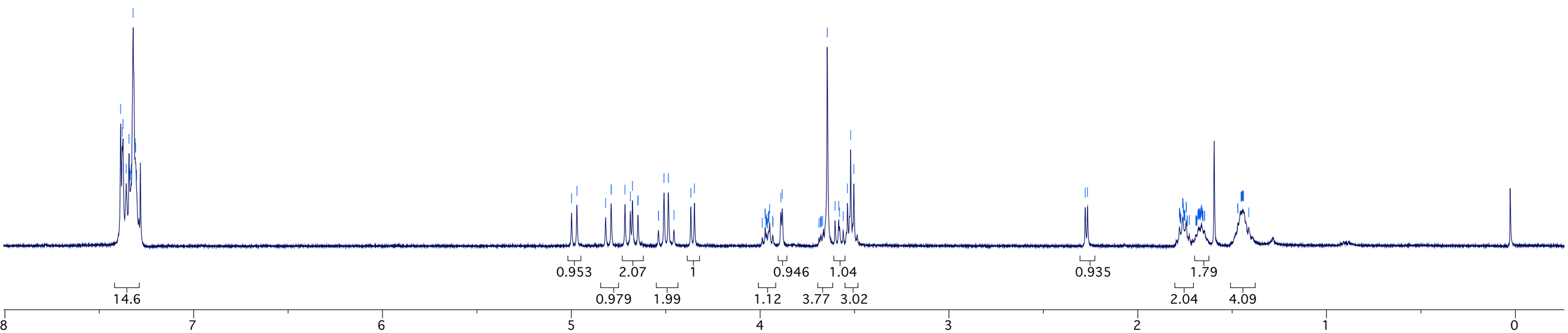

Compound 19, CDCl3, 13C

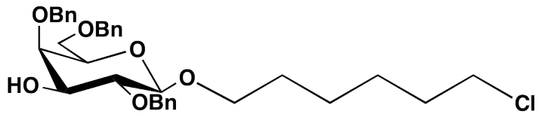

138.52
138.49
137.92
128.50
128.45
128.33
128.22
128.05
127.82
103.77
79.64
75.52
74.99
74.64
74.09
73.59
73.54
69.73
68.78
45.03
32.52
29.58
26.69
25.50

200 190 180 170 160 150 140 130 120 110 100 90 80 70 60 50 40 30 20 10 0

Compound 20, CDCl3, 1H

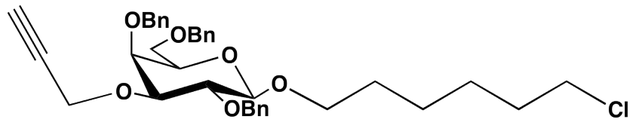

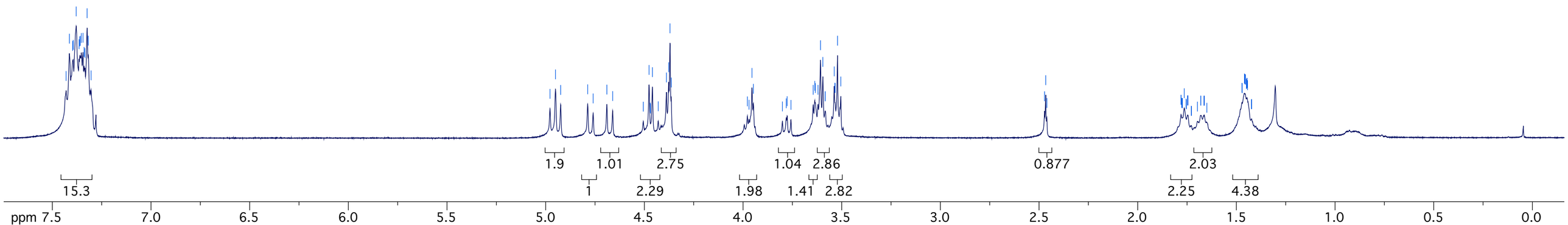

138.81
138.65
137.98
128.50
128.45
128.32
128.18
127.96
127.91
127.81
127.58
103.90
81.65
80.42
79.63
77.42
77.10
76.79
75.08
74.56
74.40
73.95
73.57
73.46
69.79
68.97
58.74
45.07
32.56
29.62
26.74
25.52

Compound 20, CDCl3, 13C

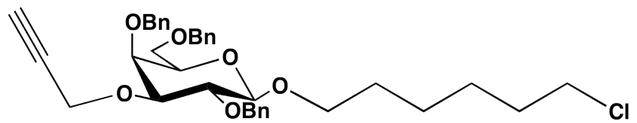

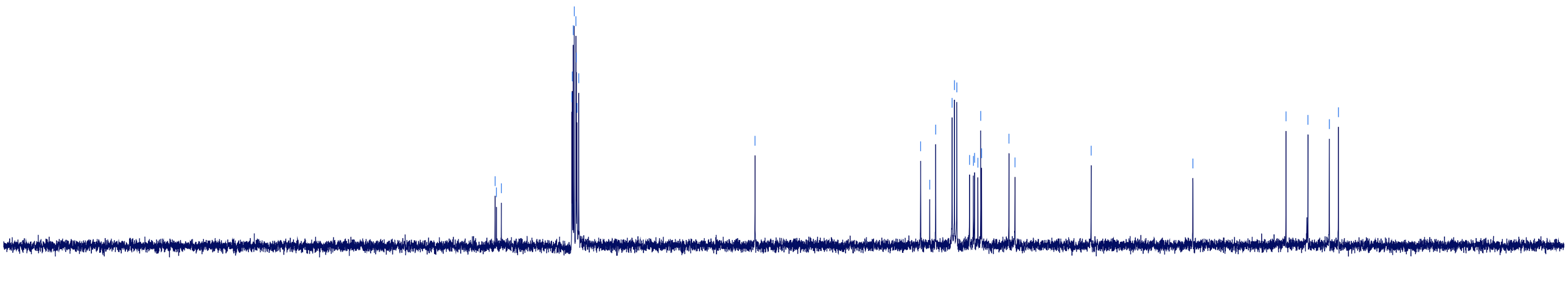

200 190 180 170 160 150 140 130 120 110 100 90 80 70 60 50 40 30 20 10 0

Compound 21, CDCl3, 1H

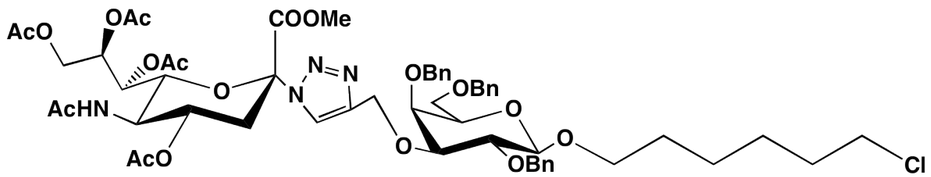

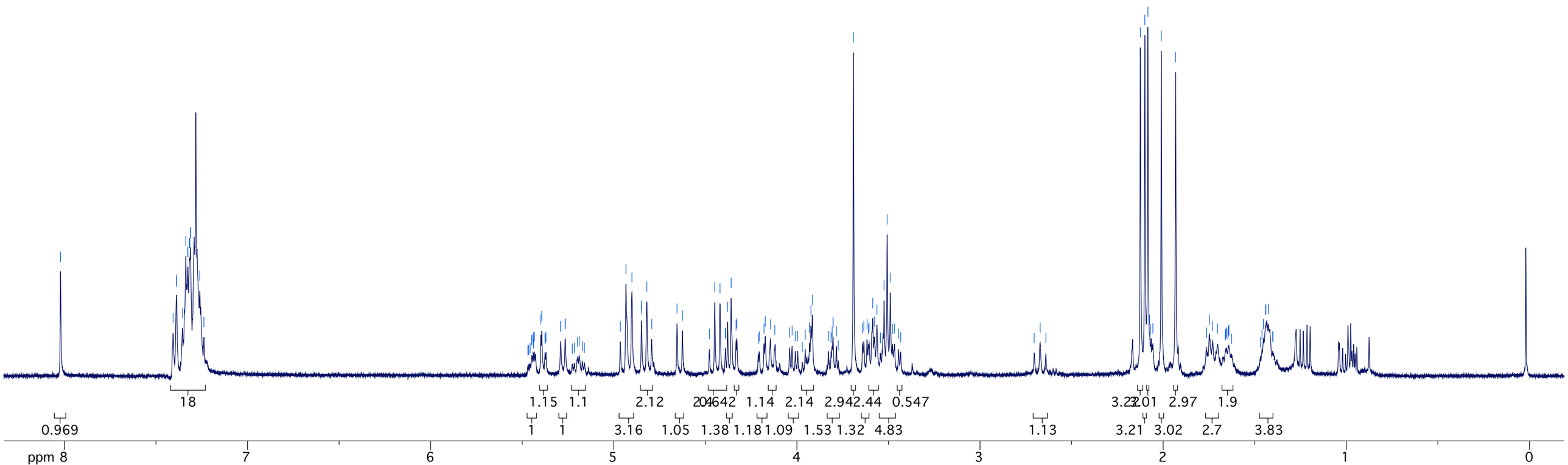

Compound 21, CDCl3, 13C

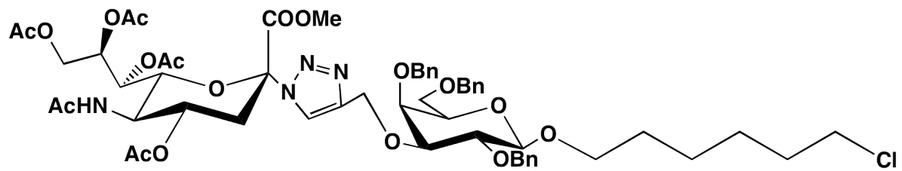

Compound 22, CDCl3, 1H

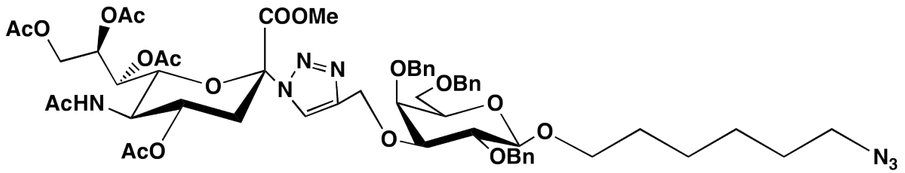

Compound 22, CDCl3, 13C

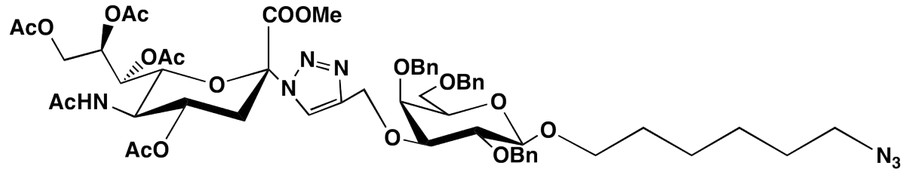

Compound 23, D2O, 1H

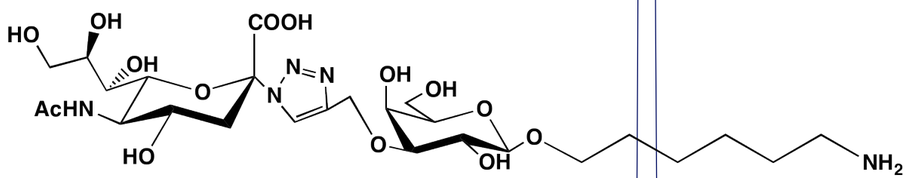

7.904

4.833 4.802 4.325 4.324 4.316 4.315 4.308 4.307 4.306 4.070 4.070 4.069 4.068 4.027 3.984 3.971 3.959 3.934 3.932 3.910 3.854 3.830 3.829 3.804 3.803 3.779 3.779 3.763 3.740 3.740 3.703 3.702 3.683 3.682 3.670 3.576 3.574 3.556 3.540 3.484 3.472 3.455 3.431 3.406 3.382 2.926 2.925 2.907 2.906 2.887 2.886 2.184 2.173 2.151 2.151 2.140 2.001 1.972 1.972 1.963 1.956 1.789 1.759 1.728 1.710 1.695 1.694 1.676 1.565 1.549 1.533 1.317 1.298

Compound 23, D2O, 13C

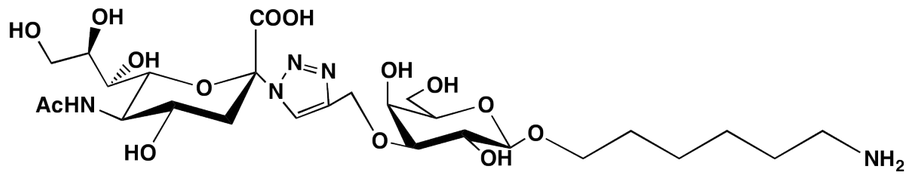

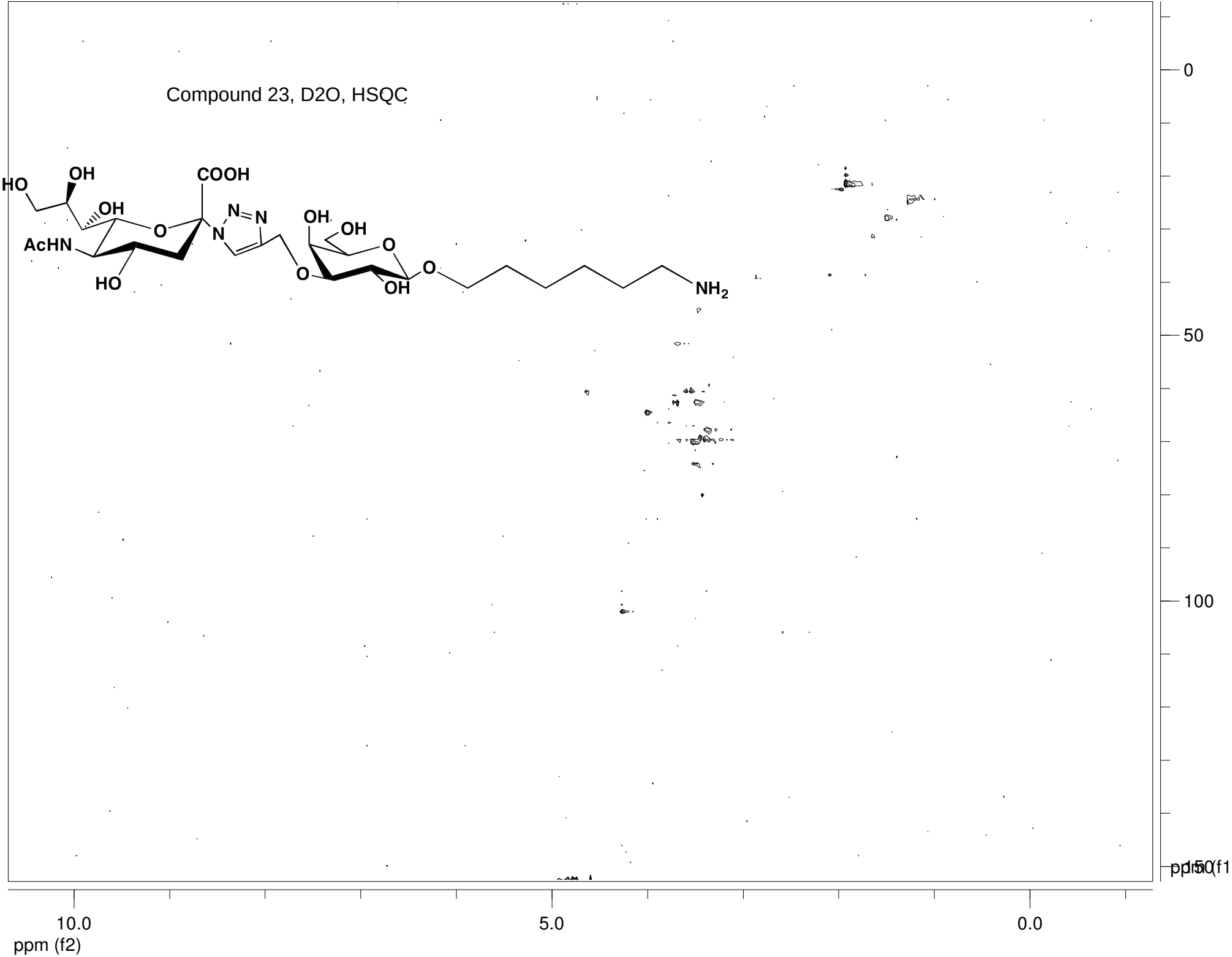
Compound 23, D2O, HSQC
HO
OH
COOH
OH
O
N
N
N
OH
OH
AcHN
O
O
HO
O
OH
NH2
0
50
100
150
ppm (f1
10.0
5.0
0.0
ppm (f2)

Compound 24, CDCl3, 1H

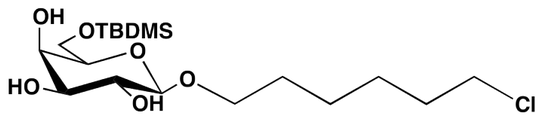

Compound 24, CDCl3, 13C

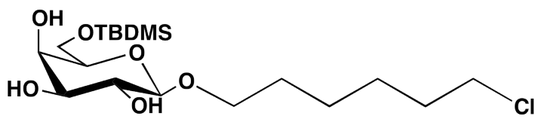

Compound 25, CDCl3, 1H

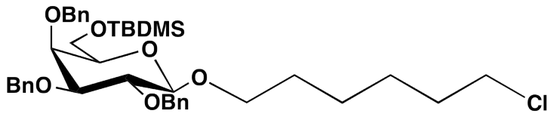

Compound 25, CDCl3, 13C

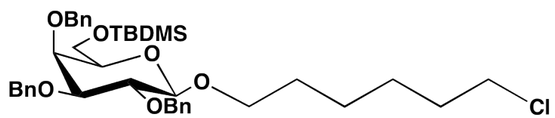

Compound 26, CDCl3, 1H

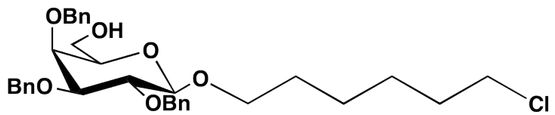

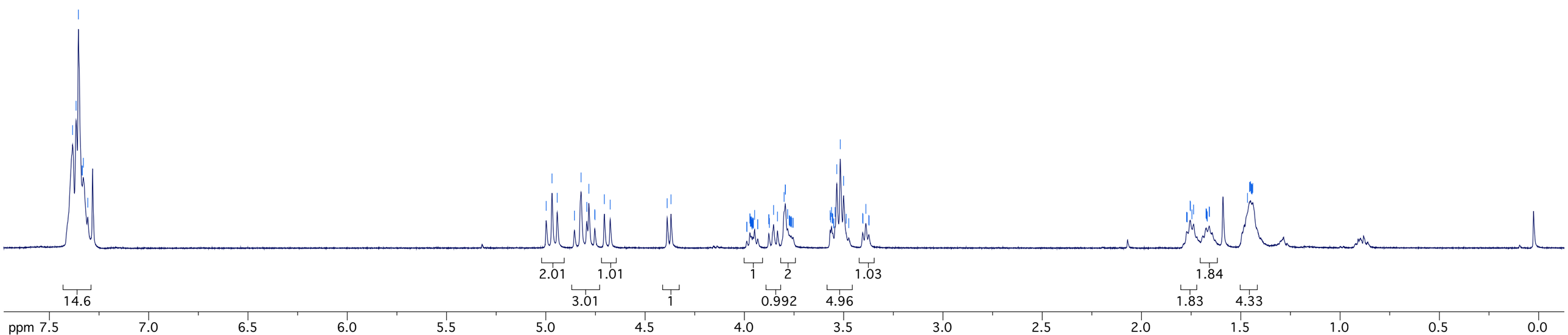

Compound 26, CDCl3, 13C

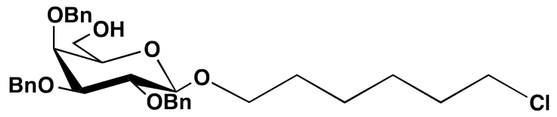

138.75
138.43
138.24
128.74
128.46
128.32
128.00
127.64
104.07
82.30
79.69
75.20
74.48
74.12
73.43
72.79
69.85
62.05
45.05
32.52
29.62
26.71
25.50

200 190 180 170 160 150 140 130 120 110 100 90 80 70 60 50 40 30 20 10 0

Compound 27, CDCl3, 1H

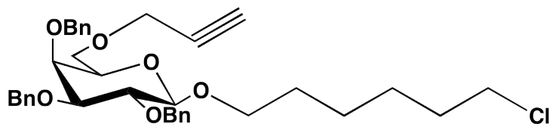

Compound 27, CDCl3, 13C

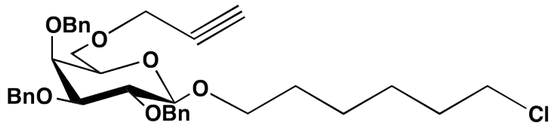

138.80
138.61
138.51
128.47
128.39
128.29
128.19
128.03
127.56
103.98
82.14
79.57
75.18
74.67
74.46
73.28
73.24
73.08
69.81
68.66
58.55
45.06
32.55
29.60
26.73
25.50

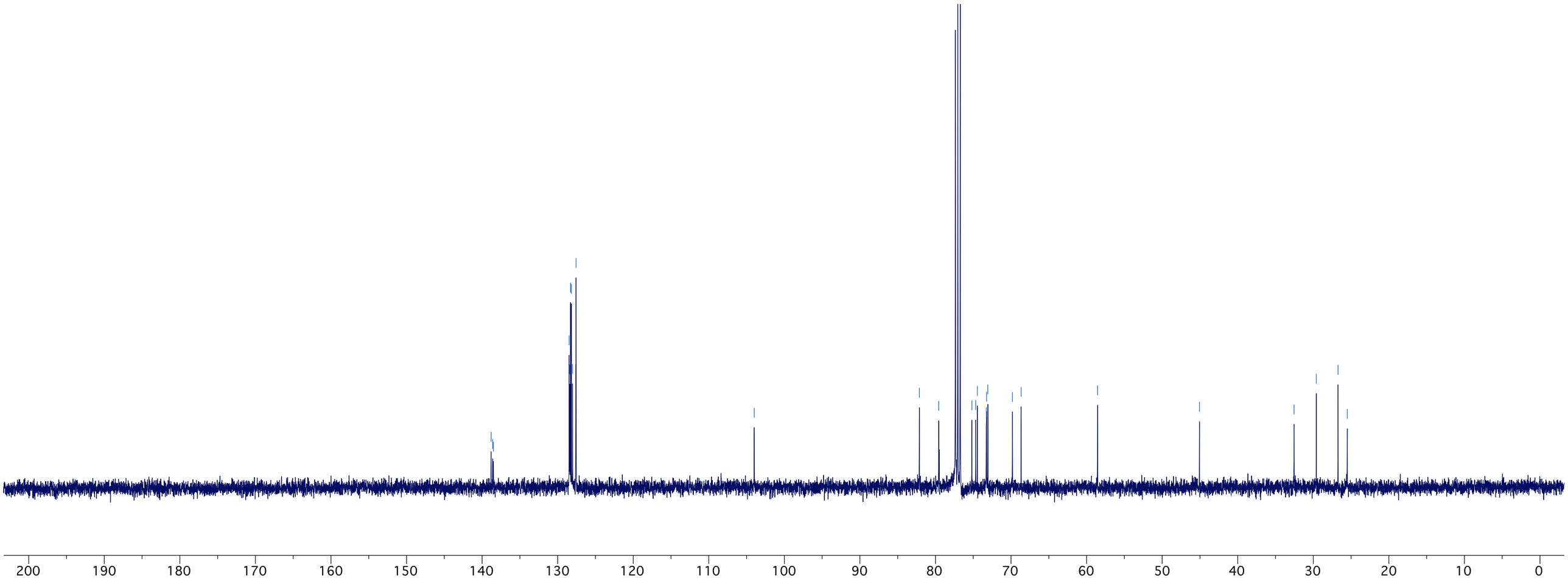

Compound 28, CDCl3, 1H

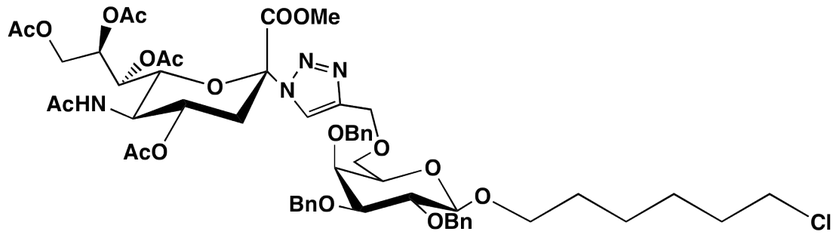

170.841
170.536
170.294
170.190
169.972
166.440
145.237
138.812
138.671
128.471
128.344
128.256
128.191
128.011
127.512
121.764
103.938
88.417
82.185
79.520
75.142
74.507
73.689
73.314
72.910
69.771
69.453
68.491
67.815
66.815
64.434
62.247
54.098
49.232
45.052
36.167
32.527
29.592
26.713
25.496
23.230
21.277
20.888
20.853
20.785
20.763

Compound 28, CDCl3, 13C

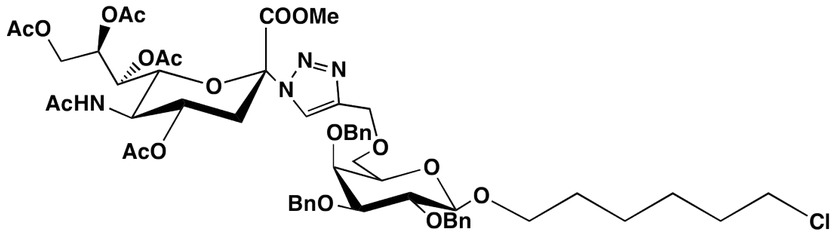

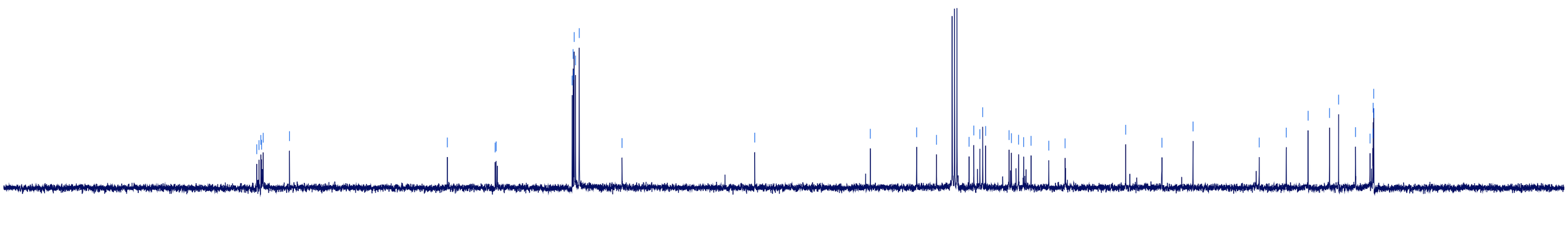

200 190 180 170 160 150 140 130 120 110 100 90 80 70 60 50 40 30 20 10 0

Compound 29, CDCl3, 1H

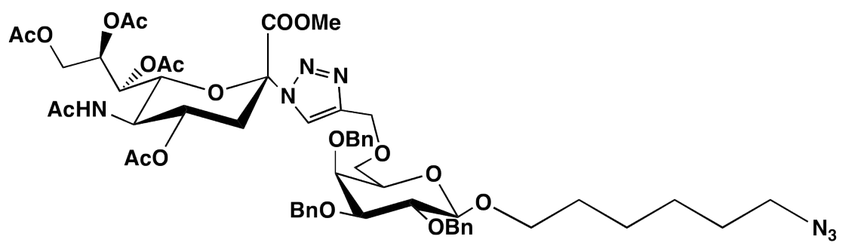

Compound 29, CDCl3, 13C

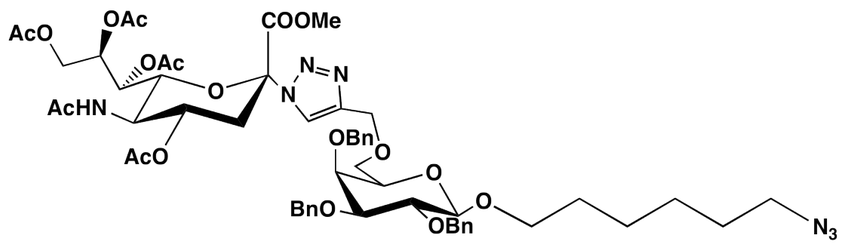

170.82
170.55
170.37
170.21
170.00
166.45
145.23
138.84
138.68
138.53
128.46
128.34
128.25
128.20
127.99
127.52
121.76
103.94
88.44
82.19
79.53
75.14
74.53
73.69
73.36
73.33
72.92
69.76
69.45
68.50
67.88
66.86
64.44
62.26
54.05
51.38
49.24
29.61
28.78
26.56
25.76
23.19
21.25
20.84
20.77
20.74

ppm 210 200 190 180 170 160 150 140 130 120 110 100 90 80 70 60 50 40 30 20 10 0 -10

Compound 30, D2O, 1H

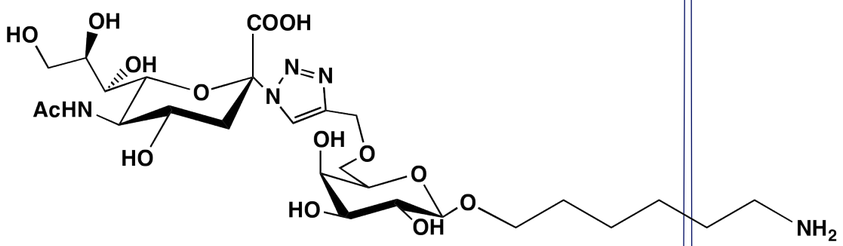

8.159

4.285 4.270 4.251 3.895 3.849 3.823 3.796 3.768 3.768 3.706 3.692 3.577 3.557 3.546 3.530 3.433 3.432 3.415 3.397 3.373 3.211 3.201 3.201 3.177 3.176 2.908 2.890 2.870 2.870 2.822 2.633 2.613 2.551 2.132 2.129 2.117 2.084 2.040 2.004 1.975 1.964 1.958 1.955 1.923 1.558 1.556 1.554 1.554 1.543 1.540 1.539 1.538 1.537 1.536 1.535 1.289 1.287 1.285 1.283 1.282 1.280

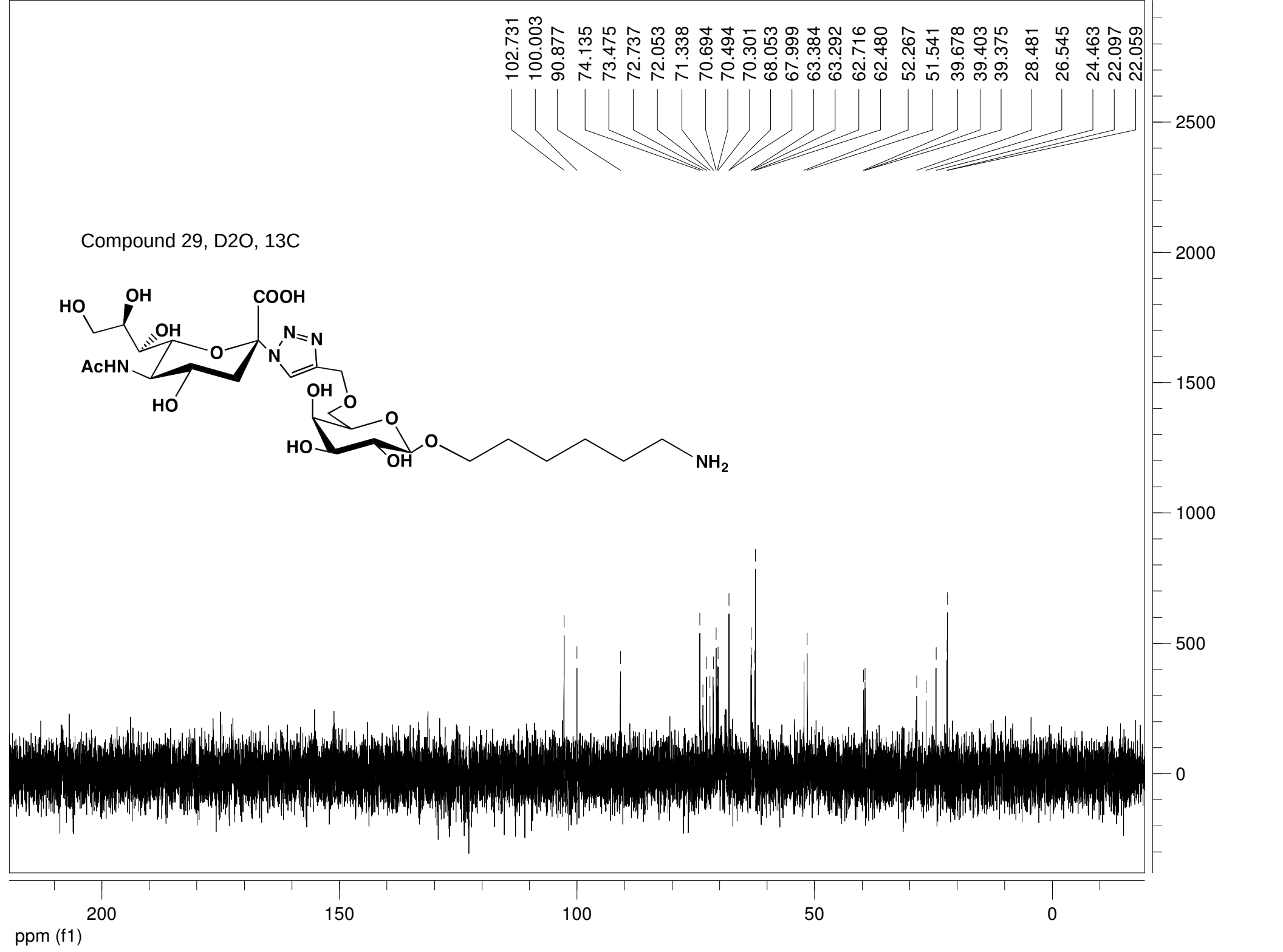
102.731
100.003
90.877
74.135
73.475
72.737
72.053
71.338
70.694
70.494
70.301
68.053
67.999
63.384
63.292
62.716
62.480
52.267
51.541
39.678
39.403
39.375
28.481
26.545
24.463
22.097
22.059
Compound 29, D2O, 13C
HO
OH
COOH
OH
O
N
N
N
AcHN
HO
OH
O
O
HO
O
OH
NH2
2500
2000
1500
1000
500
0
200
150
100
50
0
ppm (f1)